UNCLASSIFIED
SECURITY CLASSIFICATION OF THIS PAGE *(When Data Entered)*

REPORT DOCUMENTATION PAGE	READ INSTRUCTIONS BEFORE COMPLETING FORM
1. REPORT NUMBER AFOSR-TR- 31-0876 2. GOVT ACCESSION NO. AD-A111227	3. RECIPIENT'S CATALOG NUMBER
4. TITLE *(and Subtitle)* Computer Based Methods for Thermodynamic Analysis of Materials Processing	5. TYPE OF REPORT & PERIOD COVERED Annual 01 OCT 1980 to 30 SEPT 1981
	6. PERFORMING ORG. REPORT NUMBER
7. AUTHOR(s) Larry Kaufman	8. CONTRACT OR GRANT NUMBER(s) F49620-80-C-0020
9. PERFORMING ORGANIZATION NAME AND ADDRESS ManLabs, Inc. 21 Erie Street Cambridge, Mass. 02139	10. PROGRAM ELEMENT, PROJECT, TASK AREA & WORK UNIT NUMBERS 61102F 2306/A2
11. CONTROLLING OFFICE NAME AND ADDRESS Air Force Office of Scientific Research AFSC Bolling Air Force Base, D.C. 20332	12. REPORT DATE 02 November 1981
	13. NUMBER OF PAGES 84
14. MONITORING AGENCY NAME & ADDRESS*(if different from Controlling Office)*	15. SECURITY CLASS. *(of this report)* Unclassified
	15a. DECLASSIFICATION/DOWNGRADING SCHEDULE

16. DISTRIBUTION STATEMENT *(of this Report)*

Approved for public release; distribution unlimited.

17. DISTRIBUTION STATEMENT *(of the abstract entered in Block 20, if different from Report)*

18. SUPPLEMENTARY NOTES

Copy furnished to DTIC does not permit fully legible reproduction

19. KEY WORDS *(Continue on reverse side if necessary and identify by block number)*

Data Base	Thermochemical Properties	Fluoride glasses
Phases Diagrams	Ceramic Systems	III-V Compounds
Quasi Binary	Sialon Ceramics	Quasi Ternary
Iron base ternary alloys		

20. ABSTRACT *(Continue on reverse side if necessary and identify by block number)*

The data base previously developed for multicomponent SIALON Ceramic phase diagrams has been expanded to cover Ce_2O_3 additions. The Ce_2O_3-SiO_2 and Ce_2O_3-Si_3N_4 systems have been computed. Isothermal sections in the MgO-Si_3N_4-SiO_2, Y_2O_3-SiO_2-Si_3N_4 and Ce_2O_3-SiO_2-Si_3N_4 systems near 2000°K have been computed and

DD FORM 1 JAN 73 1473 EDITION OF 1 NOV 65 IS OBSOLETE -OVER-

SECURITY CLASSIFICATION OF THIS PAGE *(When Data Entered)*

compared with limited experimental data. A date base has also been developed for calculating binary, ternary and multi-component phases diagrams for III-V and II-VI compound systems. The trajectory of ordering temperatures for A2/B2 and $B2/DO_3$ reactions has been computed along the Fe_3Si-Fe_3Al composition path in the BCC of the Fe-Al-Si system and compared with experiment. The two phase (fcc +bcc) fields for disordered phases in the iron-aluminum-nickel, iron-aluminum-manganese, and the iron-nickel-manganese system between 900 and 1200°C. Contruction of a data base covering fluoride systems consisting of systems containing ZrF_4 which are employed to synthesize fluoride glasses has been initiated.

Annual Report

on

CONTRACT F 49620-80-C-0020

COMPUTER BASED METHODS FOR THERMODYNAMIC ANALYSIS OF MATERIALS PROCESSING

1 October 1980 to 30 September 1981

Submitted to

Air Force Office of Scientific Research (AFSC)

Bolling Air Force Base, D.C. 20332

2 November 1981

by

Larry Kaufman

ManLabs, Inc.
21 Erie Street
Cambridge, Massachusetts 02139

DISCLAIMER NOTICE

THIS DOCUMENT IS BEST QUALITY PRACTICABLE. THE COPY FURNISHED TO DTIC CONTAINED A SIGNIFICANT NUMBER OF PAGES WHICH DO NOT REPRODUCE LEGIBLY.

Abstract

The data base previously developed for multicomponent SIALON Ceramic phase diagrams has been expanded to cover Ce_2O_3 additions. The Ce_2O_3-SiO_2 and Ce_2O_3-Si_3N_4 systems have been computed. Isothermal sections in the MgO-Si_3N_4-SiO_2, Y_2O_3-SiO_2-Si_3N_4 and Ce_2O_3-SiO_2-Si_3N_4 systems near 2000°K have been computed and compared with limited experimental data. The trajectory of ordering temperatures for A2/B2 and B2/DO_3 reactions has been computed along the Fe_3Si-Fe_3Al composition path in the BCC of the Fe-Al-Si system and compared with experiment. The two phase (fcc + bcc) fields for disordered phases in the iron-aluminum-nickel, iron-aluminum-manganese, and the iron-nickel-manganese system between 900 and 1200°C. Construction of a data base covering fluoride systems consisting of systems containing ZrF_4 which are employed to synthesize fluoride glasses has been initiated.

I. PROGRESS DURING THE CURRENT YEAR

1. Calculation of Ceramic Materials Systems (Work statement items g,h,i,j,k) A data base is being developed for calculation of quasi-binary and quasi-ternary phase diagrams of ceramic systems (1-3). Previous segments of this base cover combinations of Cr_2O_3, MgO, Al_2O_3, Fe_2O_3, Fe_3O_4, "FeO", SiO_2, CaO, Si_3N_4 and AlN. Lattice Stability, Solution and Compound Phase Parameters were derived covering the liquid, spinel, corundum, periclase, crystobalite, tridymite, quartz, hexagonal and beta prime phases which appear in the binary systems composed of pairs of these compounds. Compound phases formed from specific binary combinations of these compounds (i.e. $MgO{\cdot}Cr_2O_3$) were also characterized. This description is based on observed thermochemistry and phase diagrams for the binary systems of interest. Selected ternary systems have been computed based on the foregoing data base for comparison with experimental sections in order to illustrate the usefulness of the data base. The present paper extends the data base to cover BeO, Y_2O_3 and Ce_2O_3 additions. Moreover, ternary sections in the SiO_2-MgO-Si_3N_4, SiO_2-Y_2O_3-Si_3N_4 and SiO_2-Ce_2O_3-Si_3N_4 were calculated between 1900K and 2100K for comparison with experiment. Pages 5-26 comprise a paper published in CALPHAD 5 (1981) 185 covering this work.

2. Calculation of III-V and II-VI Electro-Optical Materials Systems (Work statement item e) A data base covering the binary systems composed of Aluminum, Gallium Indium, Phosphorus, Arsenic and Antimony has been constructed by analyzing the fifteen combinations of these elements in terms of lattice stability, solution phase and compound parameters. Partial isothermal sections in the P-In-As, As-In-Sb, P-Ga-As, Ga-Sb-In and Al-Sb-Ga systems were then calculated using the foregoing data base for comparison with experimental isothermal sections and quasi-binary III-V phase diagrams. It was found that ternary liquid and

III-V compound interaction parameters were required to attain good agreement in some cases. Similar calculations were performed for the Te-Cd, Hg-Cd and Te-Hg binary systems and the Cd-Te-Hg ternary systems at pressures up to 74 atmospheres. Comparison of the calculated results with experimental data on tie-line compositions between Cd-Te-Hg liquid and quasi-binary CdTe-HgTe alloys is important in the liquid phase epitaxial growth of controlled band gap electro-optical materials. Pages 27-57 comprise a paper published in CALPHAD 5 (1981) 217 Covering this work.

3. Calculation of Ordering Temperatures for the Fe_3Al-Fe_3Si Quasi-Binary Section (Work statement item o) Inden's model has been employed to compute the trajectory of ordering temperatures along the quasi-binary join Fe_3Al-Fe_3Si for A2/B2 and B2/DO_3 reactions in the bcc phase of the Fe-Al-Si system. The results are compared with experimental findings on page 67, while pages 58-71 detail the method of computation.

4. Calculation of the Two Phase (FCC+BCC) Fields in Disordered Fe-Al-Ni, Fe-Al-Mn and Fe-Ni-Mn Alloys Between 900°C and 1200°C (Work statement item p) The ManLabs Data Base has been employed to carry out these calculations which are shown on pages 73-75 and detailed on pages 72-83.

5. Development of a Data Base for Calculating the Phase Diagrams of ZrF_4 Systems used in the Synthesis of Fluoride Glasses (Work statement item l) Coupled thermochemical analyses of the ZrF_4-BaF_2, ZrF_4-LaF_3, ZrF_4-PbF_2, ZrF_4-NaF, ZrF_4-KF, ZrF_4-RbF and ZrF_4-CsF binary system have been carried out. These results can be employed to locate the composition of maximum liquid stability for synthesis of fluoride glasses.

II. PROGRAM PERSONNEL

Technical activities during the past year have been carried out by L. Kaufman, F. Hayes, E.P. Warekois, J. Kozaczka, J. Nell, K. Taylor, D. Birney, C. Biddell and S. Drake of ManLabs, Inc.

III. TECHNICAL LECTURES

Technical lectures covering the work of this program were presented at the Washington, D.C. meeting of the American Ceramic Society, May 1981, CALPHAD X, Vienna Austria July 1981 and the Conference on the Chemistry of Materials at High Temperatures, AERE, Harwell, England September 1981. Discussions covering the cu-rent work were held with personnel from ESM-RADC Hanscom Field, AFOSR, WPAFB, UCLA Los Angeles, California and the Max Plank Institute-Stuttgart and Dusseldorf.

CALCULATION OF QUASIBINARY AND QUASITERNARY OXYNTIRIDE SYSTEMS-IV*

Larry Kaufman, Fred Hayes† and Dunbar Birnie
ManLabs, Inc., 21 Erie Street
Cambridge, Massachusetts 02139 USA

(This paper was presented at CALPHAD X, Vienna, Austria, July 1981)

ABSTRACT. A data base is being developed for calculation of quasi-binary and quasi-ternary phase diagrams of ceramic systems (1-3). Previous segments of this base cover combinations of Cr_2O_3, MgO, Al_2O_3, Fe_2O_3, Fe_3O_4, "FeO", SiO_2, CaO, Si_3N_4 and AlN. Lattice Stability, Solution and Compound Phase Parameters were derived covering the liquid, spinel, corundum, periclase, crystobalite, tridymite, quartz, hexagonal and beta prime phases which appear in the binary systems composed of pairs of these compounds. Compound phases formed from specific binary combinations of these compounds (i.e. $MgO{\cdot}Cr_2O_3$) were also characterized. This description is based on observed thermochemistry and phase diagrams for the binary systems of interest. Selected ternary systems have been computed based on the foregoing data base for comparison with experimental sections in order to illustrate the usefulness of the data base. The present paper extends the data base to cover BeO, Y_2O_3 and Ce_2O_3 additions. Moreover, ternary sections in the SiO_2-MgO-Si_3N_4, SiO_2-Y_2O_3-Si_3N_4 and SiO_2-Ce_2O_3-Si_3N_4 were calculated between 1900K and 2100K for comparison with experiment.

1. Introduction

The utility of computer based methods for coupling phase diagrams and thermochemical data for metallic systems has been well documented in many papers published in this journal. considerable effort is being applied toward developing an extensive base for metallic systems. Recently similar efforts have begun in order to provide a similar facility with ceramic systems. The expanded studies of SIALON composites, combining silicon and aluminum trides with oxides of silicon, aluminum, magnesium, beryllium, cerium and yttrium and other metals has provided additional motivation for predicting multicomponent phase diagrams of ceramic systems.

2. Description of the Thermochemical System Employed to Characterize Solution and Compound Phases

The method utilized for describing solution and compound phases is the same as that employed earlier (1-3) comprising some symbolic usage which facilitates data handling as indicated below. The free energy, G^L, of a liquid (solution) phase, L, in the binary system $_2O_3$-BeO is given by Equation (1) where T is in Kelvins, R=8.314 J/g. at°K, while is the atomic fraction of BO(i.e. BO=½BeO) and(1-x)is the fraction of YO(i.e. $1/5Y_2O_3$). The mass basis is thus one mole of atoms (i.e. a gram-atom)

This work has been sponsored by the Air Force Office of Scientific Research, Bolling AFB, Washington, D.C. under Contract F44620-80-C-0020

† On leave from Department of Metallurgy, University of Manchester-UMIST, Manchester, England.

$$G=(1-x)\,{}^{\circ}G^{L}_{YO}+x\,{}^{\circ}G^{L}_{BO}+RT(x\ln x+(1-x)\ln(1-x))+x(1-x)\,[LYOBO(1-x)+xLBOYO]\ J/g.at \qquad (1)$$

where ${}^{\circ}G^{L}_{YO}$ and ${}^{\circ}G^{L}_{BO}$ are the free energies of one gram atom of pure liquid YO and BO. Table 1 defines the lattice stabilities of the liquid and solid forms of YO, BO and the other components of current interest. These data derived from earlier studies and compilations of thermochemical and phase diagram data, (1-8), when combined with the solution and compound phase parameters shown in Tables 2 and 3 permit calculation of the binary phase diagrams shown in Figures 1-12. The solution parameters LYOBO and LBOYO, which describe the liquid Y_2O_3-BeO solution are listed in Table 2 (LYOBO=LBOYO=-2092 Joules/g.at). Similar parameters for the liquid and solid phases are listed in Table 2. The free energy of the solid phases are described in a manner similar to equation (1). Thus, for example, the free energy of the body centered cubic (Mn_2O_3)Y phase in the YO-BO system is given by

$$G=(1-x)\,{}^{\circ}G^{Y}_{YO}+x\,{}^{\circ}G^{Y}_{BO}+RT(x\ln x+(1-x)\ln(1-x))+x(1-x)\,[YYOBO(1-x)+xYBOYO]\ J/g.at. \qquad (2)$$

The solution parameters for the Y phase (YYOBO=YBOYO=-2092 J/g.at) are listed in Table 2. The free energy difference between the L and Y forms of YO and BO, i.e. $YOYOLY={}^{\circ}G^{L}_{YO}-{}^{\circ}G^{Y}_{YO}$ and $G^{L}_{BO}-{}^{\circ}G^{Y}_{BO}=BOBOLY$ are listed in Table 1. The free energy of a compound phase such as $C=(1/7)(SiO_2\cdot 2BeO)=SO_{0.429}BO_{0.571}$ is defined on the basis of Table 3 in terms of the base phase, the compound parameter, C, and the stoichiometry by equation (3)

$$G=0.429G^{N}_{SO}+0.571G^{N}_{BO}+(0.429)(0.571)\,[0.429LSOBO+0.571LBOSO-C]\ J/g.at. \qquad (3)$$

Reference to Table 2 shows that LSOBO=LBOSO=41840 J/g.at while Table 3 shows that C=62132-7.406T. Thus

$$G=0.429G^{N}_{SO}+0.571G^{N}_{BO}-4971+1.813T\ J/g.at. \qquad (4)$$

At 298K reference to Figure 1 shows that the stable form of quartz is the beta form (designated R). Table 1 shows that

$$G^{N}_{SO}-G^{R}_{SO}=SOSOLR-SOSOLN=5042-1.004T\ J/g.at. \qquad (5)$$

Substitution of equation (5) into equation (4) yields an expression for the free energy of formation of $(1/7)(SiO_2\cdot BeO)$ at 298K from the stable forms of it s compound components as,

$$G_f[298K]=G^{C}-0.429G^{R}_{SO}-0.571G^{N}_{BO}=-2808+1.382T\ J/g.at. \qquad (6)$$

Reference to Table 4 shows that this result is in keeping with the experimental (8) thermochemical data on the free energy of formation of $2BeO\cdot SiO_2$. Table 4 also displays the calculated free energy of formation for the remaining compounds listed in Table 3 and shown in Figures 1-12. It should be noted that this compound parameter for $SN_{0.7}SO_{0.3}$ currently shown as C=62760-1.255T J/g.at. has been revised from the previously stated value C=115060-25.10T J/g.at.(3) The current value is based on the assessment of Doerner et al (5) and leads to slight revisions in the previously calculated SN-SO and SO-AO-SN phase diagrams presented earlier (3). The revised versions, which differ slightly from the earlier results are shown in Figures 8 and 13.

3. Calculation of Quasi-Ternary Phase Diagrams

The free energy of ternary solution phases was synthesized from the binary solution phases on the basis of Kohler's equation as in the previous papers (1-3). On this basis the free energy of the liquid phase in the SO-MO-SN system where x is the atom fraction MO, y is the atom fraction SN and 1-x-y is the atom fraction SO is given by

TABLE 1

SUMMARY OF LATTICE STABILITY PARAMETERS
(All units in Joules per gram atom (mole of atoms), T in Kelvins)

AO = (1/5)Al_2O_3, SO = (1/3)SiO_2, MO = (1/2)MgO, AN = (1/2)AlN, SN = (1/7)Si_3N_4

BO = (1/2)BeO, YO = (1/5)Y_2O_3, CE = (1/5)Ce_2O_3

P = Periclase, C = Corundum, X = Crystobalite, T = Tridymite, H = α quartz

R = ℓ quartz, B = beta Si_3N_4, N = hexagonal AlN and BeO, Y = body centered cubic $(Mn_2O_3)Y_2O_3$ and Ce_2O_3 structure

BOBOLN* = (1/2)BeO(Liquid)-(1/2)BeO(hexagonal)

YOYOLY = (1/5)Y_2O_3(Liquid)-(1/5)Y_2O_3 (body centered cubic)

YOYOLY =	22694 - 8.368T	CECELY =	20334 - 8.368T
YOYOLN =	0 - 14.142T	CECELN =	0 - 14.142T
YOYOLX =	0 - 2.092T	CECELX =	0 - 2.092T
YOYOLB =	0 - 12.510T	CECELB =	0 - 12.510T
YOYOLC =	0 - 10.209T	CECELC =	0 - 10.209T
BOBOLN =	40376 - 14.142T	AOAOLY =	0 - 8.368T
BOBOLX =	0 - 1.674T	ANANLY =	0 - 8.368T
BOBOLC =	0 - 10.209T	SNSNLB =	33949 - 12.510T
BOBOLB =	0 - 12.510T	SNSNLY =	0 - 8.368T
BOBOLY =	0 - 8.368T	SOSOLY =	0 - 2.092T
		SOSOLN =	0 - 2.092T
		SOSOLX =	3347 - 1.674T
		SOSOLR =	5042 - 3.096T

* These differences specify the free energy of one phase (i.e. liquid) minus the free energy of the second phase (i.e. hexagonal) for a given compound.

$$G^L=(1-x-y)\,{}^oG^L_{SO}+x\,{}^oG^L_{MO}+y\,{}^oG^L_{SN}+RT[(1-x-y)\ell n(1-x-y)+x\ell nx+y\ell ny]$$
$$+(1-x-y)x(1-y)^{-1}[(1-x-y)LSOMO+xLMOSO]+xy(x+y)^{-1}[xLMOSN+yLSNMO]$$
$$+(1-x-y)y(1-x)^{-1}[(1-x-y)LSOSN+yLSNSO] \quad J/g.at. \quad (7)$$

The solution parameters required to specify G^L were defined previously (2,3) as LSOSN=LSNSO=LMOSN=LSNMO=29288 J/g.at. and LSOMO=LMOSO=-106274+42.01T for $0.4\leq x_{MO}\leq 1.0$ and LSOMO=-24267+24.27T; LMOSO=-229283+68.62T for $0.0\leq x_{MO}\leq 0.40$. These parameters permit explicit definition of G^L in composition ranges where (x/1-x-y) is more than 0.667 and ranges where (x/1-x-y) is less than 0.667. In the latter range the miscibility gap present in the SO-MO binary system propagates into the ternary SO-MO-SN as shown in Figure 14a. Here the ternary miscibility gap shows the tie lines connecting the coexisting liquid compositions L_1 and L_2.

The remaining solution phases in this system, i.e. P, X, B, etc. are defined in similar fashion to Equation 7. The resulting equilibria between the L and P solutions are depicted by the tie lines traversing the two phase L+P field shown in Figure 14(b). The compound phases F,R and BP which appear in the SO-MO, SO-SN and MO-SN binary systems are defined along the lines previously established (1-3) and are specified in Table 3. Thus for example the free energy of the $SN_{0.7}SO_{0.3}$ (R) phase in the SO-MO-SN system is defined by Equation 8 as

TABLE 2

SUMMARY OF SOLUTION PHASE PARAMETERS
(All units in Joules per gram atom (mole of atoms), T in Kelvins)

L = Liquid, N = hexagonal, X = Crystobalite, T = Tridymite, Y = body centered cubic

B = beta Si_3N_4, AO = (1/5)Al_2O_3, SO = (1/3)SiO_2, AN = (1/2)AlN, SN = (1/7)Si_3N_4, BO = (1/2)BeO

YO = (1/5)Y_2O_3, CE = (1/5)Ce_2O_3

LSOBO = LBOSO = 41840
NSOBO = NBOSO = 83680
XSOBO = XBOSO = 83680
TSOBO = TBOSO = 83680

LYOBO = LBOYO = -2092
YYOBO = YBOYO = -2092
NYOBO = NBOYO = 83680

LAOBO = LBOAO = 8368
CAOBO = CBOAO = 83680
NAOBO = NBOAO = 83680

LBOAN = LANBO = 20920
NBOAN = NANBO = 83680

LCESN = LSNCE = 4180
BCESN = BSNCE = 62760
YCESN = YSNCE = 62760

LBOSN = LSNBO = 20920
BBOSN = BSNBO = 83680
NBOSN = NSNBO = 83680

LYOAO = LAOYO = 12552
YYOAO = YAOYO = 83680
CYOAO = CAOYA = 83680

LYOAN = LANYO = 20920
YYOAN = YANYO = 83680
NYOAN = NANYO = 83680

LSNSO = LSOSN = 29288
XSNSO = XSOSN = 125520
TSNSO = TSOSN = 125520

LYOSN = LSNYO = 4180
BYOSN = BSNYO = 83680
YYOSN = YSNYO = 83680

$0 \leq x_{SO} \leq 0.60$*
LYOSO = LSOYO = -92048+36.82T
$0.6 \leq x_{SO} \leq 1.0$
LYOSO = -216,000+66.94T
LSOYO = -9414+16.74T
YYOSO = YSOYO = 83680
XYOSO = XSOYO = 83680
TYOSO = TSOYO = 83680

$0 \leq x_{SO} \leq 0.60$
LCESO = LSOCE = -92048 + 36.82T
$0.6 \leq x_{SO} \leq 1.0$
LCESO + -216,000+66.94T
LSOCE = -9414+16.74T
YCESO = YSOCE = 83680
XCESO = XSOCE = 83680
TCESO = TSOCE = 83680

*x_{SO} = atomic fraction SO in YO-SO or CE-SO

$$G^R = z^\circ G^B_{SN} + x^\circ G^B_{SO} + y^\circ G^B_{MO} + (1-(y/(1-x)))\Delta G_A + (y/(1-x))\Delta G_B + RT(y\ell ny + z\ell nz - (1-x)\ell n(1-x)) + \Delta G_E \quad J/g.at. \qquad (8)$$

where $x=x_{SO}$, $y=y_{MO}$ and $z=z_{SN}$. Since the compound phase runs from $SN_{0.70}SO_{0.30}$ to $MO_{0.70}SO_{0.30}$, $p=(x_*-x'_*)/(1-x_*)=0$ and $x=x'_*+yp=x_*=0.3$, and $z=1-x'_*-y(1+p)=0.7-y$. Since

$$\Delta G_A = (0.3)(0.7)[0.7LSNSO+0.3LSOSN-C] = -7029 + 0.263T \quad J/g.at. \qquad (9)$$

and $\Delta G_B = (0.3)(0.7)[0.7LMOSO+0.3LSOMO-C] = -22318 + 8.822T$ J/g.at.

from Tables 3 and 5 and the previous values of LSNSO, LSOSN, LMOSO and LSOMO (2) given in the above text. The excess free energy of mixing, ΔG_E, for the compound is given (3) by

$$\Delta G_E = CAByz/(1-x)$$

However, CAB is taken as zero in all the cases treated here thus Equation 8 can be written explicitly as follows:

$$G^R = (0.70-y)^\circ G^B_{SN} + 0.3^\circ G^B_{SO} + y^\circ G^B_{MO} - (1-(y/0.7))(7029-0.263T) - (y/0.7)(22318-8.822T) + RT(y\ell ny + (0.7-y)\ell n(0.7-y) - 0.7\ell n0.7) \qquad (11)$$

where $y=y_{MO}$. Since the lattice stabilities of SN, SO and MO (i.e. SNSNLB, SOSOLB and MOMOLB) have already been specified the R-L equilibria (Figure 14c) can be computed. Figs. (14a) through

TABLE 3

SUMMARY OF COMPOUND PARAMETERS FOR BINARY SYSTEMS
(All units in Joules per gram atom (mole of atoms) T in Kelvins)

Compound	Name	Stoichiometry	Stability	Base	Compound Parameter (Joules/g.at.)
$(1/7)(SiO_2 \cdot 2BeO)$	G	$SO_{0.429}BO_{0.571}$	stable	N	62132-7.406T
$(1/17)(3Al_2O_3 \cdot BeO)$	Q	$AO_{0.882}BO_{0.118}$	stable	C	75312
$(1/7)(Al_2O_3 \cdot BeO)$	I	$AO_{0.714}BO_{0.286}$	stable	C	76567
$(1/11)(Al_2O_3 \cdot 3BeO)$	J	$AO_{0.455}BO_{0.545}$	stable	N	61923+9.916T
$(1/15)(2Y_2O_3 \cdot Al_2O_3)$	U	$YO_{0.667}AO_{0.333}$	stable	Y	70291
$(1/10)(Y_2O_3 \cdot Al_2O_3)$	V	$YO_{0.500}AO_{0.500}$	stable	C	48534+20.083T
$(1/40)(3Y_2O_3 \cdot 5Al_2O_3)$	WA	$YO_{0.375}AO_{0.625}$	stable	C	82425
$(1/5)(Si_2N_2O)$	R	$SN_{0.7}SO_{0.3}$	stable	B	62760-1.255T
$(1/12)(Y_2O_3 \cdot Si_3N_4)$	S	$YO_{0.417}SN_{0.583}$	stable	B	44769+14.644T
$(1/8)(Y_2O_3 \cdot SiO_2)$	M	$YO_{0.625}SO_{0.375}$	stable	Y	-15900+29.288T
$(1/19)(2Y_2O_3 \cdot 3SiO_2)$	K	$YO_{0.527}SO_{0.473}$	stable	Y	-30334+36.819T
$(1/11)(Y_2O_3 \cdot 2SiO_2)$	O	$YO_{0.455}SO_{0.545}$	stable	Y	-2218+23.849T
$(1/12)(Ce_2O_3 \cdot Si_3N_4)$	S	$CE_{0.417}SN_{0.583}$	stable	B	44769+14.644T
$(1/8)(Ce_2O_3 \cdot SiO_2)$	M	$CE_{0.625}SO_{0.375}$	stable	Y	418+24.058T
$(1/62)(7Ce_2O_3 \cdot 9SiO_2)$	Z	$CE_{0.565}SO_{0.435}$	stable	Y	6276+24.434T
$(1/11)(Ce_2O_3 \cdot 2SiO_2)$	O	$CE_{0.455}SO_{0.545}$	stable	Y	7531+25.230T
$0.01(14Si_3N_4 \cdot BeO)$	BP	$SN_{0.98}BO_{0.02}$	stable	B	83680+4.184T
$(1/150)(21Si_3N_4 \cdot SiO_2)$	BP	$SN_{0.98}SO_{0.02}$	stable	B	71128+4.184T
$0.0040(35Si_3N_4 \cdot Y_2O_3)$	BP	$SN_{0.98}YO_{0.02}$	stable	B	83680+4.184T
$0.0040(35Si_3N_4 \cdot Ce_2O_3)$	BP	$SN_{0.98}CE_{0.02}$	stable	B	83680+4.180T

14(d) illustrate the steps which are taken in sythesizing the ternary system SO-MO-SN, (i.e. $1/3SiO_2$-$1/2MgO$-$1/7Si_3N_4$) from the component binary systems. Initially each of the equilibria between pairs of solution and or compound phases are calculated individually. In the present case these pairs consist first of the liquid miscibility gap (L_1-L_2 in 14a) followed by L-Periclase in Figure 14b. Next the L-F and L-R equilibria which are shown in Figures 14a and 14c are calculated. Overlaying the L_1-L_2, L-F, L-P, and L-R equilibria shows that there are no interactions between any of the phase pairs except in the case of the L-R/L_1L_2 interaction. The latter, which is shown in Figure 14c results in a three phase field between R, L_1 and L_2. The boundaries of this three phase field are the lines traversing the L_1+L_2 miscibility gap illustrated in Figure 14a and the tie lines which define the R-L equilibria shown in Figure 14c.

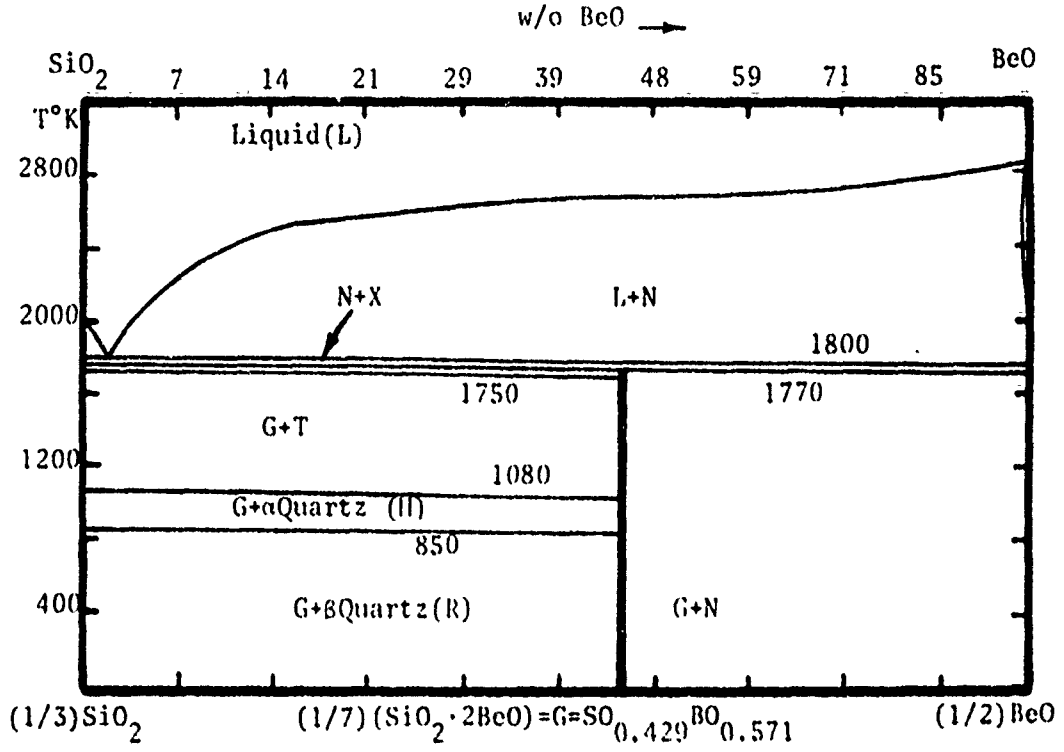

Figure 1. Calculated $(1/3)SiO_2$-(1/2)BeO Phase Diagram.

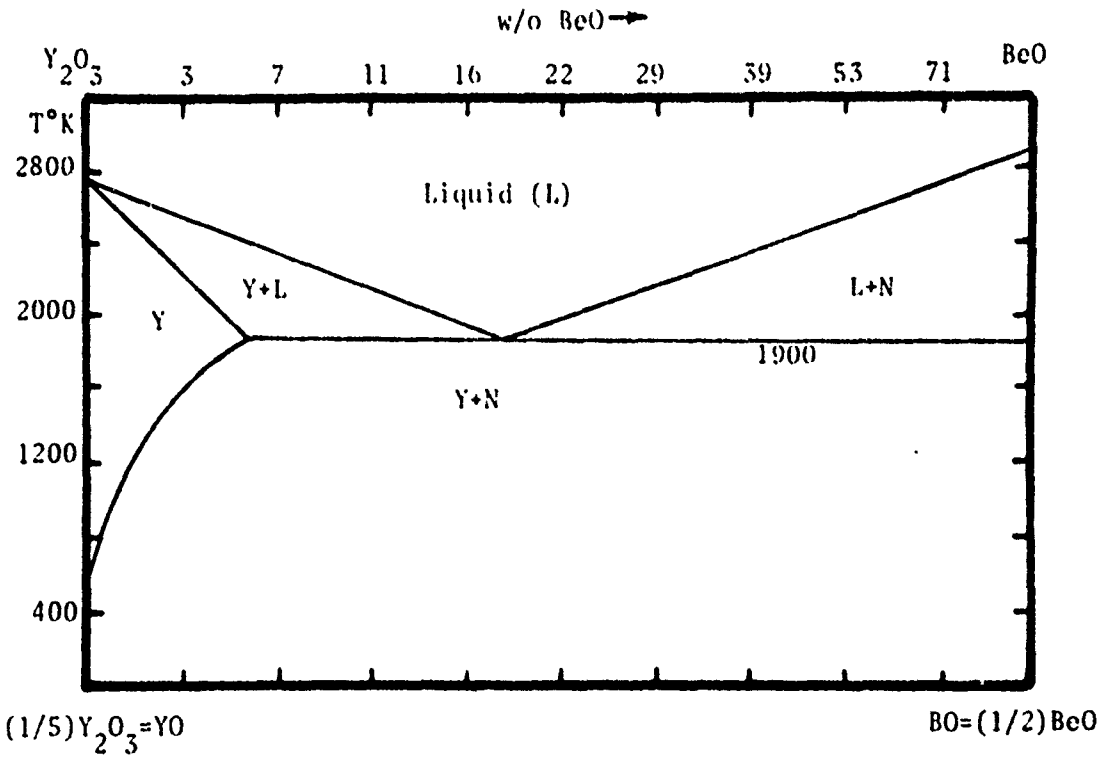

Figure 2. Calculated $(1/5)Y_2O_3$-(1/2)BeO Phase Diagram.

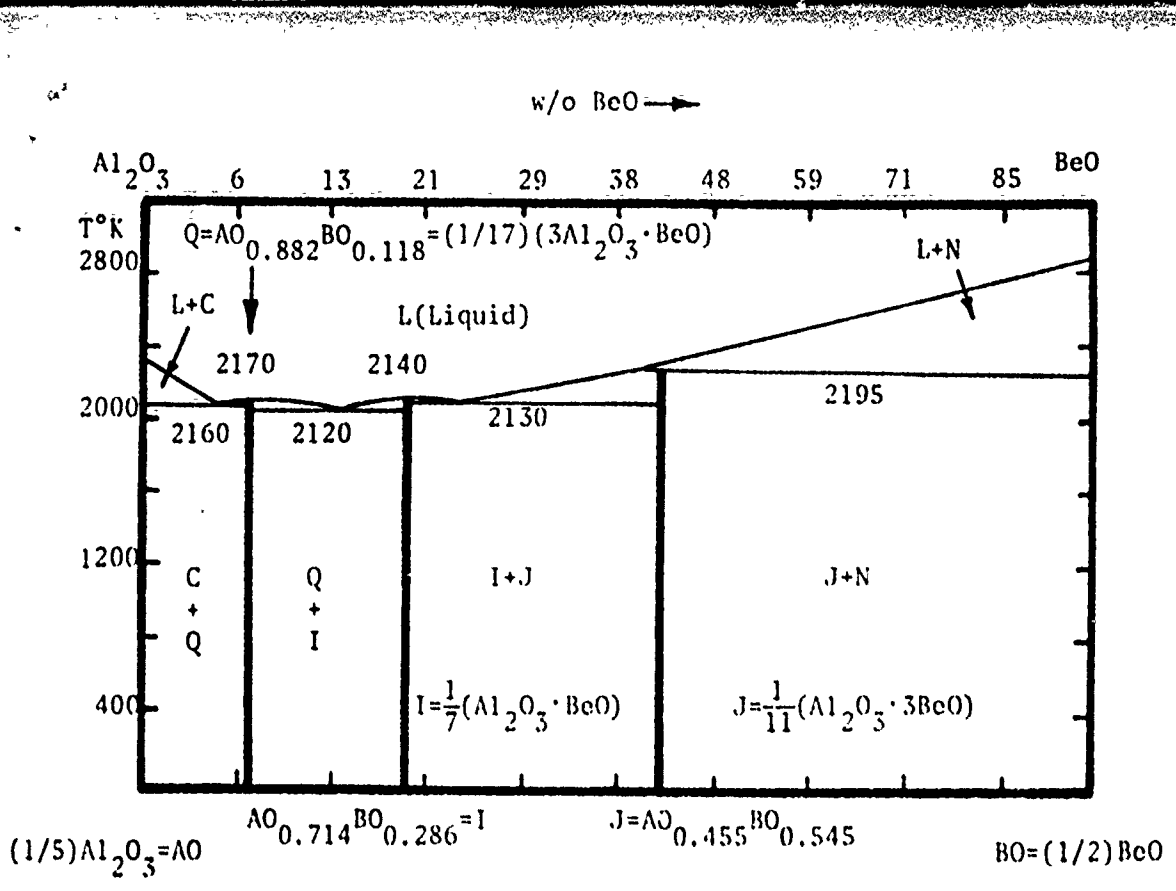

Figure 3. Calculated $(1/5)Al_2O_3$-(1/2)BeO Phase Diagram.

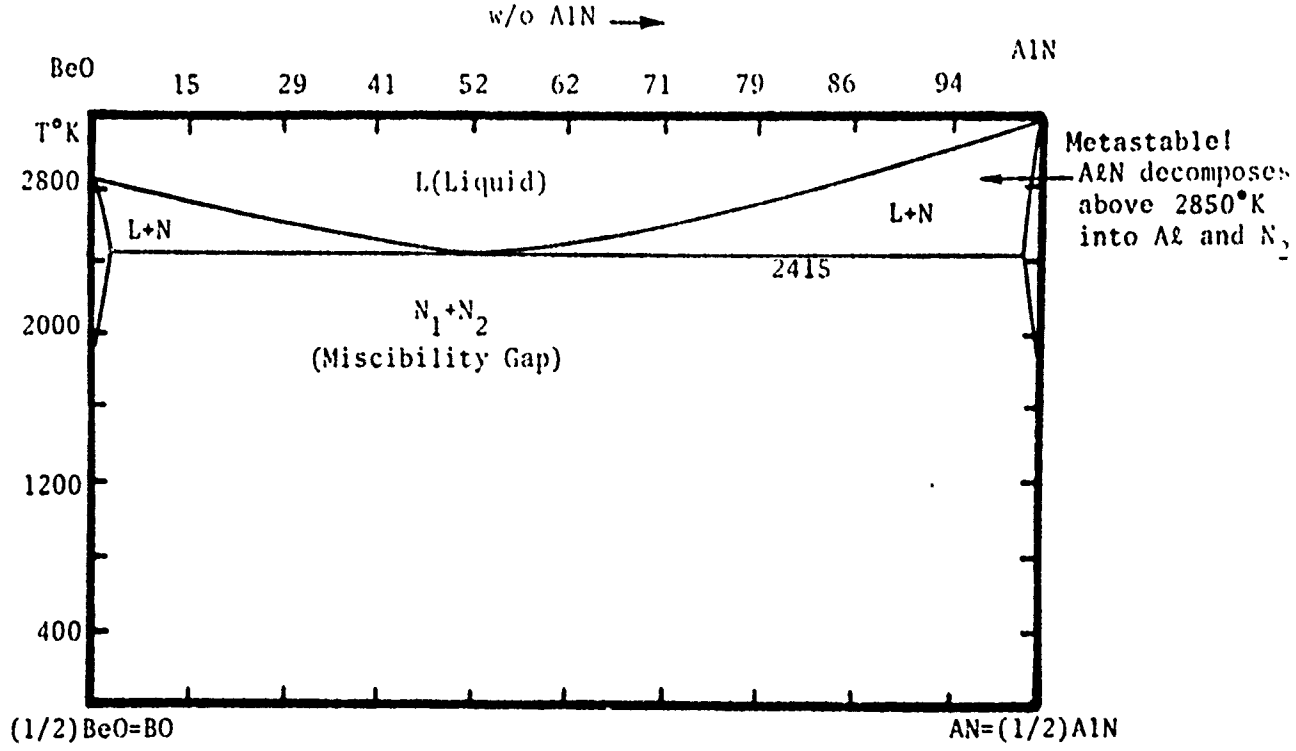

Figure 4. Calculated (1/2)BeO-(1/2)AlN Phase Diagram.

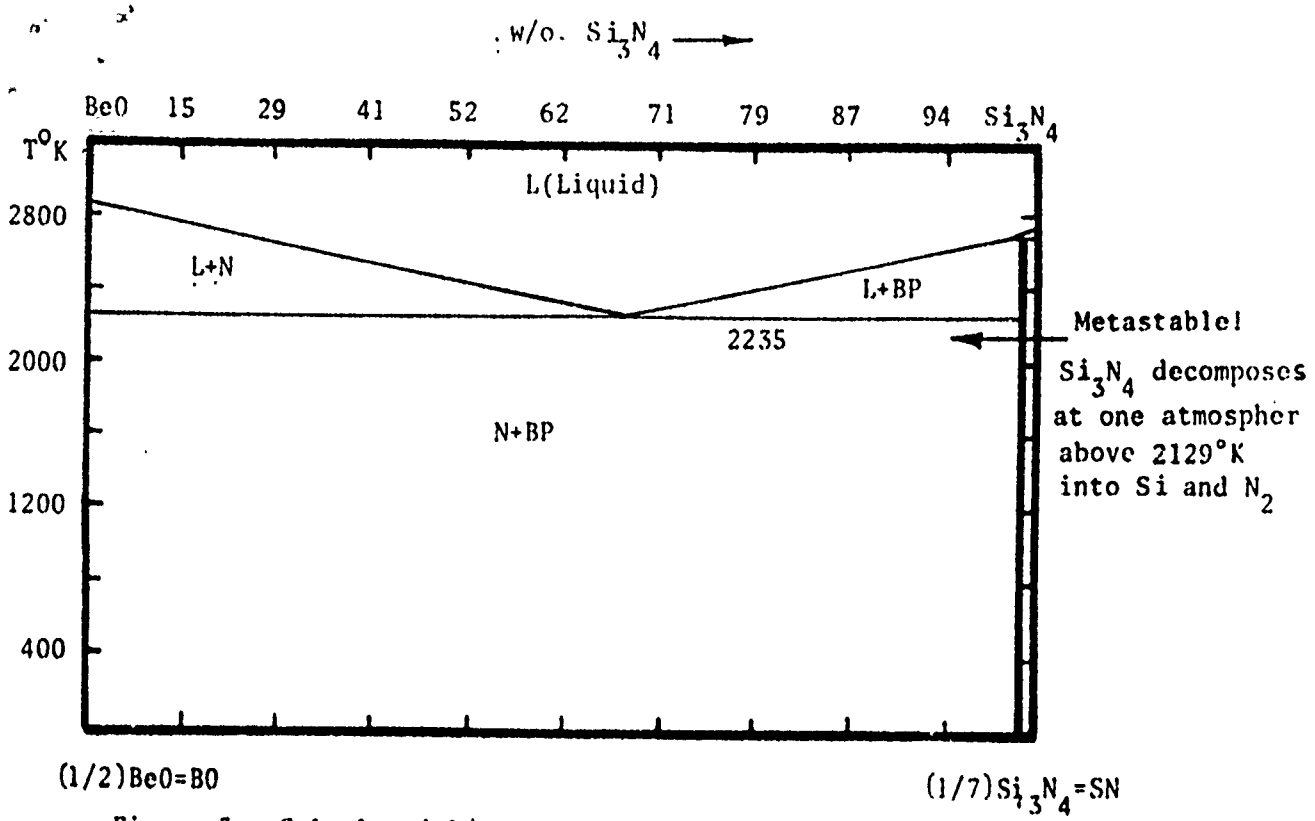

Figure 5. Calculated 1/2BeO - 1/7 Si_3N_4 Phase Diagram

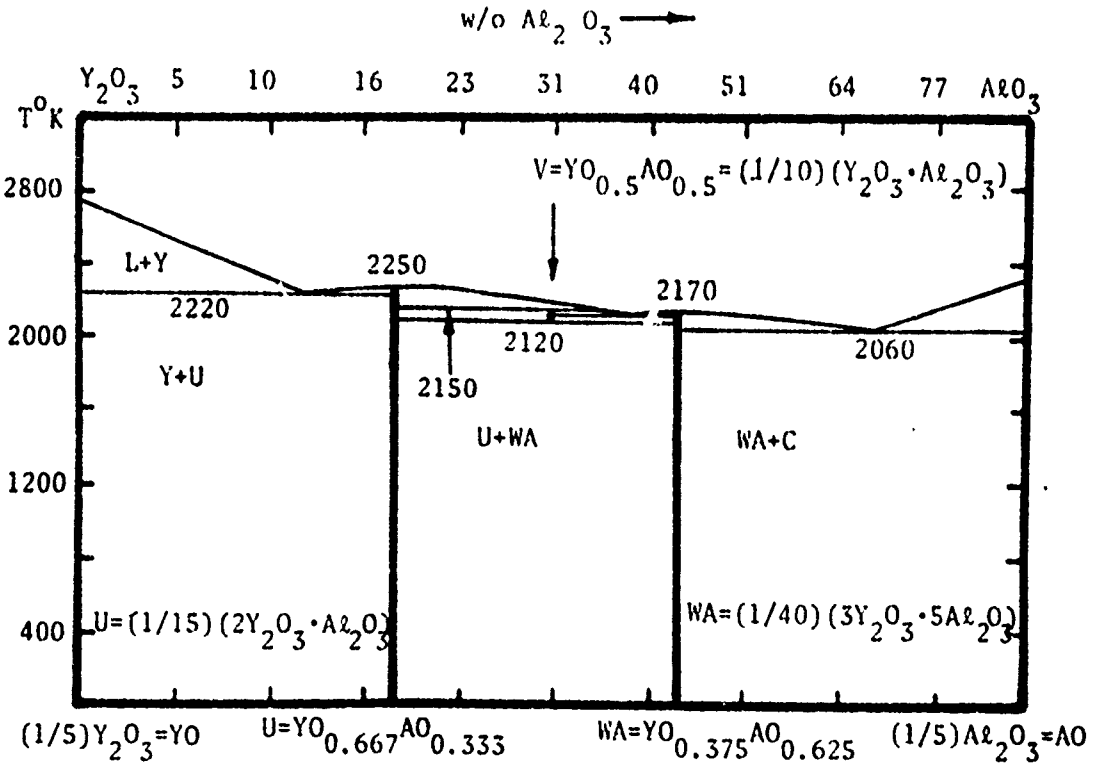

Figure 6. Calculated 1/5Y_2O_3 - 1/5Al_2O_3 Phase Diagram

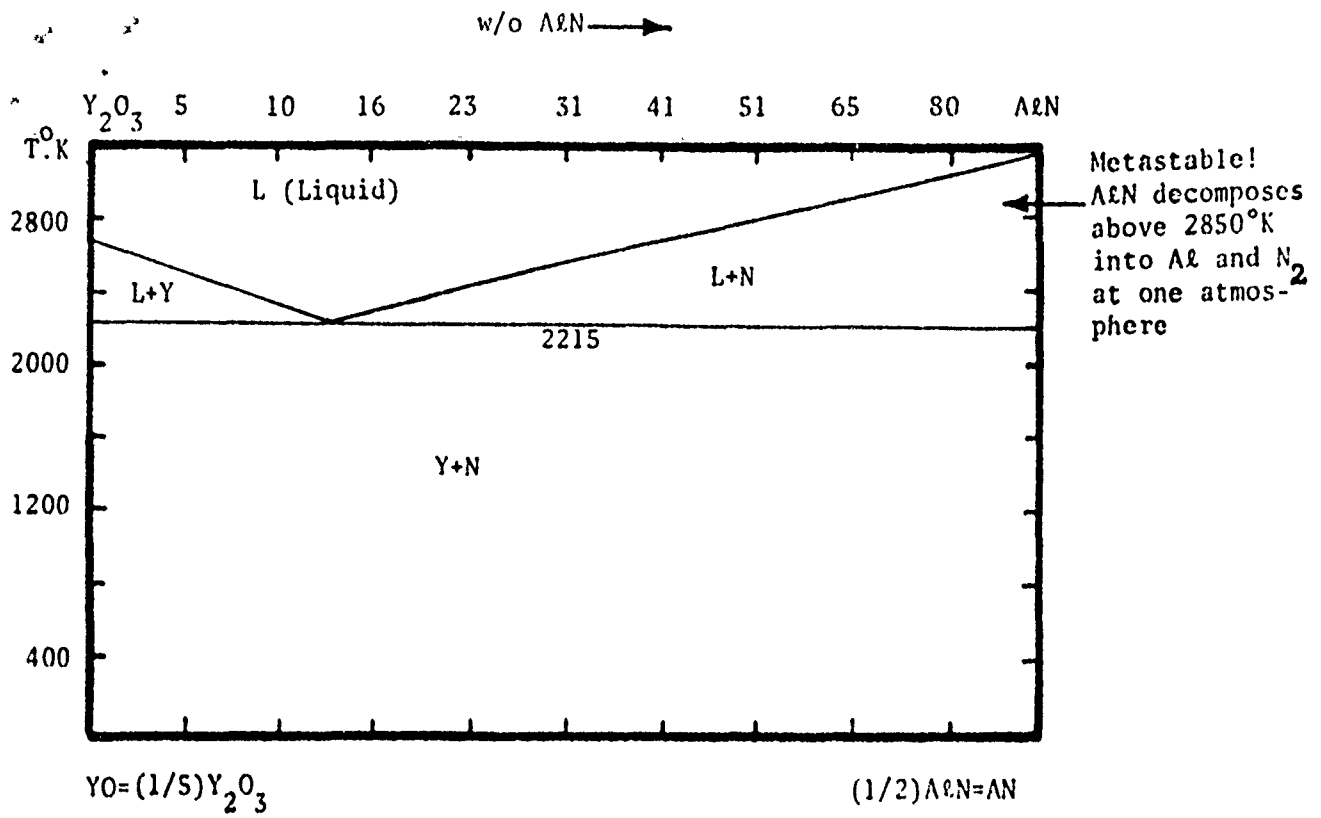

Figure 7. Calculated 1/5Y_2O_3 - 1/2AlN Phase Diagram

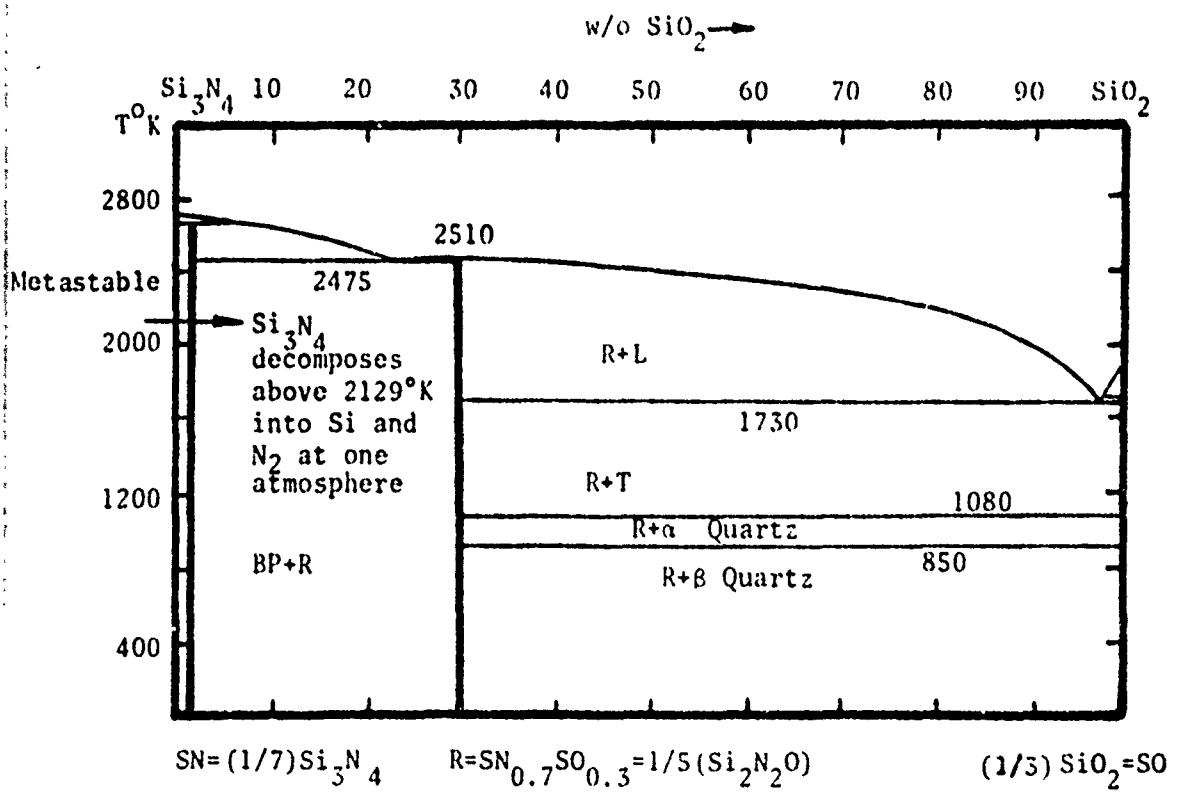

Figure 8. Calculated 1/7Si_3N_4 - 1/3SiO_2 Phase Diagram

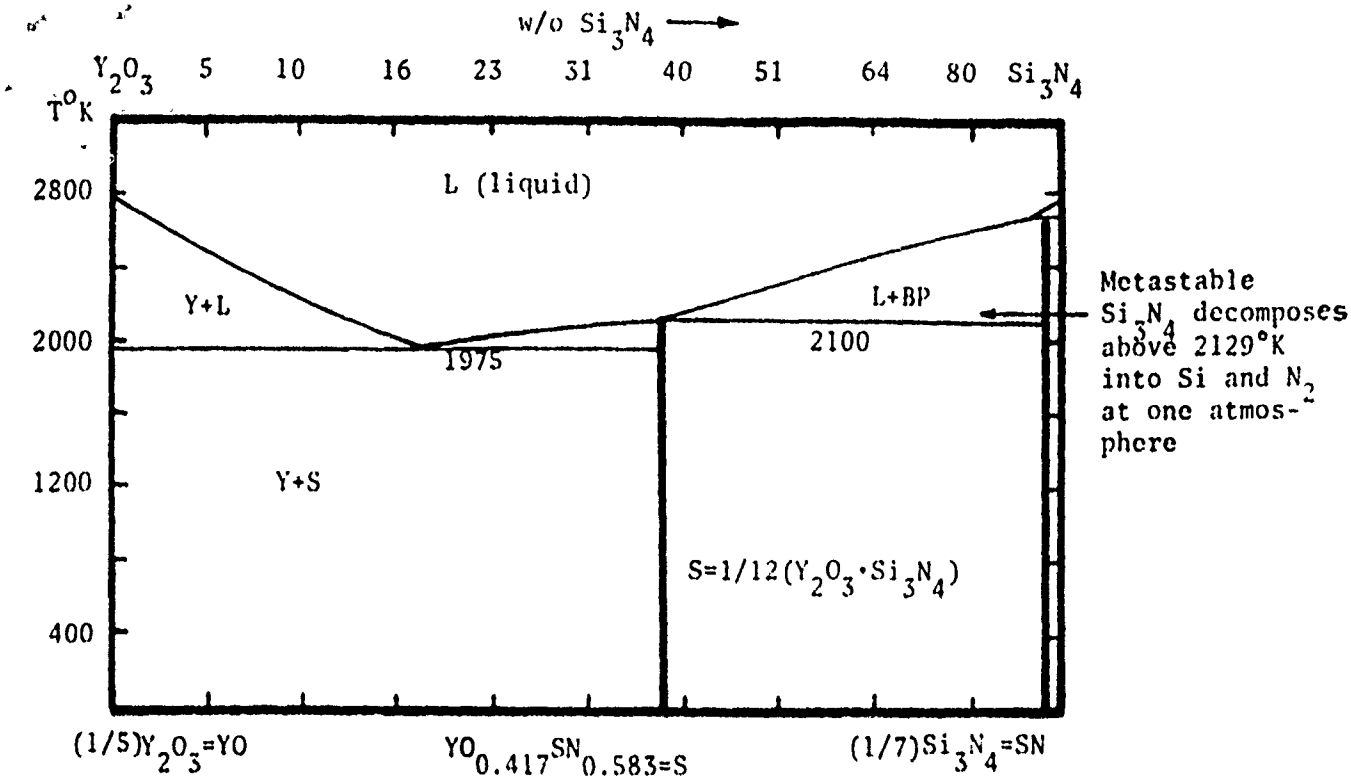

Figure 9. Calculated $1/5Y_2O_3$ - $1/7Si_3N_4$ Phase Diagram

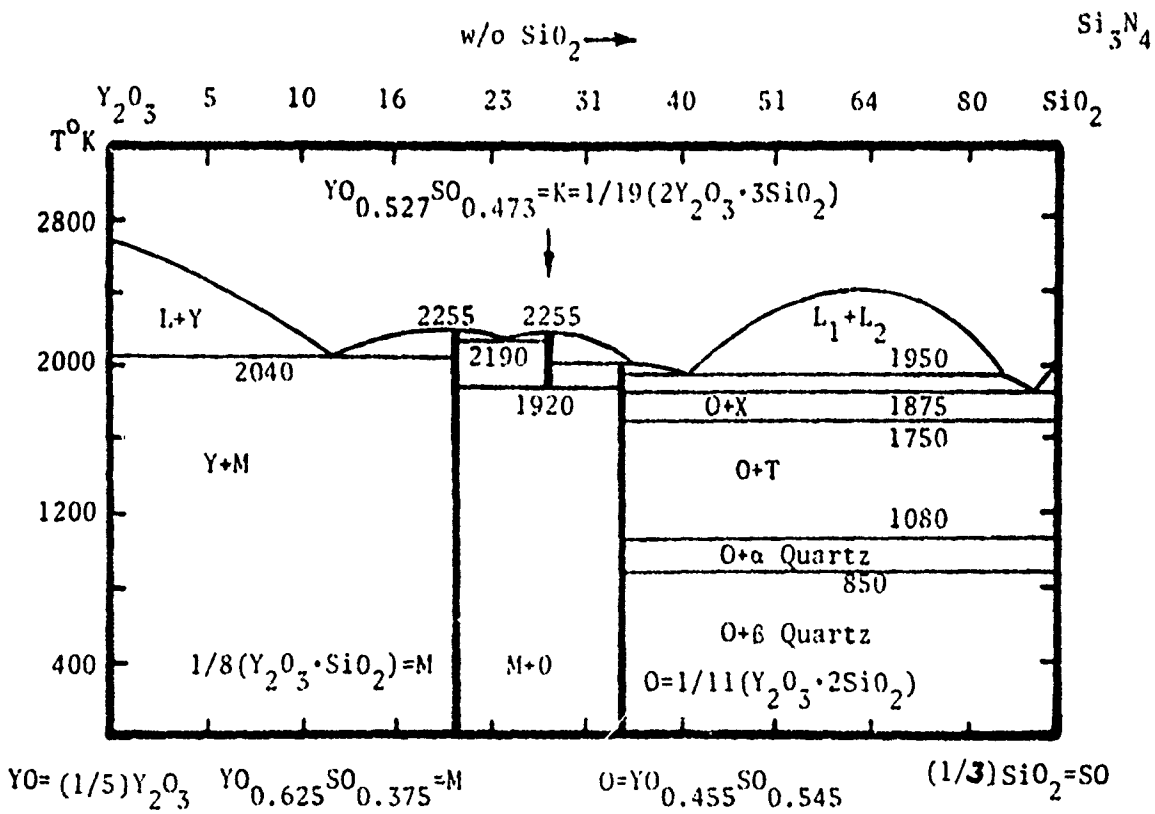

Figure 10. Calculated $1/5Y_2O_3$ - $1/3SiO_2$ Phase Diagram

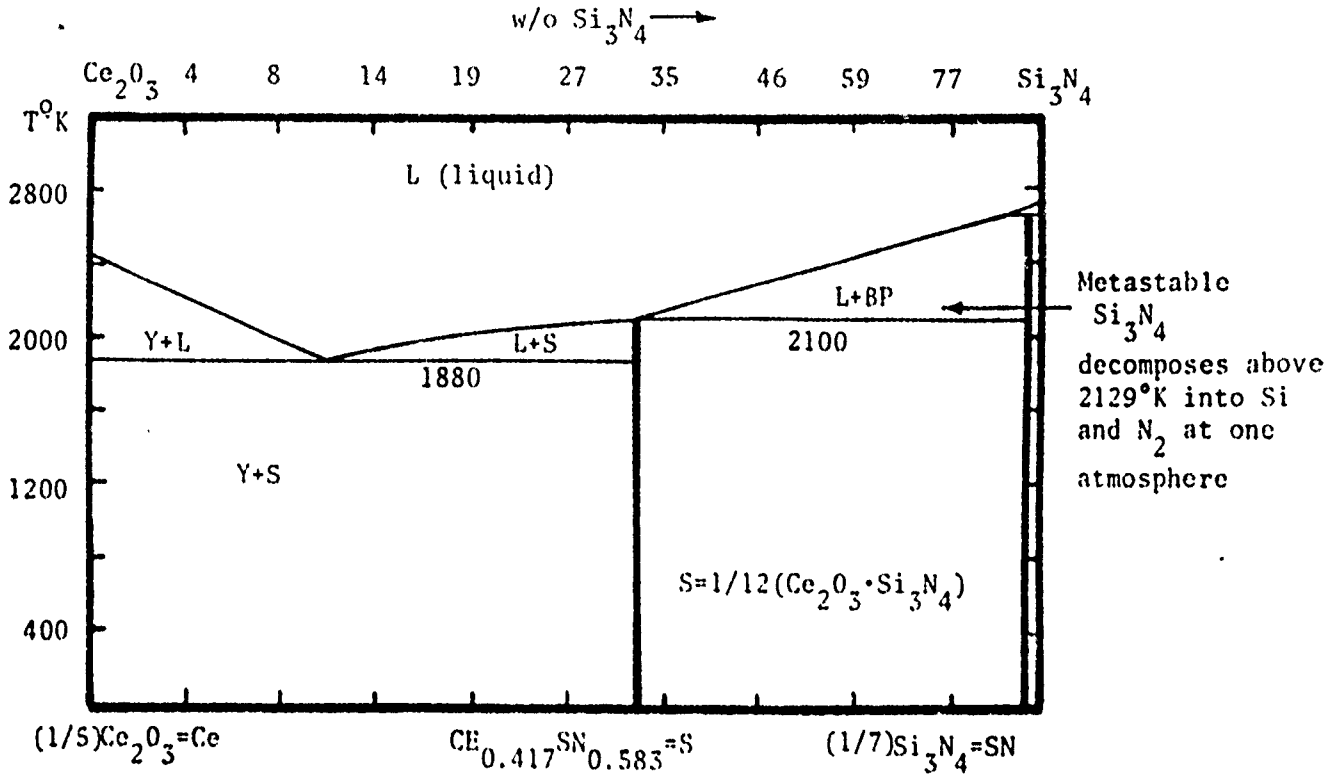

Figure 11. Calculated 1/5 Ce_2O_3 - 1/7Si_3N_4 Phase Diagram

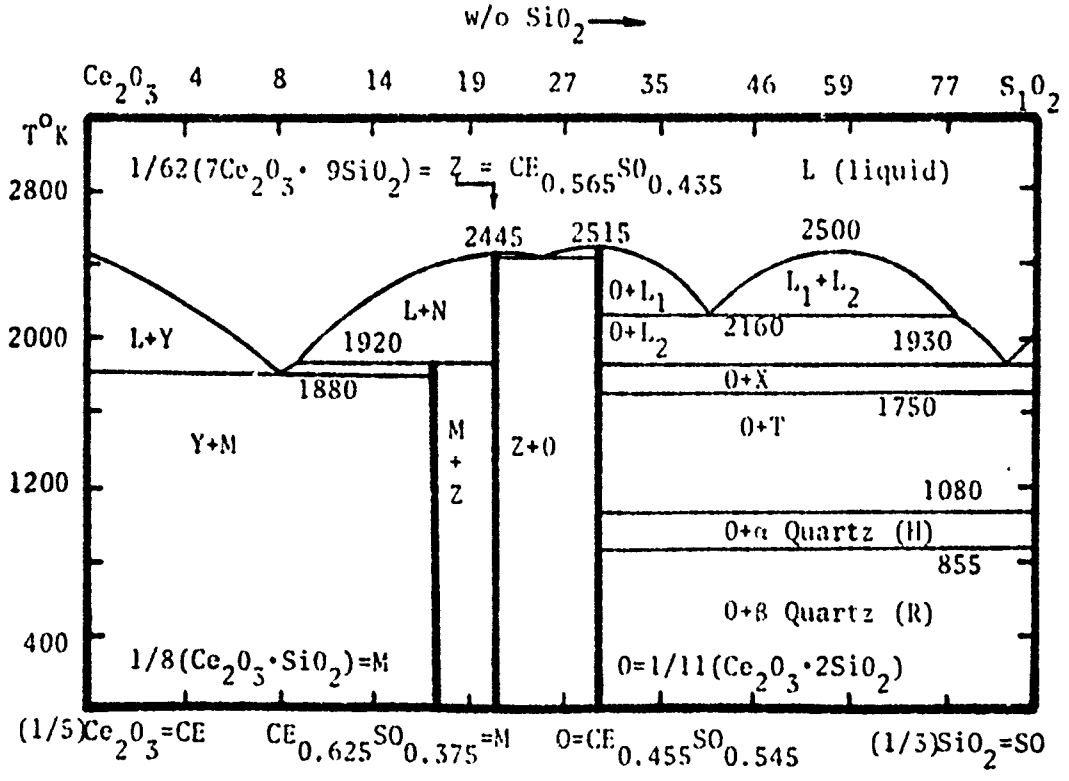

Figure 12. Calculated 1/5Ce_2O_3 - 1/3SiO_2 Phase Diagram

TABLE 4

CALCULATED FREE ENERGY OF FORMATION OF COMPOUND PHASES
(All Units in Joules per gram atom (mole of atoms), T in Kelvins)

Compound	Name	Stoichiometry	Free Energy of Formation, ΔG_f[298K] from Component Compounds
(1/7)($SiO_2 \cdot 2BeO$)	G	$SO_{0.429}BO_{0.571}$	-2808 + 1.382T/-2809+0.777T(8)
(1/17)($3Al_2O_3 \cdot BeO$)	Q	$AO_{0.882}BO_{0.118}$	-2203 - 0.464T
(1/7)($Al_2O_3 \cdot BeO$)	I	$AO_{0.714}BO_{0.286}$	-2381 - 1.125T
(1/11)($Al_2O_3 \cdot 3BeO$)	J	$AO_{0.455}BO_{0.545}$	-2524 - 1.049T
(1/15)($2Y_2O_3 \cdot Al_2O_3$)	U	$YO_{0.667}AO_{0.333}$	-4950 - 0.615T
(1/10)($Y_2O_3 \cdot Al_2O_3$)	V	$YO_{0.500}AO_{0.500}$	-2351 - 4.100T
(1/40)($3Y_2O_3 \cdot 5Al_2O_3$)	WA	$YO_{0.375}AO_{0.625}$	-7866 + 0.690T
(1/5)(Si_2N_2O)	R	$SN_{0.700}SO_{0.300}$	-5514 - 0.038T/-5781 + 0.40T(5)
(1/12)($Y_2O_3 \cdot Si_3N_4$)	S	$YO_{0.417}SN_{0.583}$	-404 - 1.833T
(1/8)($Y_2O_3 \cdot SiO_2$)	M	$YO_{0.625}SO_{0.375}$	-15958 + 1.389T
(1/19)($2Y_2O_3 \cdot 3SiO_2$)	K	$YO_{0.527}SO_{0.473}$	-13000 - 0.475T
(1/11)($Y_2O_3 \cdot 2SiO_2$)	O	$YO_{0.455}SO_{0.545}$	-19527 - 2.669T
(1/12)($Ce_2O_3 \cdot Si_3N_4$)	S	$CE_{0.417}SN_{0.583}$	-1389 - 1.828T
(1/8)($Ce_2O_3 \cdot SiO_2$)	M	$CE_{0.625}SO_{0.375}$	-19787 + 2.615T
(1/62)($7Ce_2O_3 \cdot 9SiO_2$)	Z	$CE_{0.565}SO_{0.435}$	-21974 + 2.606T
(1/11)($Ce_2O_3 \cdot 2SiO_2$)	O	$CE_{0.455}SO_{0.545}$	-21945 + 2.326T
0.01($14Si_3N_4 \cdot BeO$)	BP	$SN_{0.980}BO_{0.020}$	-423 - 0.113T
(1/150)($21Si_3N_4 \cdot SiO_2$)	BP	$SN_{0.980}SO_{0.020}$	-720 - 0.102T
0.004($35Si_3N_4 \cdot Y_2O_3$)	BP	$SN_{0.980}YO_{0.020}$	-1104
0.004($35Si_3N_4 \cdot Ce_2O_3$	BP	$SN_{0.980}CE_{0.020}$	-1158

The calculation of the isothermal section at 2'00K can be concluded by adding the L-BP equilibria as shown in Figure 14d. In this case, as in the R-L case, there are interactions with phase pairs which have been previously considered. First there is an interaction between L-BP and the liquid gap, L_1-L_2, as illustrated in Figure 14d, then there is a second interaction between the L-BP and L-P pairs. Comparison of Figures 14b and 14c with 14d shows that while the L-R/L-BP and the L-BP/L-P interaction pairs form stable three phase fields, the L-BP/L_1-L_2 interaction pair which is shown in Figure 14d is metastable. This can be seen by comparing 14c and 14d and noting that the three phase BP+L_1+L_2 field is "covered" by the R+L_1+L_2 and R+L fields. Detailed calculation of the L-BP equilibria can be performed by defining the free energy of the BP phase on the bases of Tables 1-4.

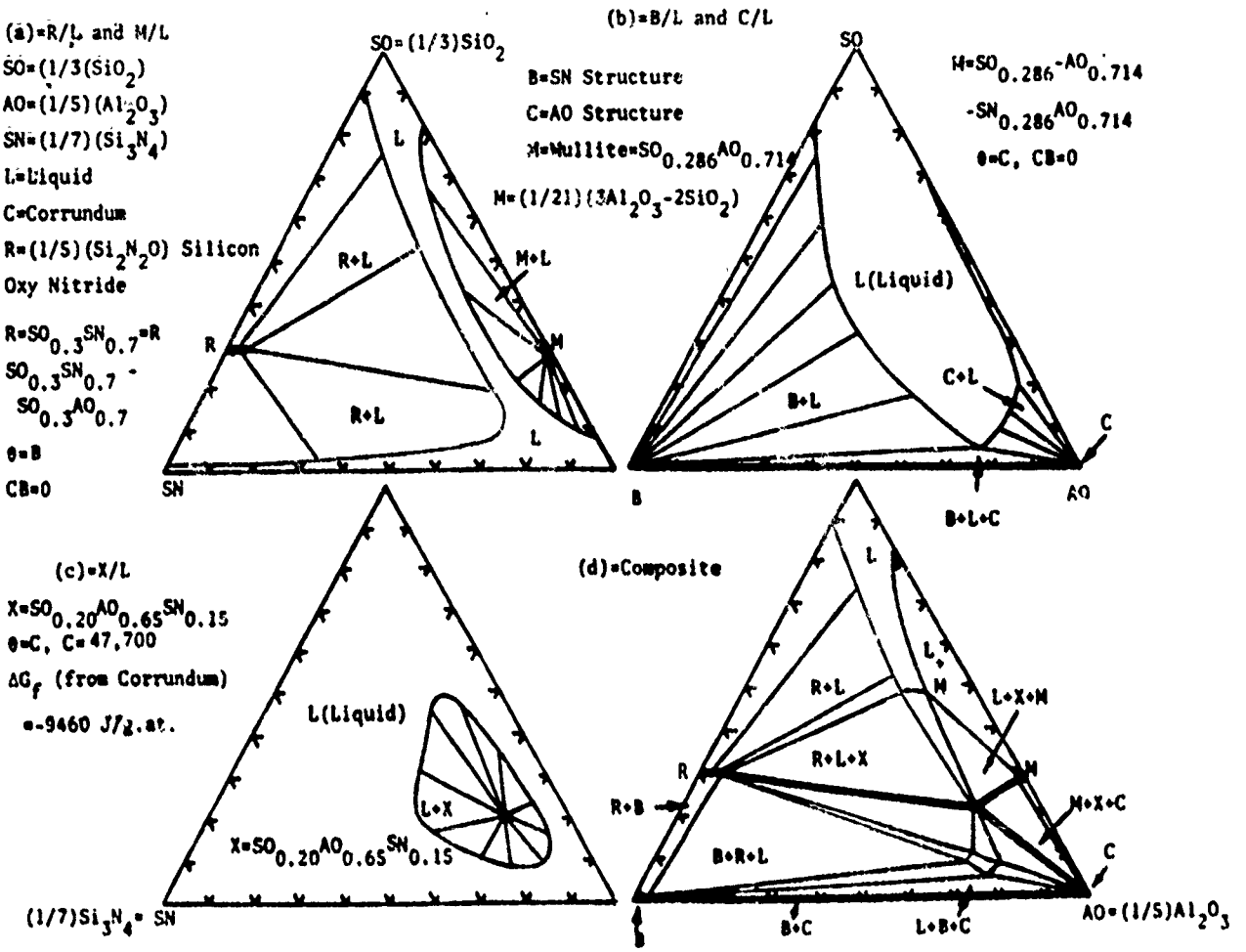

Figure 13 Calculated Pairwise (a-c) and Composite Equilibrium (d) in the $(1/3)(SiO_2)$ - $(1/7)(Si_3N_4)$-$(1/5)Al_2O_3$ System at 2000K and one atmosphere

For the case of the SO-MO-SN (BP) phase, where the compound runs from $SN_{0.980}SO_{0.020}$ to $SO_{0.50}M_{0.50}$ and from $SN_{0.98}MO_{0.20}$ to $MO_{0.50}SO_{0.50}$ similar procedures are followed. For the former case

$$G^{BP} = z\,{}^{\circ}G^{B}_{SN}+x\,{}^{\circ}G^{B}_{SO}+y\,{}^{\circ}G^{B}_{MO}+(1-(y/(1-x)))\Delta G_A+(y/(1-x))\Delta G_B+\Delta G_E$$
$$+RT(y\ell ny+z\ell nz-(1-x)\ell n(1-x)) \qquad (11)$$

here $x_*=0.50$ and $x'_*=0.02$ so that $p=0.96$, $x=x'_*+yp=0.02+0.96y=x_{SO}$, $y=y_{MO}$ and $z=1-x-y=0.98-1.96y=z_{SN}$. Moreover, $\Delta G_E=0$ and ΔG_A and ΔG_B can be explicitly defined as

$$\Delta G_A = (0.02)(0.98)(0.98\ LSNSO+0.02\ LSOSN-C)=-820-0.082T\ \ J/g.at. \qquad (12)$$

$$\Delta G_B = (0.50)(0.50)(0.50\ LSOMO+0.50\ LMOSO-C)=-26568+10.503T\ \ J/g.at. \qquad (13)$$

with $\Delta G_E=0$, and $y=y_{MO}$

$$G^{BP} = (0.98-1.96y)\,{}^{\circ}G^{B}_{SN}+(0.02+0.96y)\,{}^{\circ}G^{B}_{SO}+y\,{}^{\circ}G^{B}_{MO}-(1-(y/(1-x))\ (820+0.082T)$$
$$-(y/(1-x))(26568-10.503T)+RT(y\ell ny+(0.98-1.96y)\ell n(0.98-1.96y)-(0.98-0.96y)\ell n$$
$$(0.98-0.96y)) \qquad (14)$$

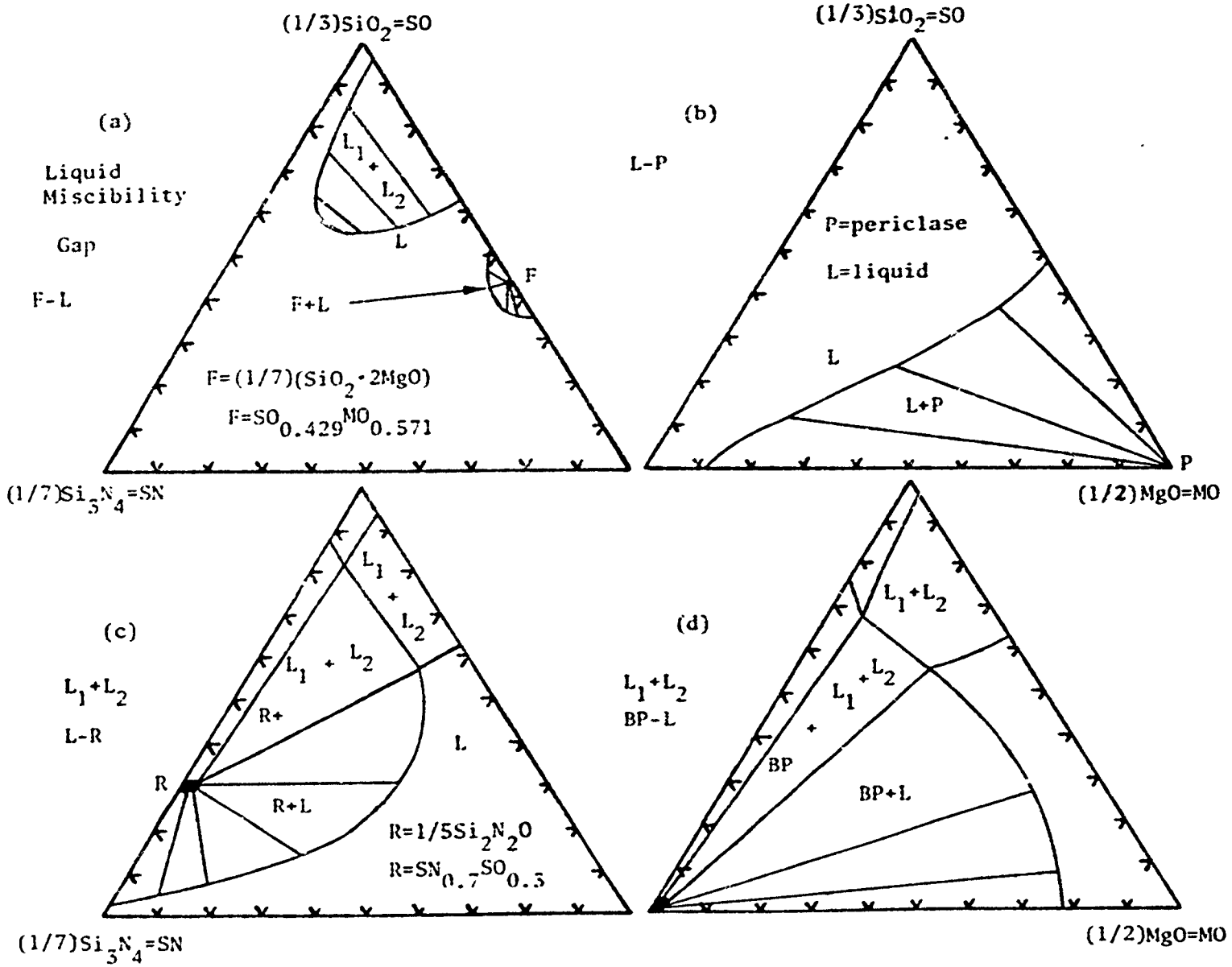

Figure 14. Calculated Pairwise Equilibria in the SiO_2- MgO -Si_3N_4 System at 2100°K

TABLE 5

SUMMARY OF COUNTERPHASE STOICHIOMETRY AND PARAMETERS EMPLOYED IN TERNARY CALCULATIONS

System	Stable Phase (Name)	Base	Counterphase	Base	Counterphase Parameter
SO-MO-SN	$SO_{0.429}MO_{0.571}$(F)	P	$SN_{0.429}MO_{0.571}$	P	0
	$SO_{0.300}SN_{0.700}$(R)	B	$SO_{0.300}MO_{0.700}$	B	0
	$SN_{0.980}SO_{0.020}$(BP)	B	$SO_{0.500}MO_{0.500}$	B	0
	$SN_{0.980}MO_{0.020}$(BP)	B	$MO_{0.500}SO_{0.500}$	B	0
SO-YO-SN	$YO_{0.625}SO_{0.375}$(M)	Y	$YO_{0.625}SN_{0.375}$	Y	0
	$YO_{0.527}SO_{0.473}$(K)	Y	$YO_{0.527}SN_{0.473}$	Y	0
	$YO_{0.455}SO_{0.545}$(O)	Y	$YO_{0.455}SN_{0.545}$	Y	0
	$SO_{0.300}SN_{0.700}$(R)	B	$SO_{0.300}YO_{0.700}$	B	0
	$SN_{0.980}SO_{0.020}$(BP)	B	$SO_{0.500}YO_{0.500}$	B	0
	$SN_{0.980}YO_{0.020}$(BP)	B	$YO_{0.500}SO_{0.500}$	B	0
SO-CE-SN	$CE_{0.625}SO_{0.375}$(M)	Y	$CE_{0.625}SN_{0.375}$	Y	0
	$CE_{0.565}SO_{0.435}$(Z)	Y	$CE_{0.565}SN_{0.435}$	Y	0
	$CE_{0.455}SO_{0.545}$(O)	Y	$CE_{0.455}SN_{0.545}$	Y	0
	$SO_{0.300}SN_{0.700}$(R)	B	$SO_{0.300}CE_{0.700}$	B	0
	$SN_{0.980}SO_{0.020}$(BP)	B	$SO_{0.500}CE_{0.500}$	B	0
	$SN_{0.980}CE_{0.020}$(BP)	B	$CE_{0.500}SO_{0.500}$	B	0

Thus the equilibrium between the liquid and BP phase can be computed as in Figure 14(d). Combination of the pairwise equilibrium in Figure 11 yields the computed isothermal section at 2100K shown in Figure 15. Isothermal sections similarly derived at 2000K and 1900 are shown in Figure 15 along with an observed section due to Mueller (9) at 1500K. The latter is in keeping with the calculations shown at 1900K. (See "Note in Proof")

Similar calculations were performed in the SO-YO-SN and SO-CE-SN systems. The results, which are complicated by the existence of stable quasi-ternary compounds (listed in Table 6) are displayed in Figures 16-19. The SO-YO-SN and SO-CE-SN sections were computed in a manner similar to the SO-MO-SN case in that the systems were first computed as if the ternary phases were absent. Subsequently the ternary phases, designated as C,D and E were inserted. In keeping with previous practice (1-3) the free energy of the ternary phases C, D and E were defined by choosing a base phase and then defining a compound parameter in conformity with experimental observation. In the present case the Y structure was chosen as the base phase since the ternary phase composition occurs near the YO and CE corners of the SO-YO-SN and SO-CE-YO systems as is seen in Figures 17 and 18.

The free energy of the ternary compound D in the SO-YO-SN system $D=(1/15)Y_4Si_2O_7N_2=$ $SO_{0.100}YO_{0.667}SN_{0.223}$ is defined as

TABLE 6

DESCRIPTION OF QUASI-TERNARY COMPOUNDS IN THE SiO_2-Y_2O_3-Si_3N_4 AND SiO_2-Ce_2O_3-Si_3N_4 SYSTEMS

Compound	Base	Stoichiometry	Compound Parameter (C) (Joules/g.at.)	Melting Point (°K)	Free Energy of Formation from Component Compounds (ΔG_f[298K]) (Joules/g.at.)
C= (1/5)$YSiO_2N$	Y	$SO_{0.150}YO_{0.500}SN_{0.350}$	29096+8.368T	1953	-4393-2.410T
D=(1/15)$Y_4Si_2O_7N_2$	Y	$SO_{0.100}YO_{0.667}SN_{0.233}$	13004+16.736T	2110	-678-4.127T
E=(1/21)$Y_5(SiO_4)_3N$	Y	$SO_{0.322}YO_{0.595}SN_{0.083}$	-2155+20.92T	1996	-11456-0.883T
C=(1/5)$CeSiO_2N$	Y	$SO_{0.150}CE_{0.500}SN_{0.350}$	31505+8.368T	1914	-5422-2.410T
D=(1/15)$Ce_4Si_2O_7N_2$	Y	$SO_{0.100}CE_{0.667}SN_{0.233}$	14769+16.736T	2020	-1259-4.127T
E=(1/21)$Ce_5(SiO_4)_3N$	Y	$SO_{0.322}CE_{0.595}SN_{0.083}$	3975+20.92T	2109*	-13585-0.883T

*$SO_{0.322}CE_{0.595}SN_{0.083}$ decomposes peritectically into Z and Liquid above 2100K

$$G^D=0.10°G^Y_{SO}+0.667°G^Y_{YO}+0.233°G^Y_{SN}+(0.10)(0.667)(0.767)^{-1}[0.1LSOYO+0.667LYOSO-C]$$
$$+(0.10)(0.233)(0.333)^{-1}[0.1LSOSN+0.233LSNSO-C]+(0.667)(0.233)(0.90)^{-1}[0.667LYOSN+0.223LSNYO-C] \quad J/g.at. \qquad (15)$$

since C=13004+16.736T for this phase

$$G^D=0.10°G^Y_{SO}+0.667°G^Y_{YO}+0.233°G^Y_{SN}-9094-3.062T \quad J/g.at. \qquad (16)$$

Thus the free energy of formation of D from the Y form of SO, YO and SN is -9094-3.062T J/g.at.. The free energy of formation of D from the stable forms of SO, YO and SN (i.e. R, Y and B respectively) can be computed by using the lattice stability values given in Table 1. With SOSOYR=5042-1.004T and SNSNYB=33949-4.142T J/g.at.

$$G^D=0.10°G^R_{SO}+0.667°G^Y_{YO}+0.233°G^B_{SN}-678-4.127T \quad J/g.at. \qquad (17)$$

or

$$\Delta G_f[298K]=-678-4.127T \quad J/g.at. \qquad (18)$$

The free energy and free energy of formation of the remaining compounds listed in Table 6 can be computed in a similar fashion. On this basis the isothermal sections and pairwise equilibria shown in Figures 16-19 were developed. Figure 16 shows the computed sections at 2100 and 2000K in which phases present in the binary systems and the ternary compound D are present. Figures 16(a) and 16(b) and Figure 17(a) illustrate pairwise interactions at 1900K in SO-YO-SN. These pairwise interactions combine to yield the calculated isothermal section at 1900K which contains two small liquid regions. A computed section at 1823K given in Figure 17(c) shows how these regions have grown smaller with decreasing temperature. This section is in good agreement with the observed section (10) at 1823 shown in Figure 17(d) which illustrates the ternary compounds and the existence of a small liquid field as well.

The computation of isothermal sections in SO-CE-SN is displayed in a similar manner at 2100, 2000 and 1900K. At 2100K the calculated isothermal section given in Figure 18 contains only the phases stable in the edge binary systems. At 2000K the calculated section displays the ternary D ($Ce_4Si_2O_7N_2$) and E($Ce_5(SiO_4)_3N$) phases. Pairwise equilibria calculated

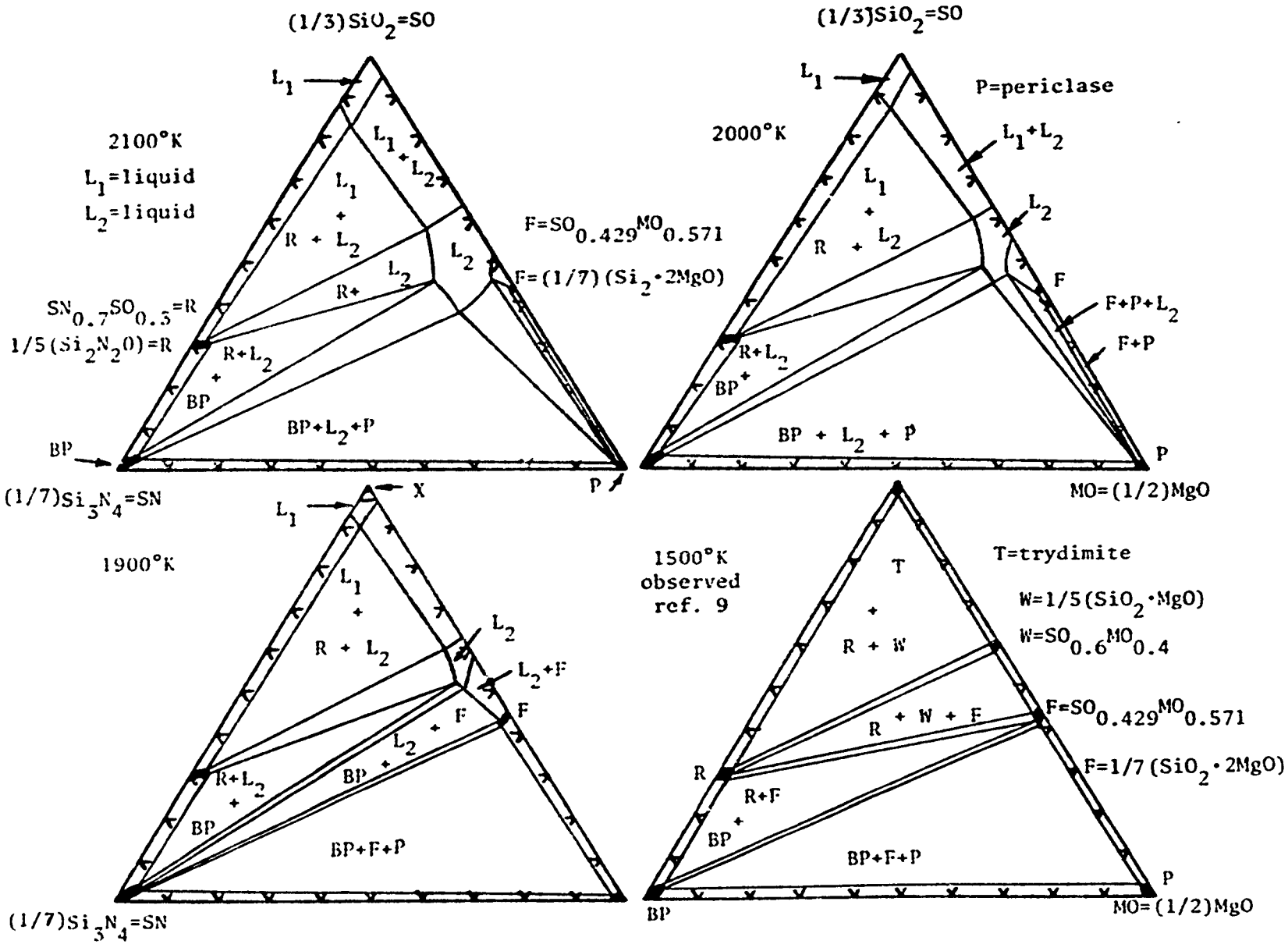

Figure 15. Calculated and Observed (9) Isothermal Sections in the SiO_2-MgO-Si_3N_4 System (See "Note in Proof")

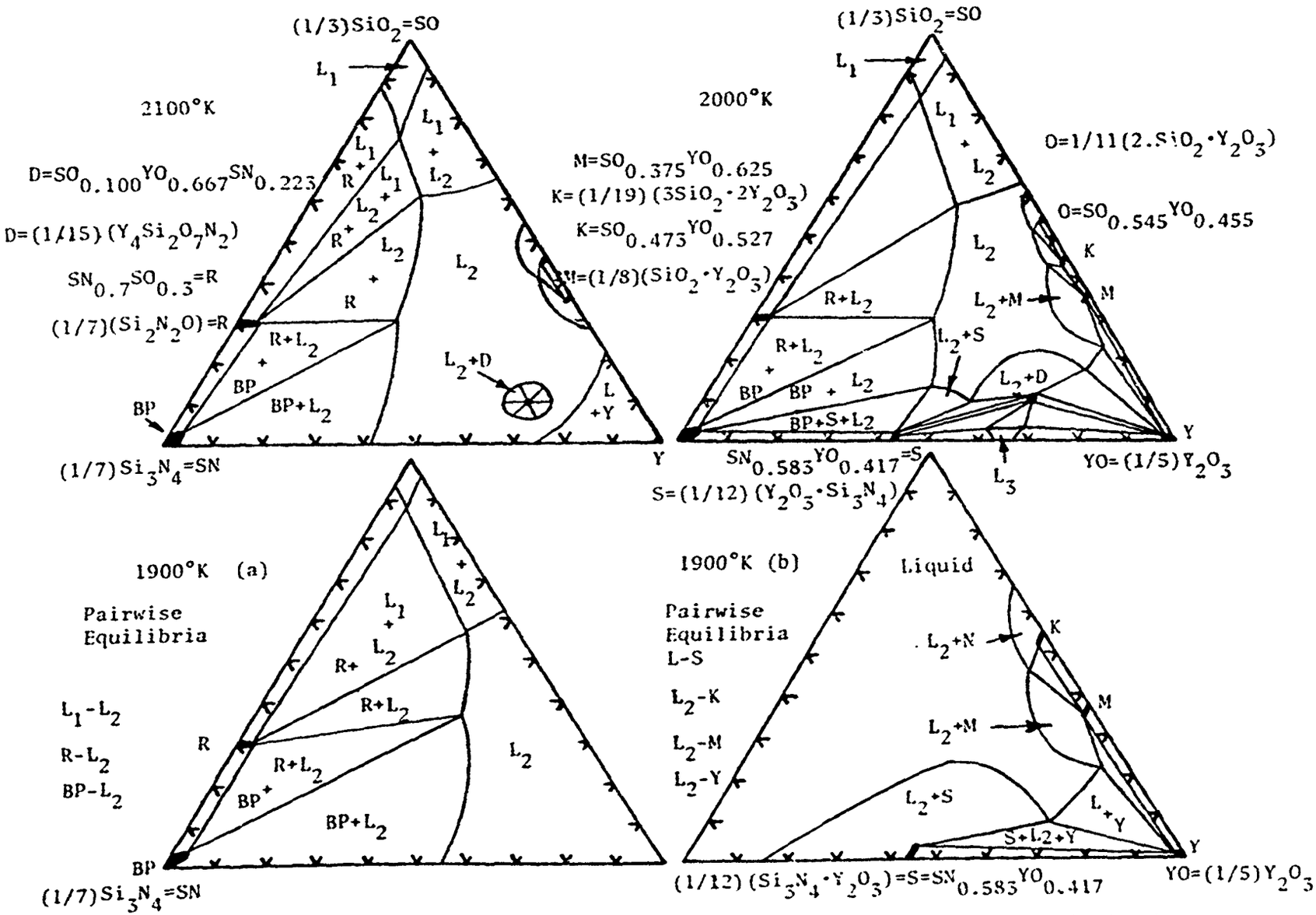

Figure 16. Calculated Isothermal Sections and Pairwise Component Equilibria in the SiO_2- Y_2O_3- Si_3N_4 System

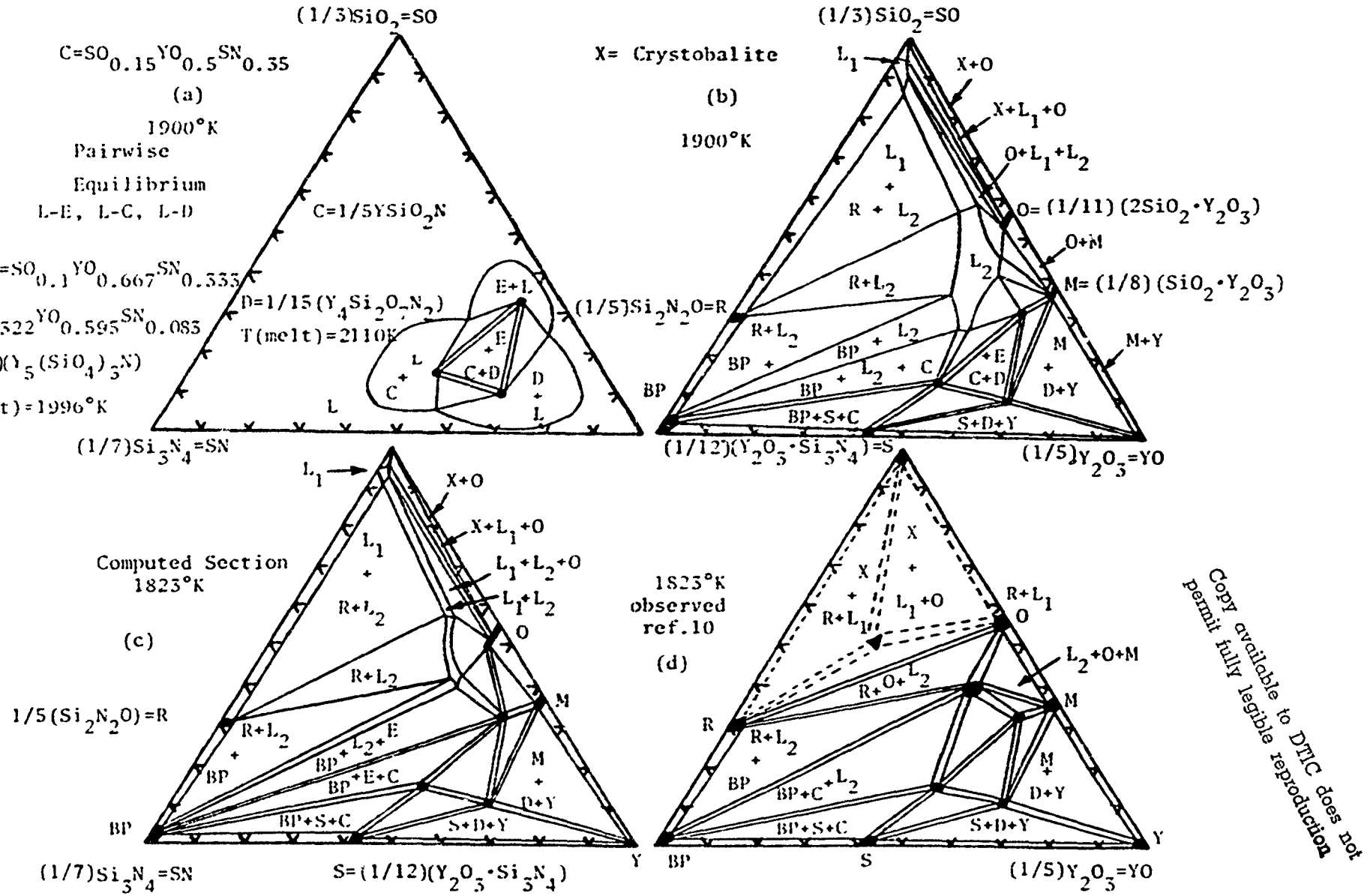

Figure 17. Calculated Pairwise Equilibria at 1900°K, Calculated Isothermal Sections at 1900°K and

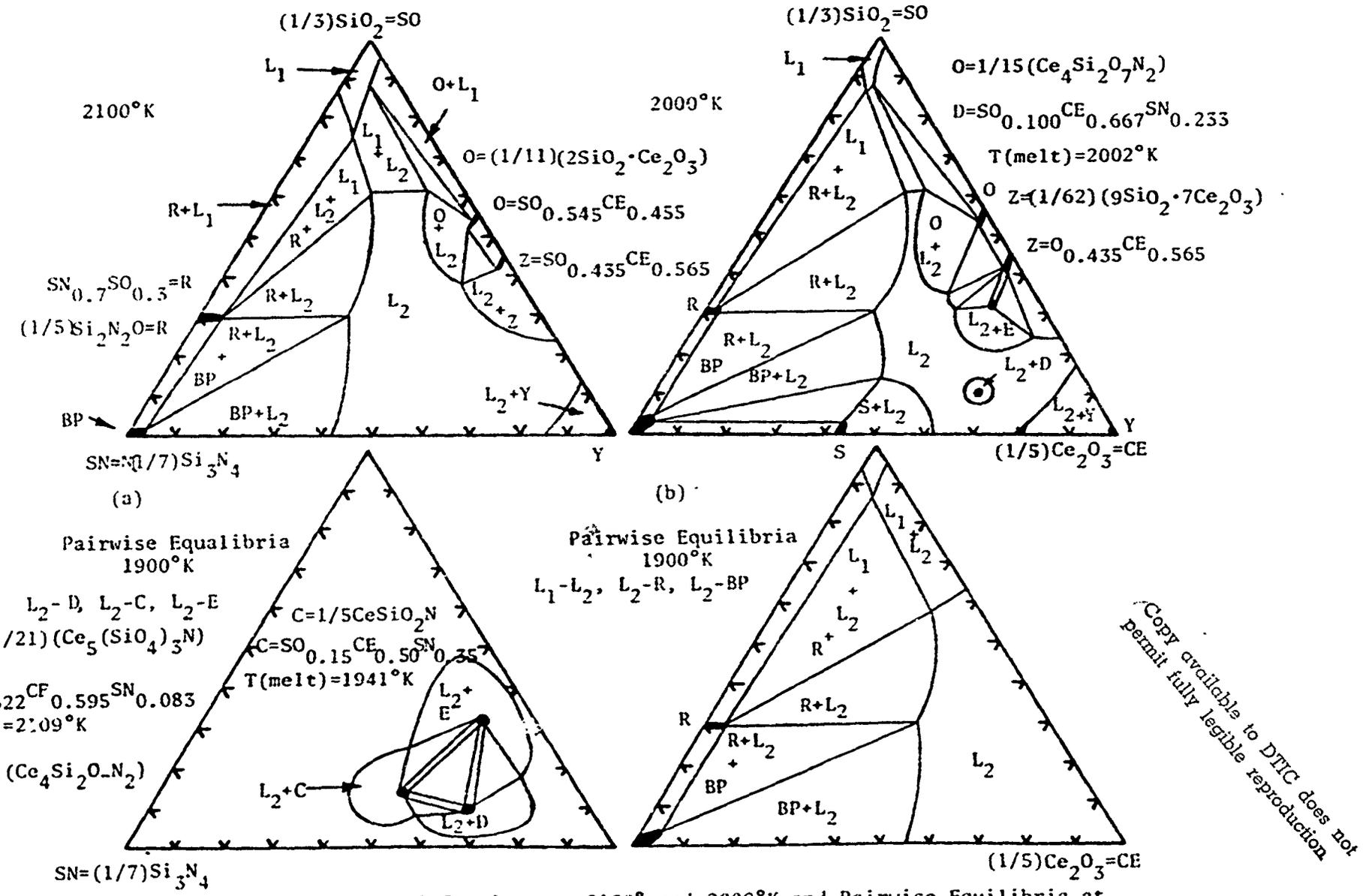

Figure 18. Calculated Isothermal Sections at 2100° and 2000°K and Pairwise Equilibria at 1900°K in the SiO_2-Ce_2O_3-Si_3N_4 System

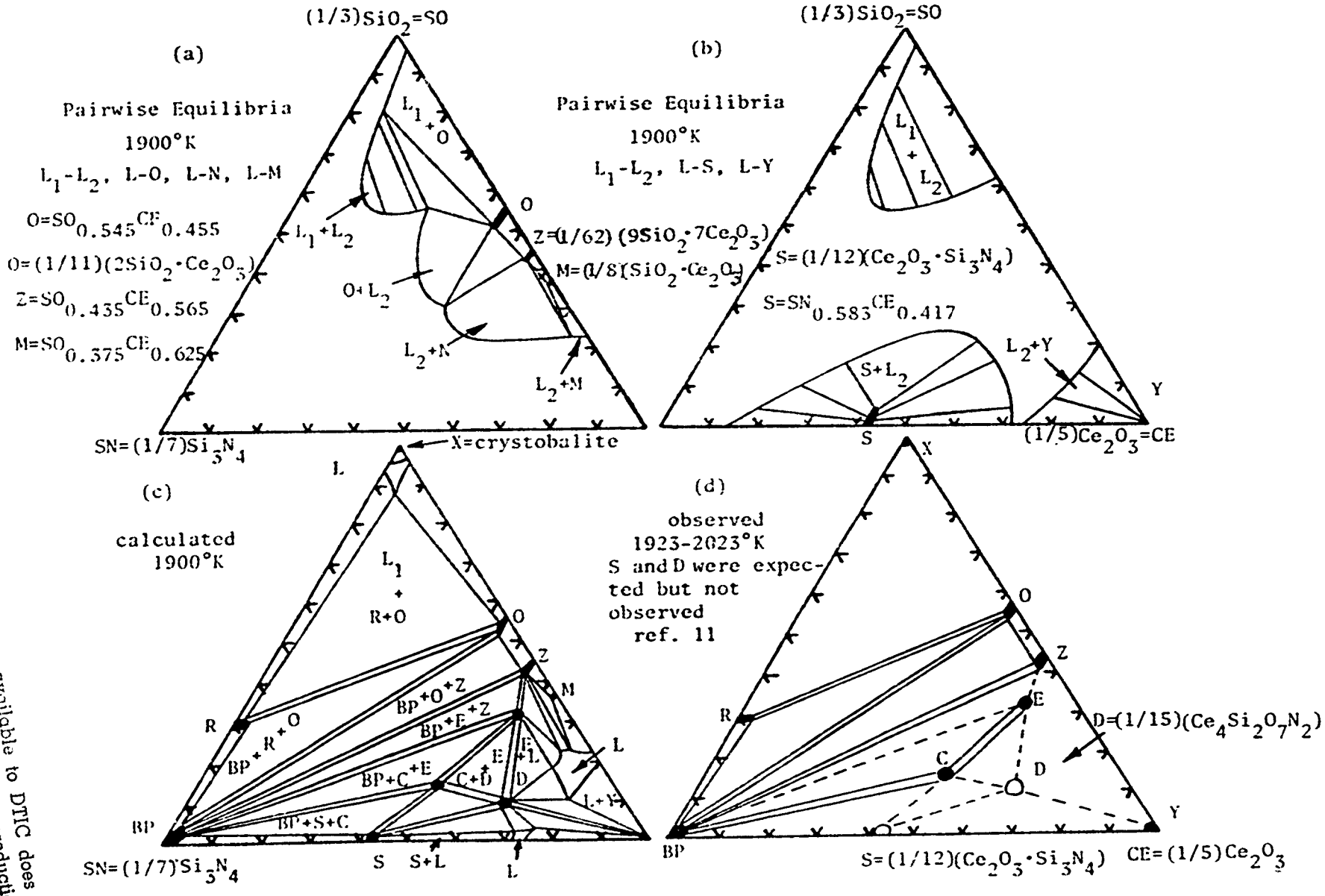

Figure 19. Calculated Pairwise Equilibria and Isothermal Sections at 1900°K and Observed (11) Subsolidus Equilibria at 1923-2023°K in the SiO_2-Ce_2O_3-Si_3N_4

at 1900K are shown in Figures 18(a), 18(b), 19(a) and 19(b). The latter combine to yield the calculated isothermal section at 1900K given in Figure 19(c). The latter is in relatively good agreement with the observed subsolidus equilibria (11) determined between 1923 and 2023K. The observed section does not show evidence of the S or D compound phases which was expected but not observed (11).

The SO-MO-SN, SO-YO-SN and SO-CE-SN sections calculated above serve to illustrate how the synthesis of multicomponent phase diagrams can be performed in support of experimental studies of practical problems which must often be performed with great difficulty and some measure of uncertainty.

References

1. L. Kaufman and H. Nesor, CALPHAD 2 35 (1978)
2. L. Kaufman, CALPHAD 3 27 (1979)
3. L. Kaufman, CALPHAD 3 279 (1979)
4. L.J. Gaukler, H.L. Lukas, E.Th. Henig and G. Petzow, CALPHAD 2 349 (1979).
5. P. Doerner, L.J. Gaukler, H. Krieg, H.L. Lukas, G. Petzow and J. Weiss, CALPHAD 3 239 (1979).
6. J. Weiss, H.L. Lukas, J. Lorenz, G. Petzow ans H. Krieg, CALPHAD 5 123 (1981).
7. E.M. Levin, C.R. Robbins and H.F. McMurdie, Phase Diagrams for Ceramists, American Ceramics Society, Columbus, Ohio (1964), First Supplement (Ibid) (1969) Second Supplement, Ibid (1975)
8. O. Kubaschewski and C.B. Alcock, Metallurgical Thermochemistry Fifth Edition (1979) Pergamon Press, Oxford.
9. R. Mueller, Thesis University of Stuttgart (1981) To be Published in CALPHAD by J. Weiss, R. Mueller, H.L. Lukas, H. Krieg, G. Petzow and T.Y. Tien.
10. L.J. Gaukler, H. Hohnke and T.Y. Tien, J. American Ceramic Society 63 35 (1980)
11. F.F. Lange, Ceramic Bulletin 59 239 (1980).

Note in Proof

Note in Proof

H. L. Lukas has pointed out that the Gibbs free energy change for the reaction between the following solid phases

$$Si_3N_4 + 4MgO \rightarrow Mg_2SiO_4 + 2Mg\ SiN_2$$

is equal to 3953 - 8.85T Joules or 264 - 0.59 T Joules/ g. at. On this basis the SN - MO binary edge is slightly metastable with respect to the formation of F (1/7 (SiO_2 · 2MgO))and 1/5 (Mg Si N_2) above 446°K. Thus the sections shown in Figure 15 represent metastable equilibria.

CALCULATION OF TERNARY SYSTEMS CONTAINING III-V AND II-VI COMPOUND PHASES*

Larry Kaufman, Janine Nell, Keith Taylor and Fred Hayes+
ManLabs, Inc., 21 Erie Street
Cambridge, Massachusetts 02139, USA

(This paper was presented at Calphad X, Vienna, Austria July 1981)

ABSTRACT. A data base covering the binary systems composed of Aluminum, Gallium, Indium, Phosphorus, Arsenic and Antimony has been constructed by analyzing the fifteen combinations of these elements in terms of lattice stability, solution phase and compound parameters. Partial isothermal sections in the P-In-As, As-In-Sb, P-Ga-As, Ga-Sb-In and Al-Sb-Ga systems were then calculated using the foregoing data base for comparison with experimental isothermal sections and quasi-binary III-V phase diagrams. It was found that ternary liquid and III-V compound interaction parameters were required to attain good agreement in some cases. Similar calculations were performed for the Te-Cd, Hg-Cd and Te-Hg binary systems and the Cd-Te-Hg ternary systems at pressures up to 74 atmospheres. Comparison of the calculated results with experimental data on tie-line compositions between Cd-Te-Hg liquid and quasi-binary CdTe-HgTe alloys is important in the liquid phase epitaxial growth of controlled band gap electro-optical materials.

1. Introduction

Alloy semiconductors are important for a wide range of electro-optical applications because their properties can be tailored by controlling the composition of the solid, which is grown from the liquid or deposited from the vapor. Although crystal growers have become very adept at controlling the temperature (and pressure) of the parent phase in order to obtain the desired characteristics of the crystalline alloy semiconductors, phase diagram data is indispensable in order to deal with the increasingly complex systems. Stringfellow and co-workers (1-6) have pioneered in developing simple, useful models for calculating quasi-binary systems based on III-V compounds. Stringfellow's pioneering work has been extended and expanded by Ansara and co-workers (7), Osamura and Murakami and co-workers (8-10), and Brebrick (11) who have used more extensive experimental thermochemical data and less restrictive models than the regular solution (and quasichemical) model employed by Stringfellow. The current paper attempts to assemble a data base for III-V compounds which can be employed to compute multicomponent phase diagrams over a wide range of temperatures (and pressures) both outside and within the quasi-binary plane. In addition, the Cd-Hg, Cd-Te and Hg-Te binary systems are analyzed and combined to calculate the Cd-Te-Hg ternary system over a range of temperatures (and pressures) in order to compute tie-line compositions between quasi-binary CdTe-HgTe alloys and the Cd-Te-Hg liquid. The former alloys are of current interest in synthesizing controlled band gap electro-optical materials. In the analyses of both the III-V and II-VI (Cd-Te-Hg) systems, the methods and formalism which are applied are those employed in dealing with metals and metallic alloys (12,13), silicides (14), and oxynitride systems (15).

2. Thermochemical System Employed to Characterize Binary III-V Phase Diagrams

The method employed for describing solution and compound phases is the same as that employed to describe a variety of metal, metalloid, and oxide systems (13-15) incorporating

* This work has been sponsored by the Air Force Office of Scientific Research, Bolling Air Force Base, Washington, D.C. under Contract F44620-80-0020 and the Electronic Systems Division, RADC-AFSC-Hanscom Field, Bedford, Mass. under Contract F19628-78-C-0060.

+ On leave from Department of Metallurgy, University of Manchester-UMIST, Manchester, England.

some sybolic usage which facilitates data handling as indicated below. The free energy of the liquid phase, G^L, in the binary system Al-In is given by equation (1), where T is in Kelvins, R=8.314 J/g.at.°K, and x is the atomic fraction of Indium:

$$G^L = (1-x)\,{}^\circ G^L_{Al} + x\,{}^\circ G^L_{In} + RT(x\ell nx + (1-x)\ell n(1-x)) + x(1-x)[(1-x)\,LALIN + x\,LINAL]. \quad (1)$$

Similarly, the free energy of the fcc phase in the Al-In is defined by Equation (2) as

$$G^{fcc} = (1-x)\,{}^\circ G^{fcc}_{Al} + x\,{}^\circ G^{fcc}_{In} + RT(x\ell nx + (1-x)\,\ell n(1-x)) + x(1-x)[(1-x)\,AALIN + x\,AINAL] \quad (2)$$

where the difference in free energy between fcc and liquid aluminum, ALALLA, and the difference in free energy between fcc and liquid indium, ININLA, are listed in Table 1, while the solution parameters LALIN, LINAL, AALIN, and AINAL are given in Table 2. The liquid parameters for the In-As and Ga-As systems were taken directly from Brebrick's analysis (11). Brebrick also provides parameters for the In-Sb and Ga-Sb systems, namely LINSB=-3431-19.782T, LSBIN=-27698+19.581T, LGASB=21652-32.108T and LSBGA=-30020+28.259T J./g.at. While these parameters provide a good description of the In-Sb and Ga-Sb phase diagrams and the excess free energy of mixing for the liquid phases in these systems, they do not describe the enthalpy of mixing for the liquid phase in the In-Sb and Ga-Sb systems as measured by Ansara et al. (7). Thus in the case of the In-Sb system, the enthalpy of mixing defined by Brebrick's LINSB and LSBIN parameters is given by Equation (3) as

$$E_H{}^L = -x(1-x)[(1-x)3431 + 27698x] \quad J/g.at. \quad (3)$$

where $x=x_{Sb}$. By contrast, the equation for $E_H{}^L$ provided by Ansara et al. (7) for In-Sb, which is based upon experimental measurements of the heat of mixing, is given by

$$E_H{}^L = -x(1-x)(11689 + 19774x - 46661x^2 + 24980x^3) \quad J/g.at. \quad (4)$$

Ansara et al. also provide the following equation for the excess entropy of mixing of the liquid as

$$E_S{}^L = x(1-x)[4.602 - 7.799x + 12.104x^2 - 6.782x^3] \quad J./g.at.°K \quad (5)$$

Although the excess free energy provided by Brebrick's parameters and those generated by Eqs. (4) and (5) in the temperature range of interest (near 700°K) are in relatively good agreement, the enthalpy of mixing described by Equations (3) and (4) differ by 800-1600 J/g.at. Consequently, Equations (4) and (5) were employed to derive LINSB=-15380-3.607T and LSBIN=-10293-2.393T shown in Table 2. These expressions provide a closer fit to Equations (4) and (5) than Brebrick's parameters and still yield a satisfactory agreement in the calculated and observed In-Sb phase diagram. A similar comparison can be made for the Ga-Sb system. In the latter case Brebrick's analysis yielded LGASB=21652-32.108T and LSBGA=-30020+28.259T J./g.at. By contrast, Ansara et al. (7) suggest that

$$E_H{}^L = x(1-x)[531 - 21599x + 32175x^2 - 15788x^3] \quad J/g.at. \quad (6)$$

where $x=x_{Sb}$ and

$$E_S{}^L = x(1-x)[4.849 - 14.456x + 24.527x^2 - 15.786x^3] \quad J/g.at.°K \quad (7)$$

The present parameters, LGASB=4962-3.209T and LSBGA=-9715-0.456T provide a better description of the experimental heat of mixing for Ga-Sb alloys embodied (12) by Equation (5) than do the parameters suggested by Brebrick. The parametric descriptions of the In-Al, Ga-Al, and In-Ga systems shown in Tables 1 and 2 were derived from the earlier description provided by Ansara et al. (12). The remaining III-V systems were characterized as shown in Tables 1-3 based on the available thermochemical and phase diagram data employing the standard compilations of such information (16-20) and available lattice stability data. Table 4 compares the calculated and observed thermochemical properties of III-V compounds based on this description while Figures 1-14 display the partial phase diagrams computed with the current description. The heat of mixing of liquid $Al_{0.5}Sb_{0.5}$ at 1400°K is given as -2477 J./g.at. based on experimental data (17) and -1126 J./g.at. on the basis of Table 2.

TABLE 1

SUMMARY OF LATTICE STABILITY PARAMETERS
(All units in Joules per gram-atom (mole of atoms), T in Kelvins)

L=liquid*, A=fcc*, T=tetragonal, O=orthorhombic,
R=rhombohedral, X=red phosphorus structure, W=white phosphorus structure

ALALLA = 10711 - 11.506T*
ALALLO = 0 - 18.451T

GAGALO = 5590 - 18.451T
GAGALA = -5021 - 8.368T
GAGALT = -1674 - 8.368T

ININLT = 3264 - 7.594T
ININLA = 2908 - 7.113T
ININLO = 0 - 18.451T

PPPPLX = 17991 - 21.506T
PPPPWX = 18171 - 19.539T
PPPPLA = -18828 - 8.368T
PPPPLR = 4184 - 23.012T

SBSBLR = 19874 - 21.966T
SBSBLA = -18828 - 8.368T

ASASLR = 24874 - 23.012T
ASASLA = -18828 - 8.368T
ASASLX = 21631 - 21.631T

*ALALLA = $G_{Al}^{liquid} - G_{Al}^{fcc}$ = 10711 - 11.506 T J./g.at.

TABLE 2

SUMMARY OF SOLUTION PHASE PARAMETERS*
(All units in Joules per gram-atom (mole of atoms), T in Kelvins)

*for Aℓ-In system, L=liquid, A=fcc, x=x_{In}

$G^{L}=(1-x)G_{A\ell}^{L} + xG_{In}^{L} + RT(x\ell nx + (1-x)\ell n(1-x)) + x(1-x)[(1-x)LALIN + xLINAL]$

$G^{fcc}=(1-x)G_{A\ell}^{fcc} + xG_{In}^{fcc} + RT(x\ell nx + (1-x)\ell n(1-x)) + x(1-x)[(1-x)AALIN + xAINAL]$

LALAS = -16317 - 41.338T
LASAL = -16317 - 41.338T

LALPP = -38911 - 26.275T
LPPAL = -38911 - 26.275T

LINPP = -29288 + 5.188T
LPPIN = -79496 + 5.188T
RINPP = 8368
RPPIN = 8368

LGAPP = -90374 + 34.225T
LPPGA = -58576 - 49.036T
XGAPP = 8368
XPPGA = 8368

LGASB = 4962 - 3.209T
LSBGA = -9715 - 0.456T
RSBGA = RGASB = 8368

LALGA = 3280 - 2.021T
LGAAL = 2071 - 0.745T
AALGA = -1046 + 5.439T
AGAAL = -20962 + 26.778T
OGAAL = OALGA = 8368

LALIN = 25522 - 3.347T
LINAL = 20502 - 2.510T
AALIN = 60250 - 3.347T
AINAL = 55229 - 2.510T

LALSB = 8050 - 9.706T
LSBAL = -17054 - 9.706T

LSBAS = LASSB = 0
RSBAS = RASSB = 8368

LSBPP = LPPSB = -15899
RSBPP = RPPSB = -20920-4.184T
XSBPP = XPPSB = -15899

LASPP = LPPAS = -15899
RASPP = RPPAS = -20920-4.184T
XASPP = XPPAS = -15899

LGAAS = -1845 - 21.209T
LASGA = -41551 + 7.192T
RGAAS = RASGA = 8368

LINAS = -243 - 29.522T
LASIN = -48124 + 17.472T
TASIN = TINAS = 8368

TABLE 2 (CONTINUED)

SUMMARY OF SOLUTION PHASE PARAMETERS
(All units in Joules per gram-atom (mole of atoms) T in Kelvins)

LINSB = -15380 - 3.607T
LSBIN = -10293 - 2.393T
TSBIN = TINSB = 8368
RSBIN = RINSB = 8368

LGAIN = 4435 + 2.268T
LINGA = 4435 + 0.954T
TGAIN = -3431 + 21.907T
TINGA = -3376 + 24.393T
OGAIN = OINGA = 12552

TABLE 3

COMPOUND PARAMETERS FOR III-V ZINC-BLENDE COMPOUNDS

$G^S = 0.5\ G_i^{fcc} + 0.5\ G_j^{fcc} + 0.25\ [0.5\ LIIJJ + 0.5\ LJJII - C]$ Joules/g.at.

Compound	Compound Parameter (C) (Joules/g.at. °K)	Compound	Compound Parameter (C) (Joules/g.at. °K)
$Al_{0.5}P_{0.5}$	364,443 - 60.517T	$Ga_{0.5}Sb_{0.5}$	179,343 - 77.571T
$Al_{0.5}As_{0.5}$	305,348 - 78.994T	$In_{0.5}P_{0.5}$	188,749 - 64.099T
$Al_{0.5}Sb_{0.5}$	174,992 - 55.815T	$In_{0.5}As_{0.5}$	187,217 - 73.806T
$Ga_{0.5}P_{0.5}$	280,328 - 75.647T	$In_{0.5}Sb_{0.5}$	125,227 - 63.011T
$Ga_{0.5}As_{0.5}$	259,525 - 83.496T		

TABLE 4

COMPARISON OF CALCULATED AND EXPERIMENTAL THERMOCHEMICAL PROPERTIES OF III-V COMPOUNDS
(J./mol., J./mol.°K)

Compound	ΔH_f[298°K]		ΔS_f[298°K]		ΔS [fusion]	
	calculated	exptl.	calculated	exptl.(16)	calculated	exptl.
AlP	-164,849	-164,431±2929(16)	-3.97	-3.85±5.0	61.66	61.50±1.6(16)
AlAs	-117,127	-122,591±5021(16)	-4.18	-3.76±4.8	70.91	70.42(43)
AlSb	-51,045	-50,208±418(16)	-9.46	-8.86±0.8	59.32	61.67(43)
GaP	-129,971	-122,173±8368(16)	-10.92	-11.51± 1.9	66.10	66.53(43)
GaAs	-86,291	-88,575(11)	-13.51	-12.47±1.3	70.015	69.63(11)
GaSb	-41,547	-41,840±1255(16)	-14.19	-9.20±1.9	67.061	67.31(11)
InP	-84,391	-75,312±8368(16)	-21.02	-20.88±1.9	59.07	59.08(43)
InAs	-61,647	-61,923(11)	-18.74	-18.83±2.5	63.92	63.36±6.89(16)
InSb	-29,974	-30,962(11)	-15.93	-15.69±1.1	58.53	59.82(11)

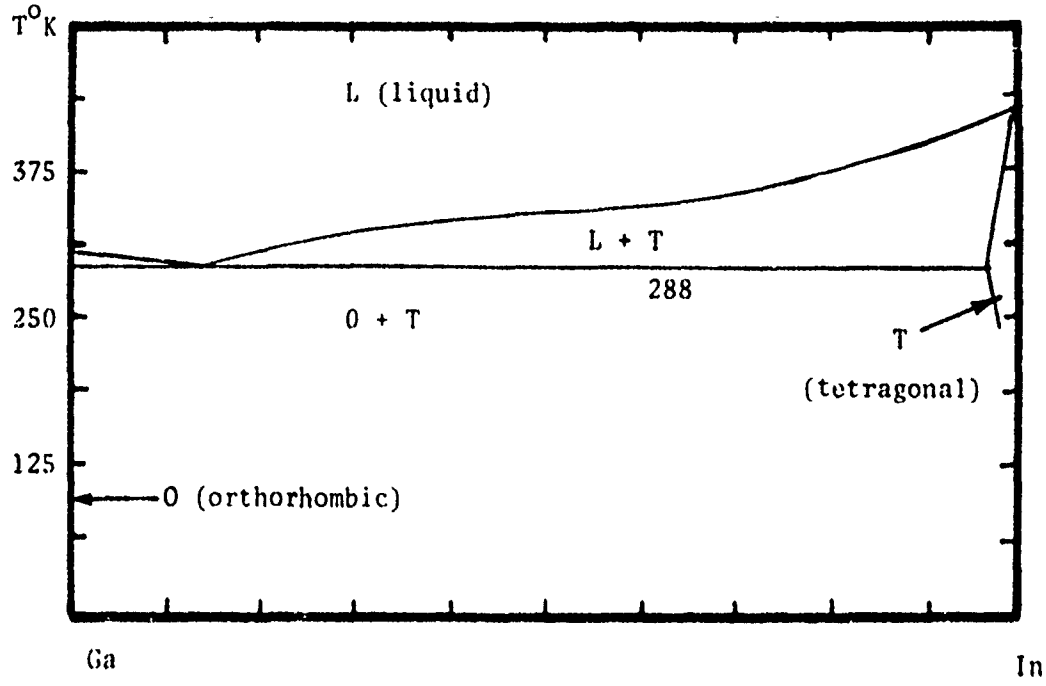

Figure 1. Calculated Ga-In Phase Diagram

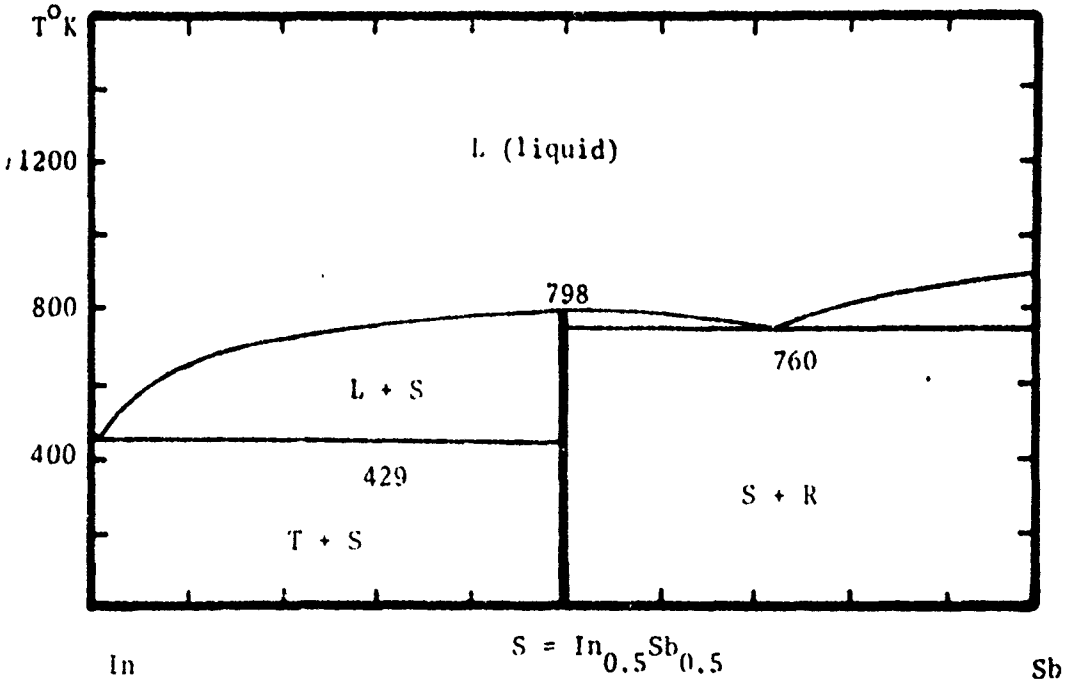

Figure 2. Calculated In - Sb Phase Diagram

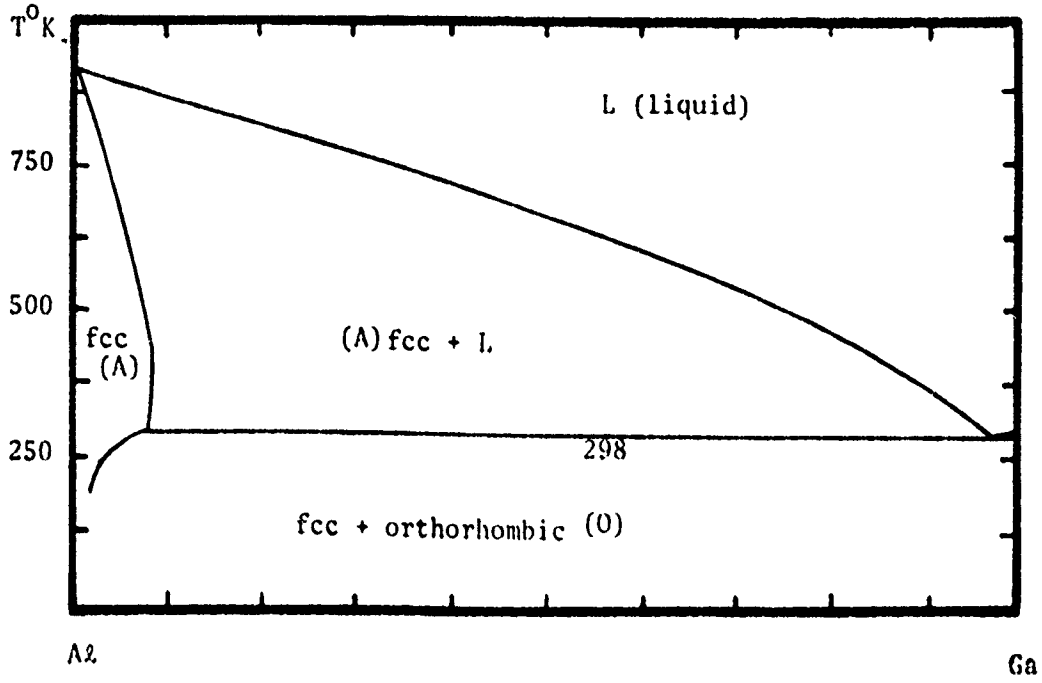

Figure 3. Calculated Aℓ-Ga Phase Diagram

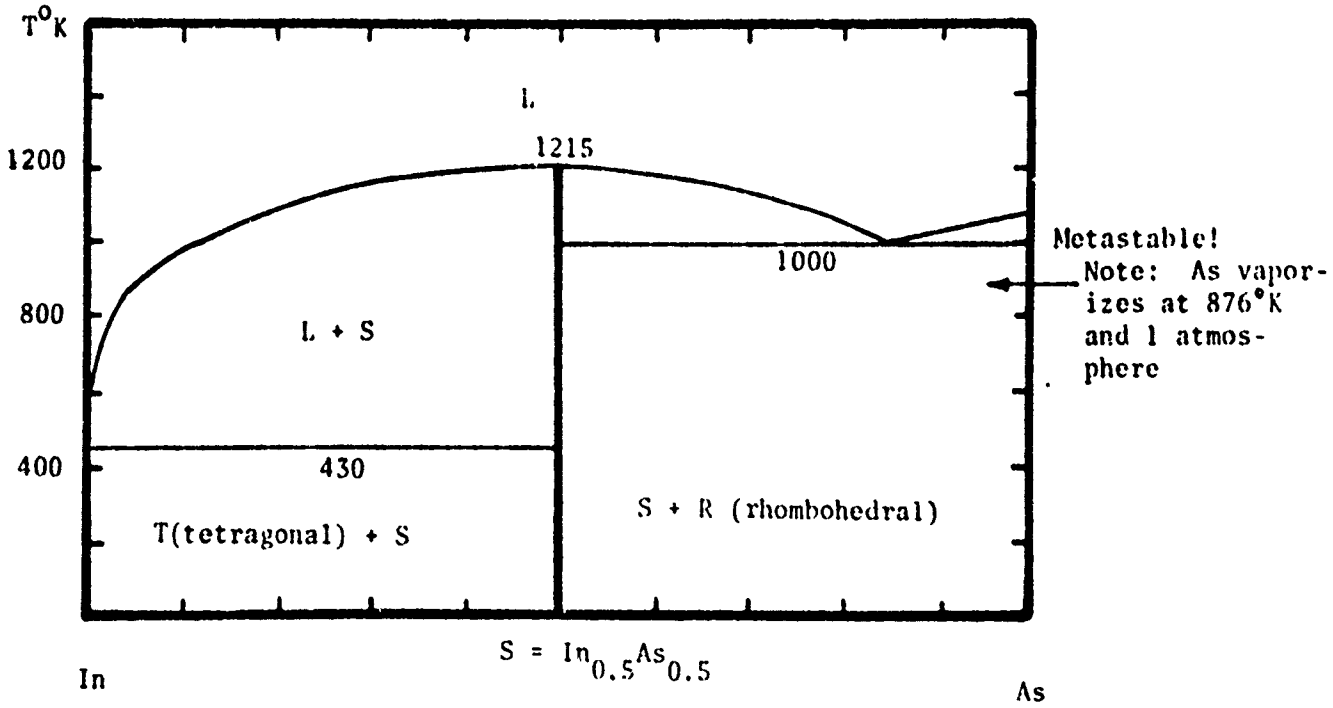

Figure 4. Calculated In - As Phase Diagram

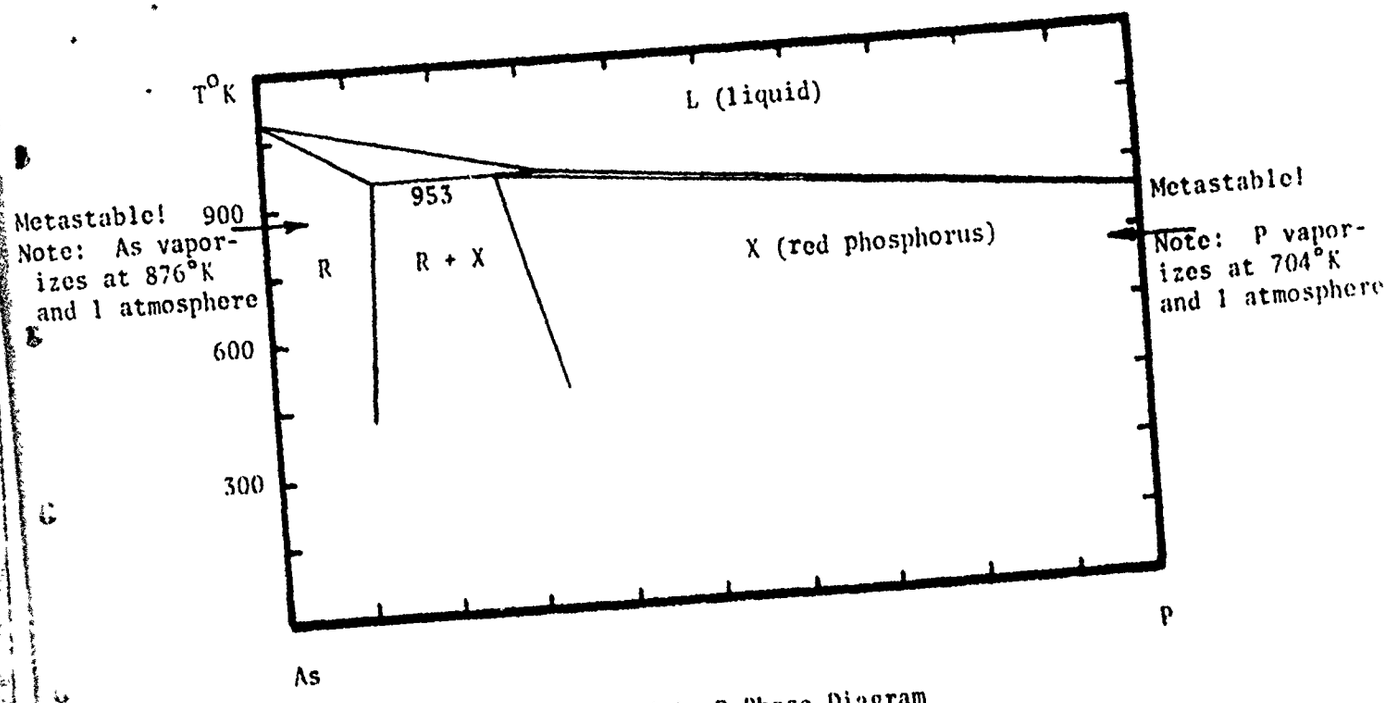

Figure 5. Calculated As-P Phase Diagram

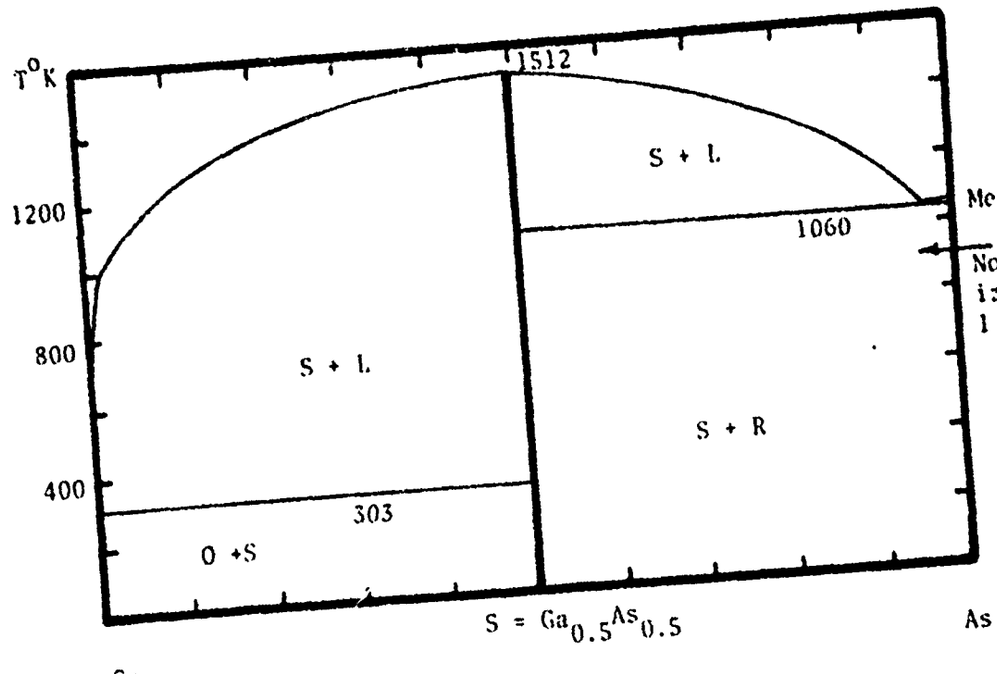

Figure 6. Calculated Ga-As Phase Diagram

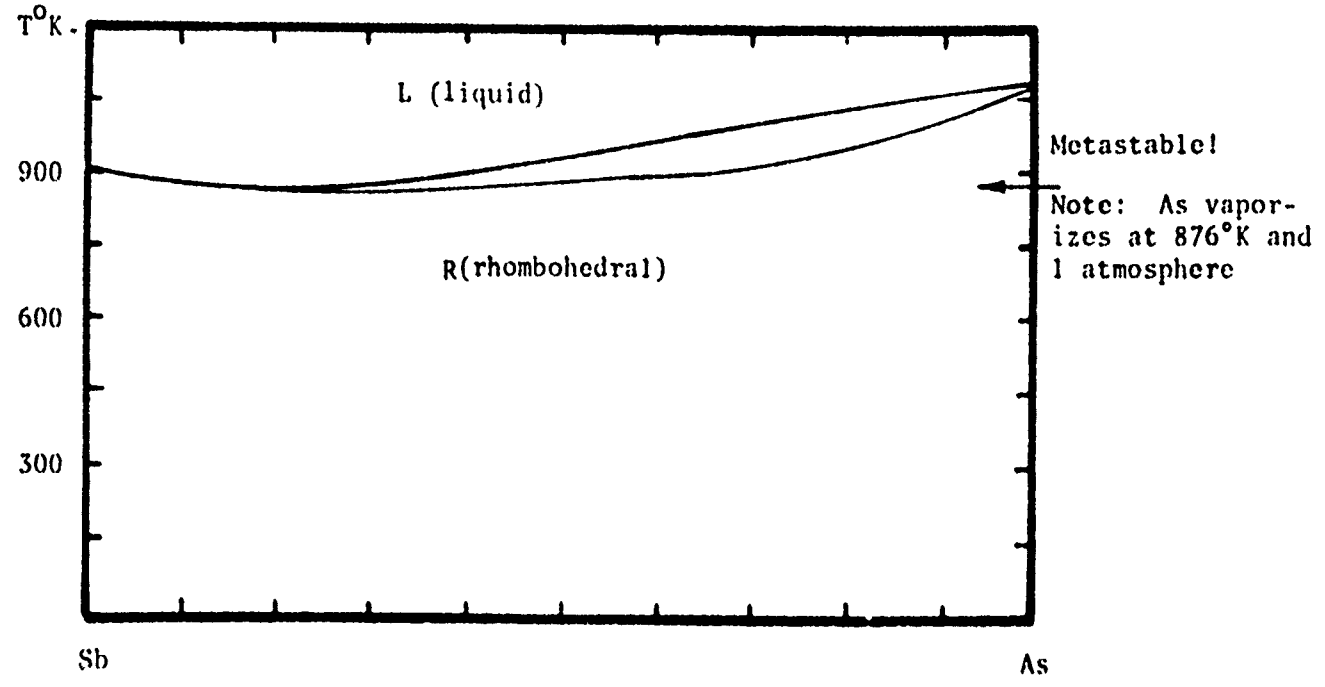

Figure 7. Calculated Sb-As Phase Diagram

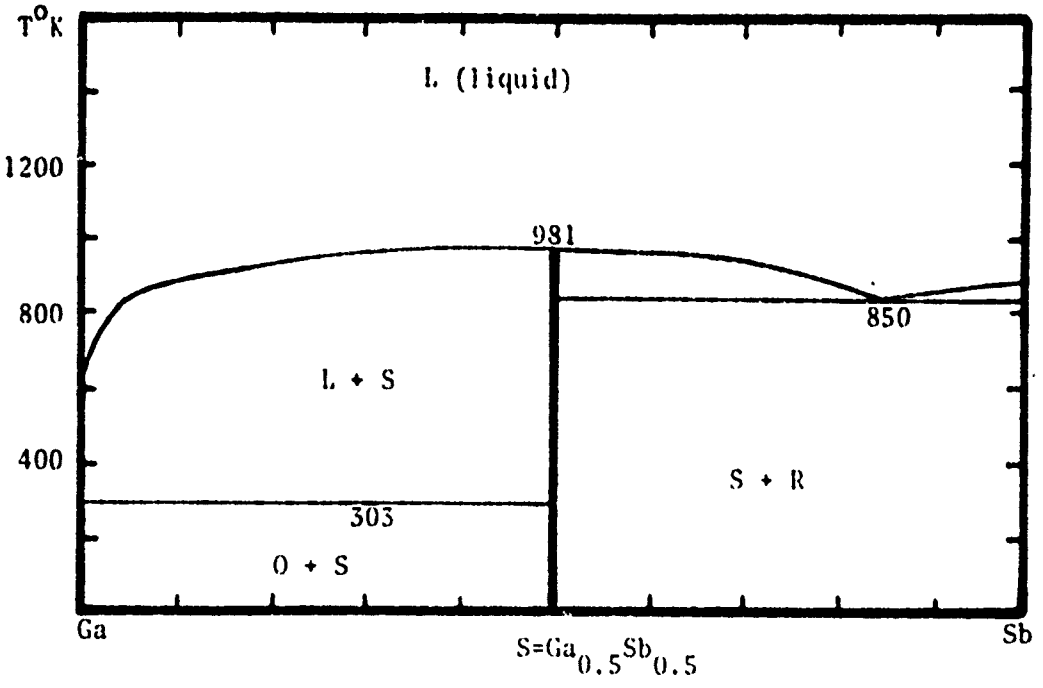

Figure 8. Calculated Ga-Sb Phase Diagram

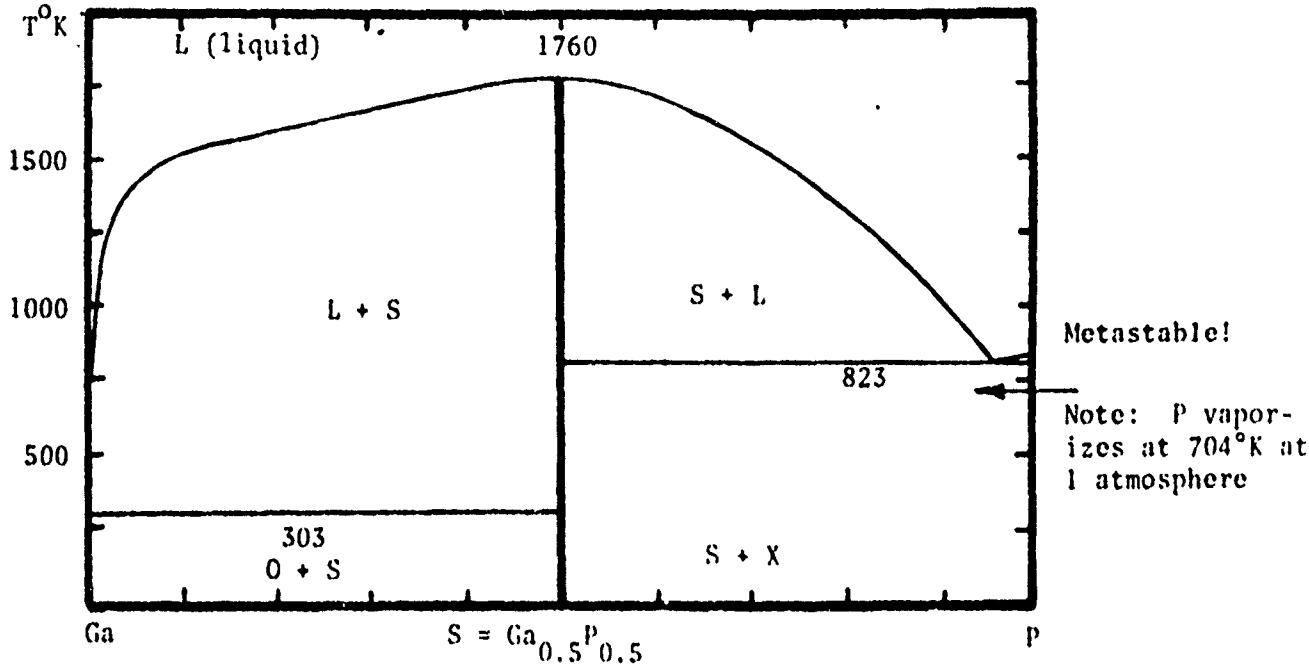

Figure 9. Calculated Ga-P Phase Diagram

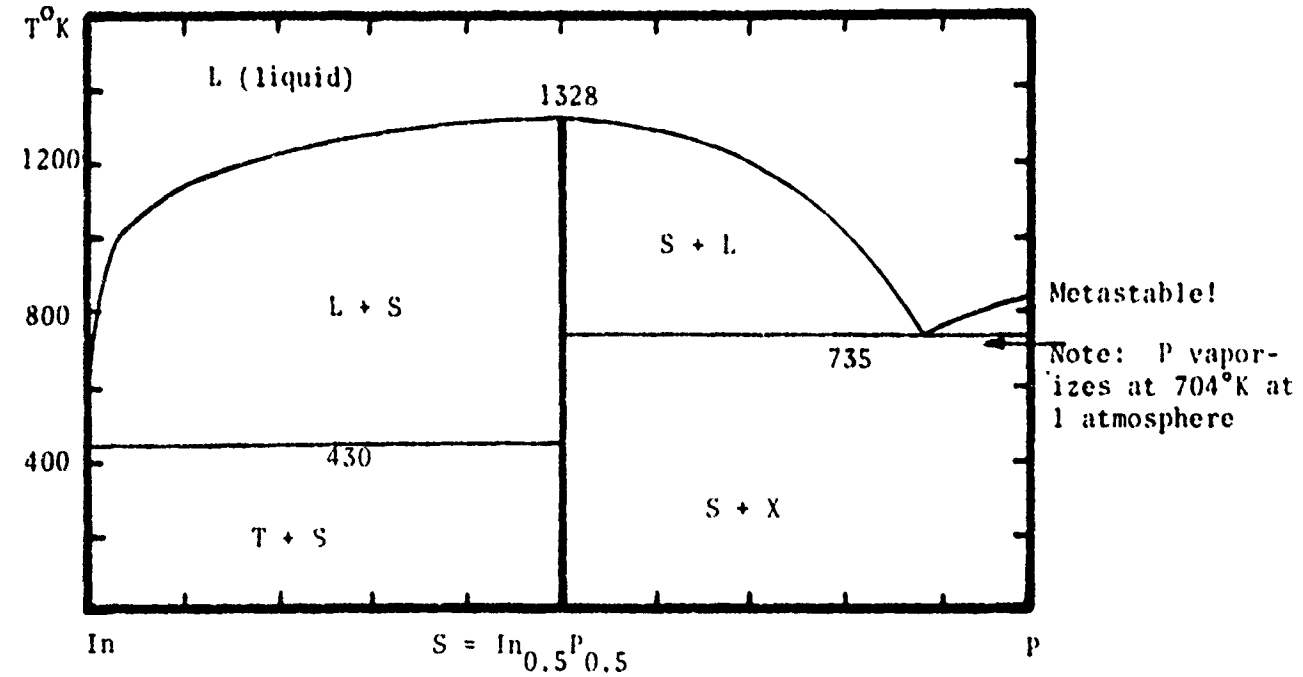

Figure 10. Calculated In-P Phase Diagram

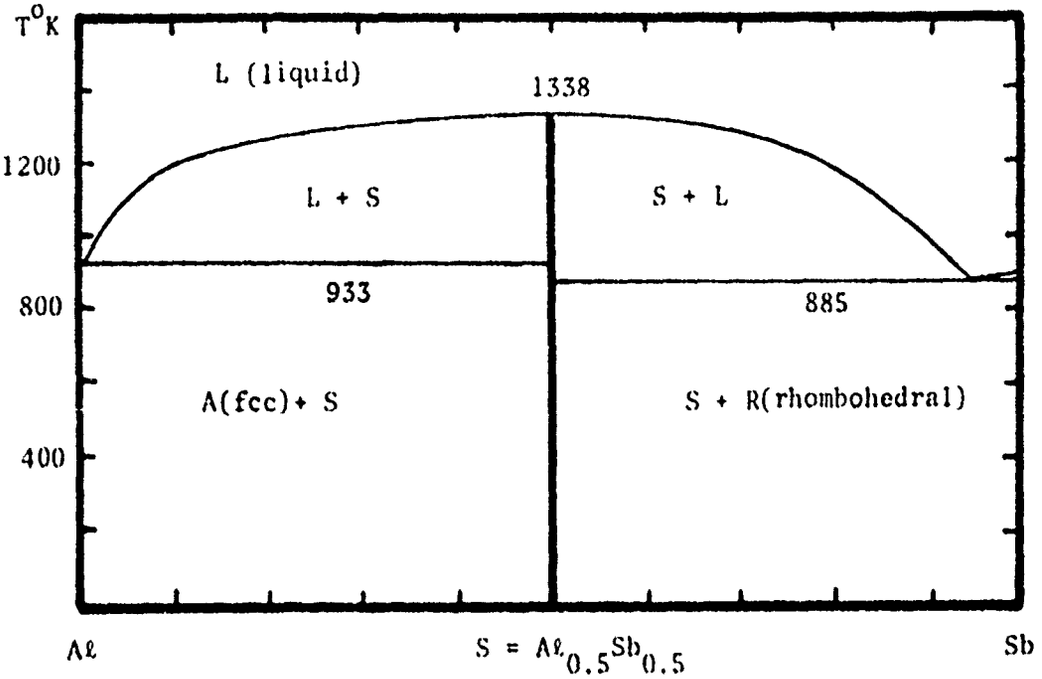

Figure 11. Calculated Aℓ-Sb Phase Diagram

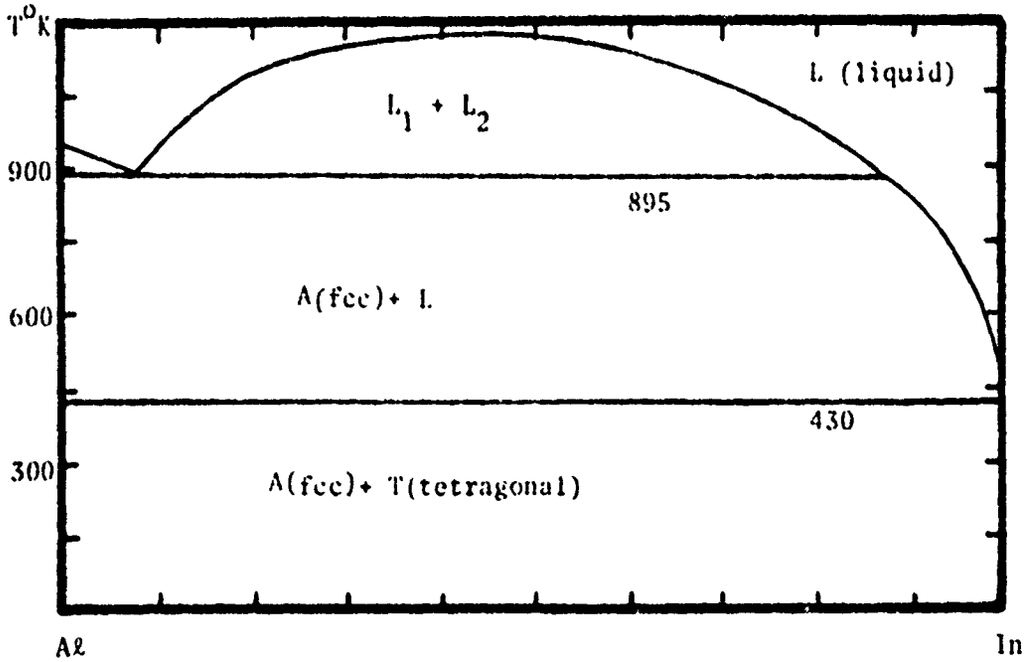

Figure 12. Calculated Aℓ-In Phase Diagram

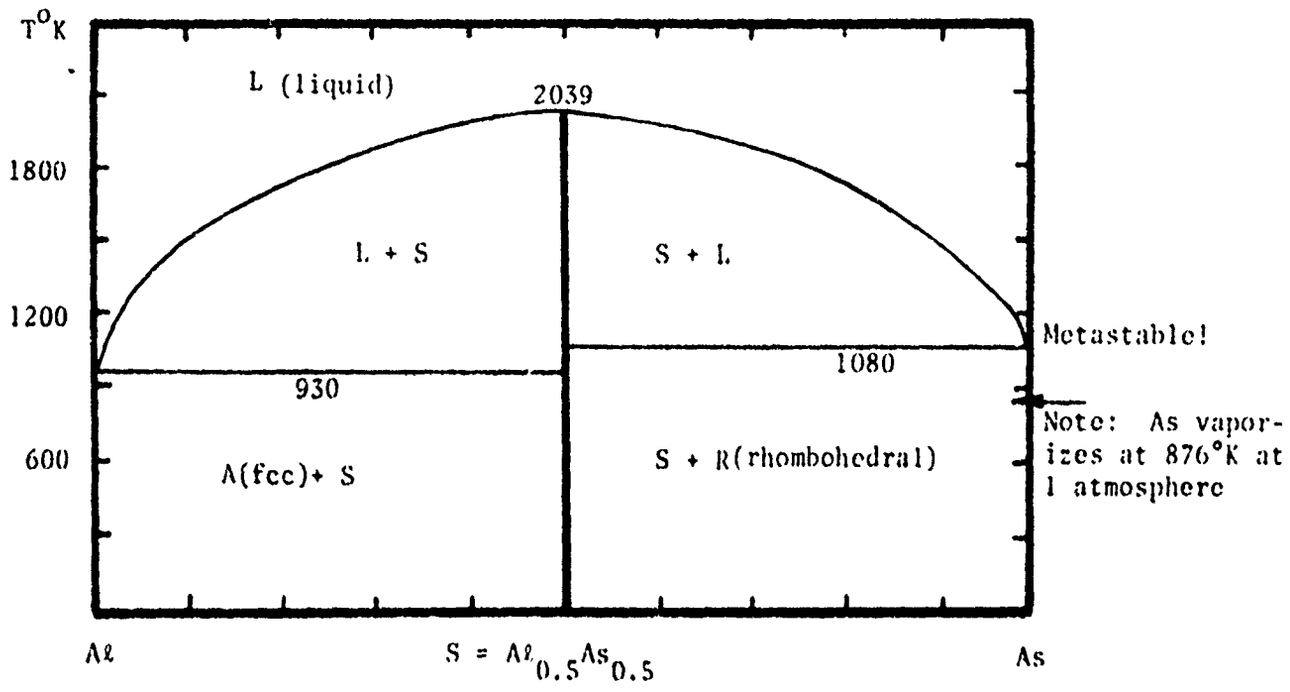

Figure 13. Calculated Al-As Phase Diagram

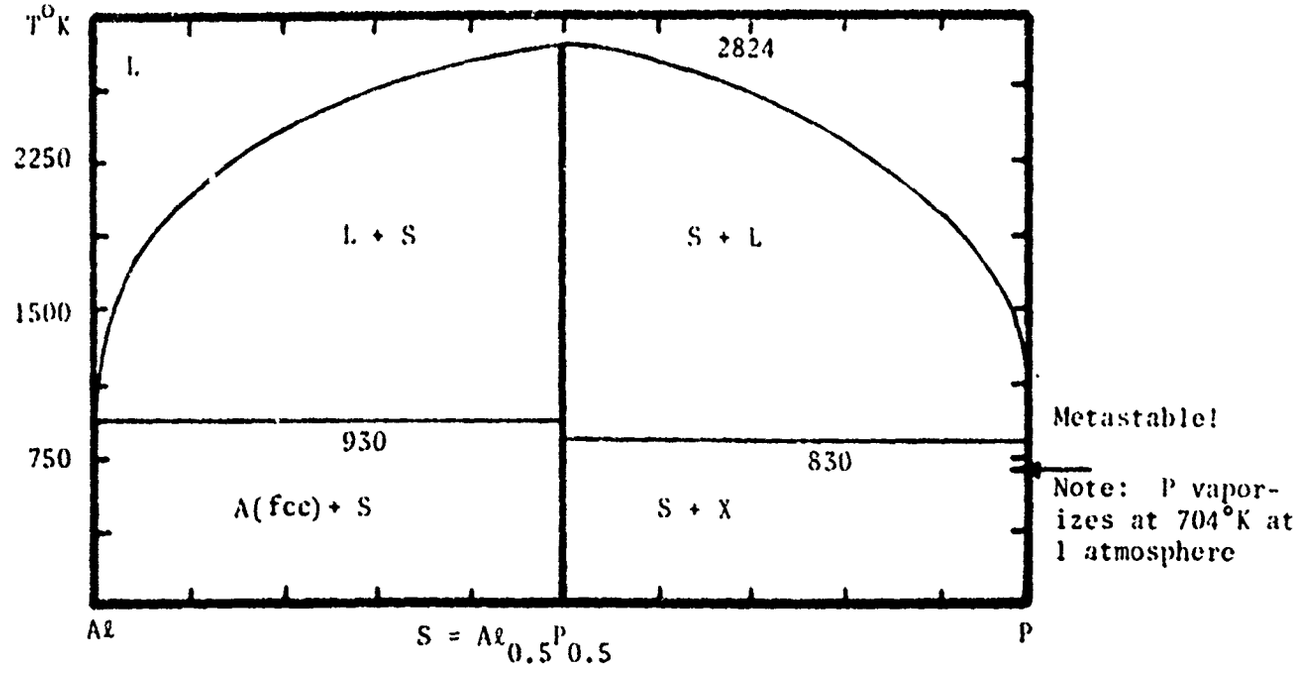

Figure 14. Calculated Al-P Phase Diagram

The free energy of the ternary liquid phase in the P-In-As system is defined on the basis of Kohler's equation as

$$G^L = (1-x-y)^oG_P^L + x^oG_{In}^L + y^oG_{As}^L + RT((1-x-y)\ln(1-x-y) + x\ln x + y\ln y)$$
$$+(1-x-y)x(1-y)^{-1}[(1-x-y)LPPIN + xLINPP] + (1-x-y)y(1-x)^{-1}[(1-x-y)LPPAS + yLASPP]$$
$$+ xy(x+y)^{-1}[xLINAS + yLASIN] + xy(1-x-y)\ TRNL \qquad J./g.at. \qquad (8)$$

where x is the atom fraction of In, y is the atom fraction of As and TRNL is the ternary interaction parameter. Values of TRNL for five ternary systems which have been investigated here are listed in Table 5. The specific value for the P-In-As system is 12552 J/g.at. This is a rather small value since the maximum value of the ternary term occurs at x=y=(1-x-y)=1/3. Thus the maximum contribution of this term is only 465 J/g.at. If attention were restricted to the quasi-binary join (i.e., where x=0.5) between $In_{0.5}P_{0.5}$ and $In_{0.5}As_{0.5}$ the maximum contribution is 390 J/g.at. when x=0.5, y=0.25 and (1-x-y)=0.25.

The free energy of the $In_{0.5}P_{0.5}$-$In_{0.5}As_{0.5}$ zinc-blende phase (S) is defined by Equation (9) as follows

$$G^S = (0.5-y)^oG_P^{fcc} + 0.5^oG_{In}^{fcc} + y^oG_{As}^{fcc} + (1-2y)(0.25)(0.5\ LPPIN + 0.5LINPP - C_1)$$
$$+2y(0.25)(0.5LINAS + 0.5LASIN - C_2) + CAB\ y(1-2y)$$
$$+RT(y\ln y + (0.5-y)\ln(0.5-y) - 0.5\ln 0.5) \qquad J./g.at. \qquad (9)$$

where C_1, the compound parameter for $In_{0.5}P_{0.5}$ = 188,749-64.099T J/g.at. and C_2, the compound parameter for $In_{0.5}As_{0.5}$ = 187,217 - 73.806T J./g.at., as given in Table 3. The interaction parameter for mixing $In_{0.5}P_{0.5}$ and $In_{0.5}As_{0.5}$, CAB, is equal to zero in this case, as shown in Table 5. Thus this compound is defined as an ideal solution of its components. Since the free energies of the liquid and zinc-blende phases can be defined explicitly, the partial ternary phase diagrams covering the L-S equilibria can be computed as a function of temperature. This procedure has been carried out for the ternary systems listed in Table 5. The results, displayed as isothermal sections or as quasi-binary joins, are compared with experimental findings and Stringfellow's calculations (1) in Figures 15-25. A calculated isothermal section due to Ansara et al. (7) for the Sb-Ga-In case at 823°K is included for comparison in Figure 21. The latter results are in good agreement with the current findings shown in Figure 23. Although it is not possible to make an exact comparison of the interaction parameters employed by Stringfellow in his quasi-binary calculations (1,6) and those employed here, an approximate comparison can be made in the following way. In Stringfellow's study, the quasi-binary system InP-InAs was treated as if the liquid and solid phases were both regular solutions. The interaction parameter for the liquid was taken to be 5238 J/mol. Since the heat of mixing is the product of the mol. fraction and the interaction parameter, the maximum value of the heat of mixing is (0.25)(5238)=1309 J/mol=655 J/g.at. for liquid $0.5In_{0.5}P_{0.5}$-$0.5In_{0.5}As_{0.5}$. This value is listed in Table 6 along with comparable parameters for the other systems of current interest cited by Stringfellow. The latter results are compared with those derived from the current study on the basis of Equations (8) and (9) and Table 5. As indicated above, the maximum contribution along the quasi-binary join is equal to TRNL/32 and CAB/8. Table 6 lists these values for comparison with Stringfellow's results in Table 6. While there is no obvious correlation between the current results and Stringfellow's values, all of the values listed are small! The analysis of the Ga-Sb-In system carried out by Ansara et al. (7) utilized a ternary heat of mixing equal to

$$E_H^L = x_{In}x_{Ga}x_{Sb}\ [23234x_{In} - 24066x_{Ga} + 582x_{Sb}]. \qquad (10)$$

The present analysis sets

$$E_H^L = -x_{In}x_{Ga}x_{Sb}\ 8368\ . \qquad (11)$$

At $x_{In}=x_{Ga}=x_{Sb}=0.333$, Equation (10) yields -3.1 J/g.at., while Equation (11) yields -309 J./g.at. At compositions near the edges of the ternary (0.1,0.4,0.5) Eq. (11) yields -167 J/g.at., while Eq. (10) yields results between +188 and -188 J.g./at. All of these contributions are small.

TABLE 5

COMPILATION OF TERNARY PARAMETERS FOR III-V LIQUID AND ZINC-BLENDE COMPOUND PHASES

(All Units in Joules per gram-atom (mole of atoms) T in Kelvins)

System	TRNL (Joules/g.at.)	Zinc-blende Phase	CAB (Joules/g. at.)
P-In-As	12552	$In_{0.5}(P,As)_{0.5}$	0
As-In-Sb	0	$In_{0.5}(As,Sb)_{0.5}$	9623
P-Ga-As	-31380	$Ga_{0.5}(P,As)_{0.5}$	2092
Ga-Sb-In	-8368	$(Ga,In)_{0.5}Sb_{0.5}$	4602
Al-Ga-Sb	-8368	$(Al,Ga)_{0.5}Sb_{0.5}$	-4184

TABLE 6

COMPARISON OF THE MAXIMUM QUASI-BINARY HEAT OF MIXING FOR THE LIQUID AND SOLID COMPOSITIONS FROM STRINGFELLOW (1,6) AND THE CURRENT ANALYSIS (Joules/g.at.)

	LIQUID		SOLID	
System	Stringfellow(1)	Current	Stringfellow	Current
$In_{0.5}P_{0.5}$-$In_{0.5}As_{0.5}$	655	392	306	0
$In_{0.5}As_{0.5}$-$In_{0.5}Sb_{0.5}$	244	0	1197	1202
$Ga_{0.5}P_{0.5}$-$Ga_{0.5}As_{0.5}$	655	-980	515	260
$Ga_{0.5}Sb_{0.5}$-$In_{0.5}Sb_{0.5}$	1409	-260	965	574
$Al_{0.5}Sb_{0.5}$-$Ga_{0.5}Sb_{0.5}$	664	-260	12	-524

Thus the current analysis suggests a simple method for calculating isothermal sections for III-IV ternary systems. In particular, if a given section is required, the data base contained in Tables 1-3 can be employed to calculate the section of interest with TRNL=TAB=0. The process can then be repeated employing a range of TRNL and CAB similar to those shown in Table 5 to predict the spread of expected results. If a few experimental data are available at a given temperature, they can be readily employed to fix TRNL and CAB, which in turn can be employed to predict the behavior at other temperatures. It is hoped that future studies will permit improvement of the current data base.

3. Thermochemical System Employed to Characterize Binary II-VI Phase Diagrams

The II-IV compounds of $Cd_{0.5}Te_{0.5}$ and $Hg_{0.5}Te_{0.5}$ form a series of cubic zinc-blende solid solutions which offer the attractive property of a variable band gap that is a function of composition. The $(Cd,Hg)_{0.5}Te_{0.5}$ solid solution displays band gaps which run in a nearly linear fashion between the wide gap semiconductor $Cd_{0.5}Te_{0.5}$ (E_g=1.6 eV) and the semimetallic compound $Hg_{0.5}Te_{0.5}$, which can be considered to be a semiconductor with a negative band gap (37). Alloys of $Cd_{0.1}Hg_{0.4}Te_{0.5}$ and $Cd_{0.2}Hg_{0.3}Te_{0.5}$, exhibiting band gaps ranging from 0.1 to 0.5 eV, respectively, are of particular interest for detection of infrared radiation in the 2 to 20 micron range. The growth of such alloy compositions from the melt presents some difficulties due to the "width" of the two phase liquid plus solid field along the

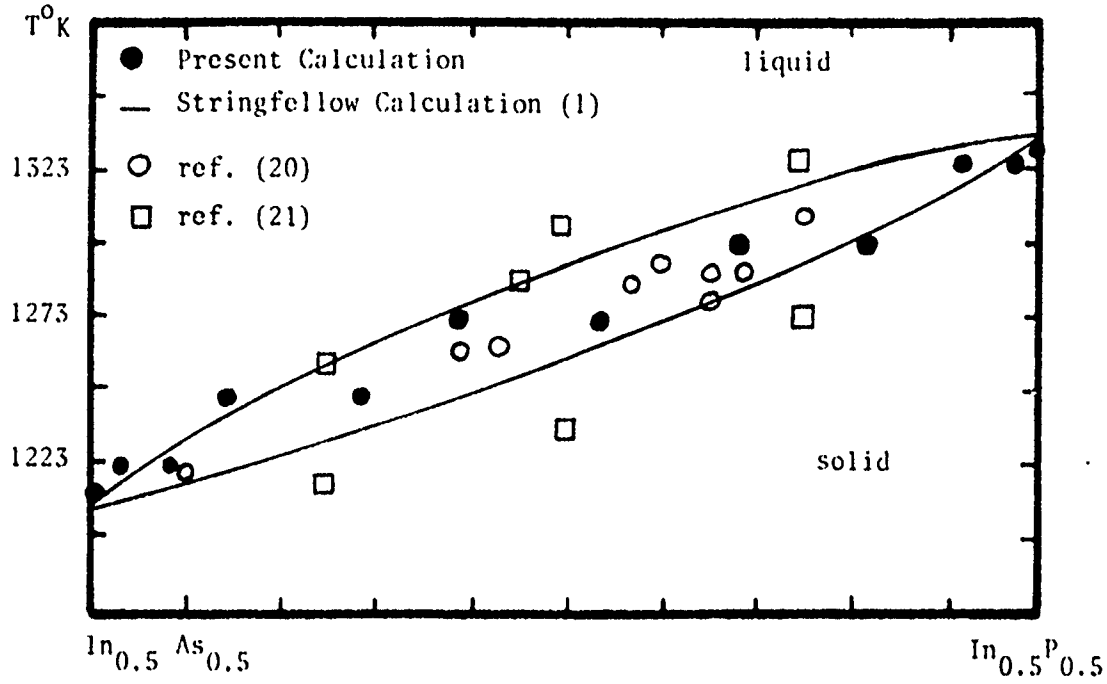

Figure 15. Calculated and Observed Equilibria Along the $In_{0.5}As_{0.5}$ - $In_{0.5}P_{0.5}$ Quasi-binary Join

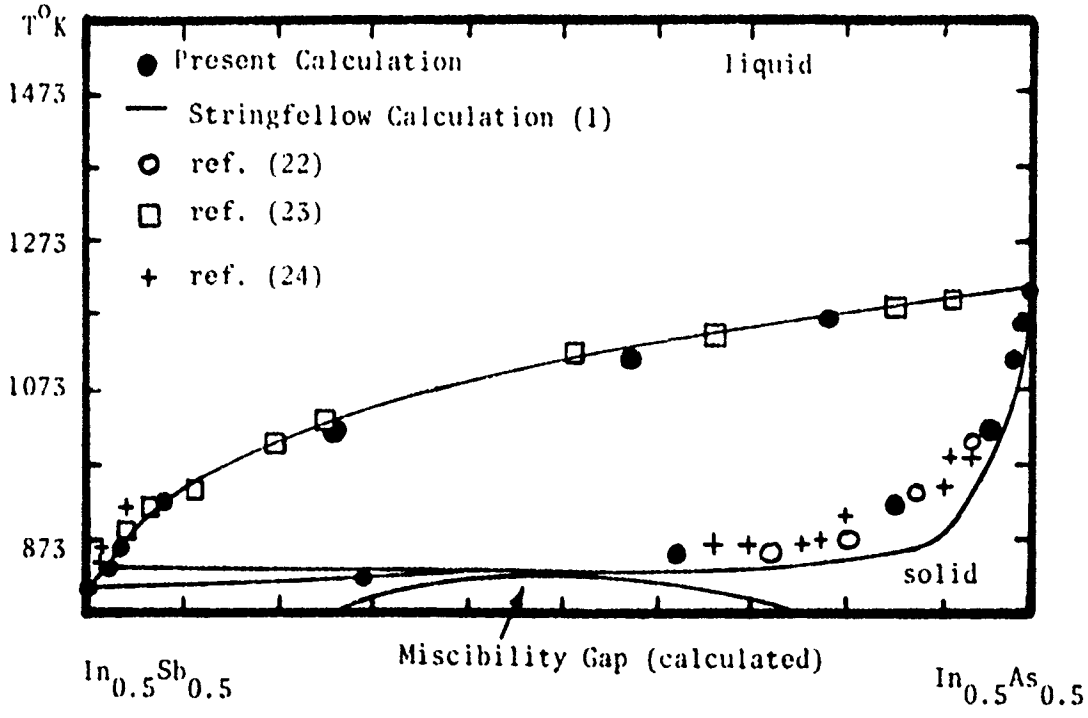

Figure 16. Calculated and Observed Equilibria Along the $In_{0.5}Sb_{0.5}$ - $In_{0.5}As_{0.5}$ Quasi-binary Join

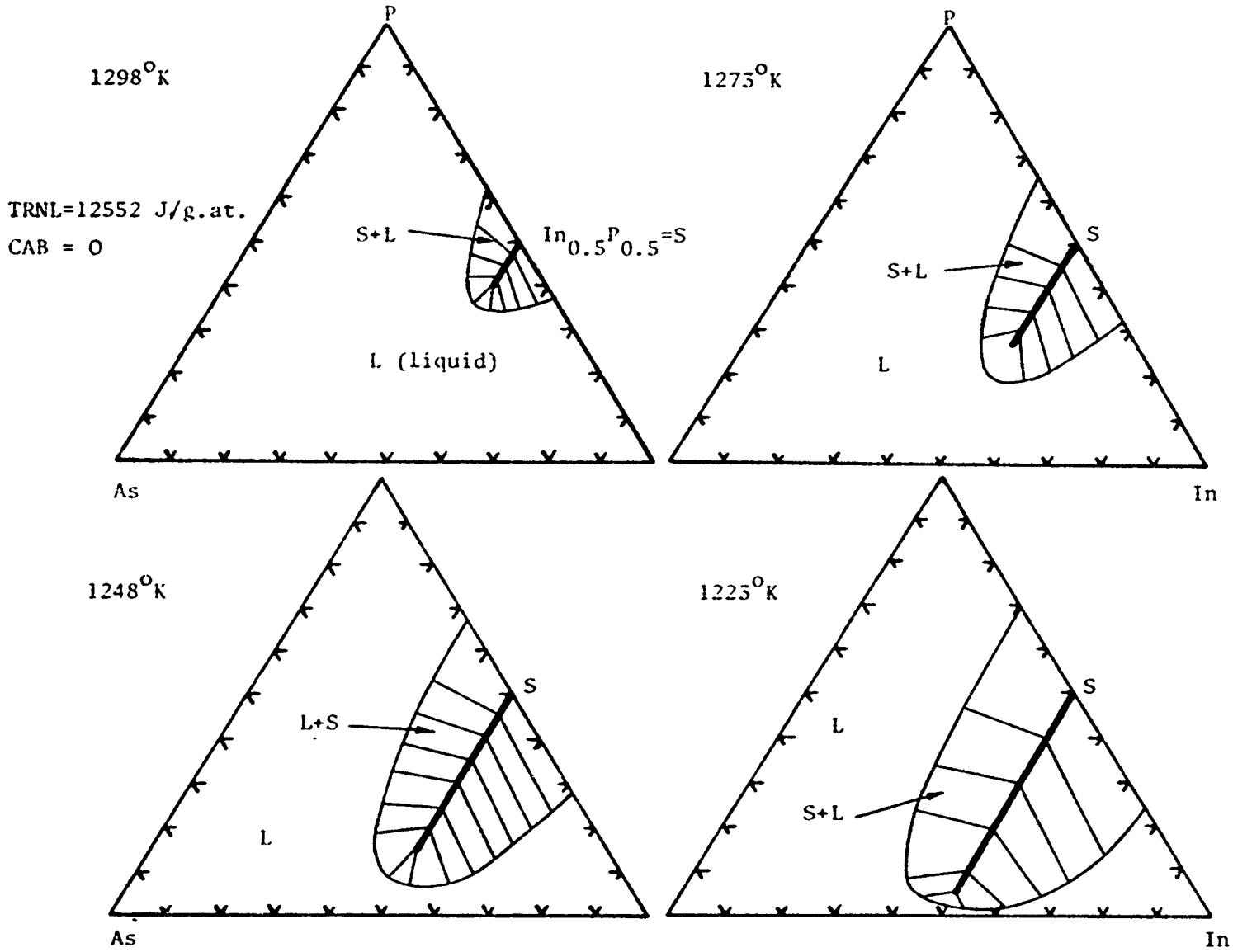

Figure 17. Calculated Partial Isothermal Sections in the Phosphorus-Indium-Arsenic System

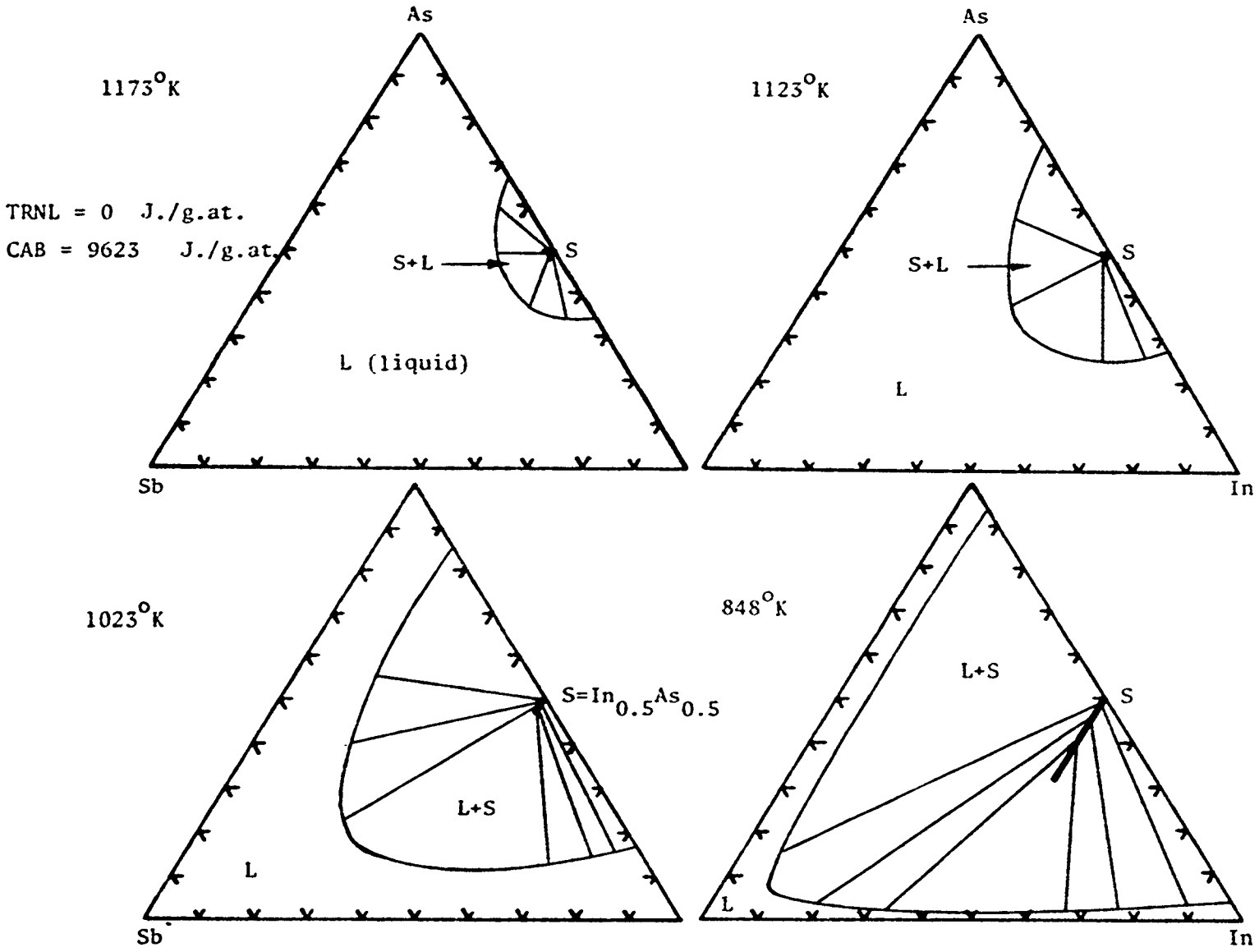

Figure 18. Calculated Partial Isothermal Sections in the Arsenic-Indium-Antimony System

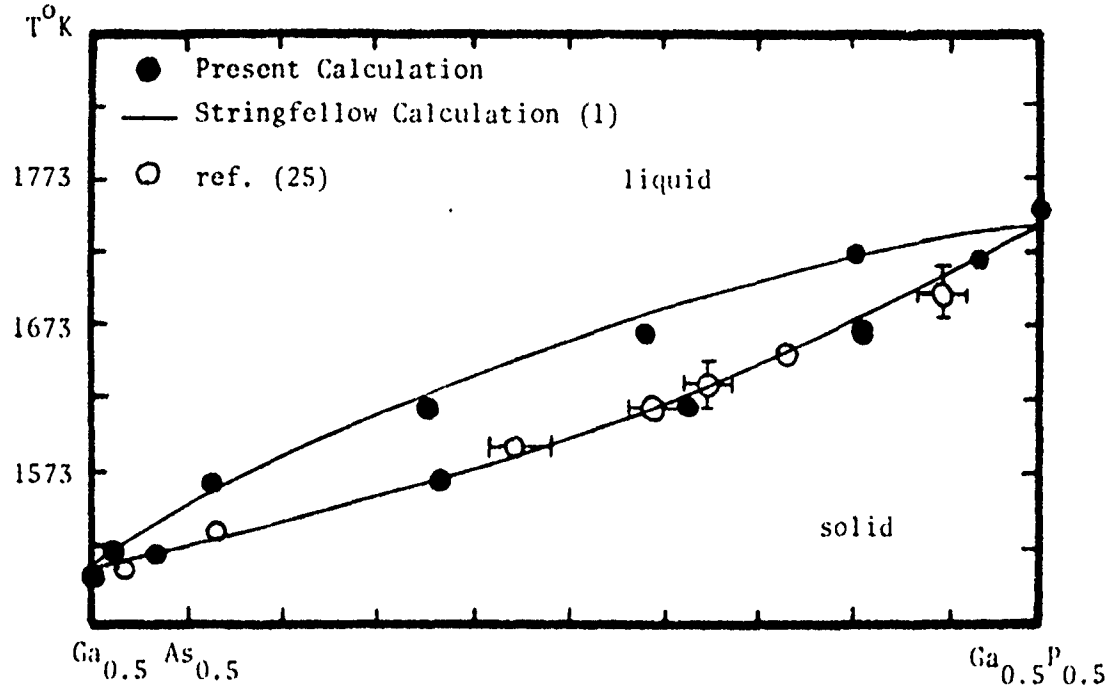

Figure 19. Calculated and Observed Equilibria Along the $Ga_{0.5}As_{0.5}$ - $Ga_{0.5}P_{0.5}$ Quasi-binary Join

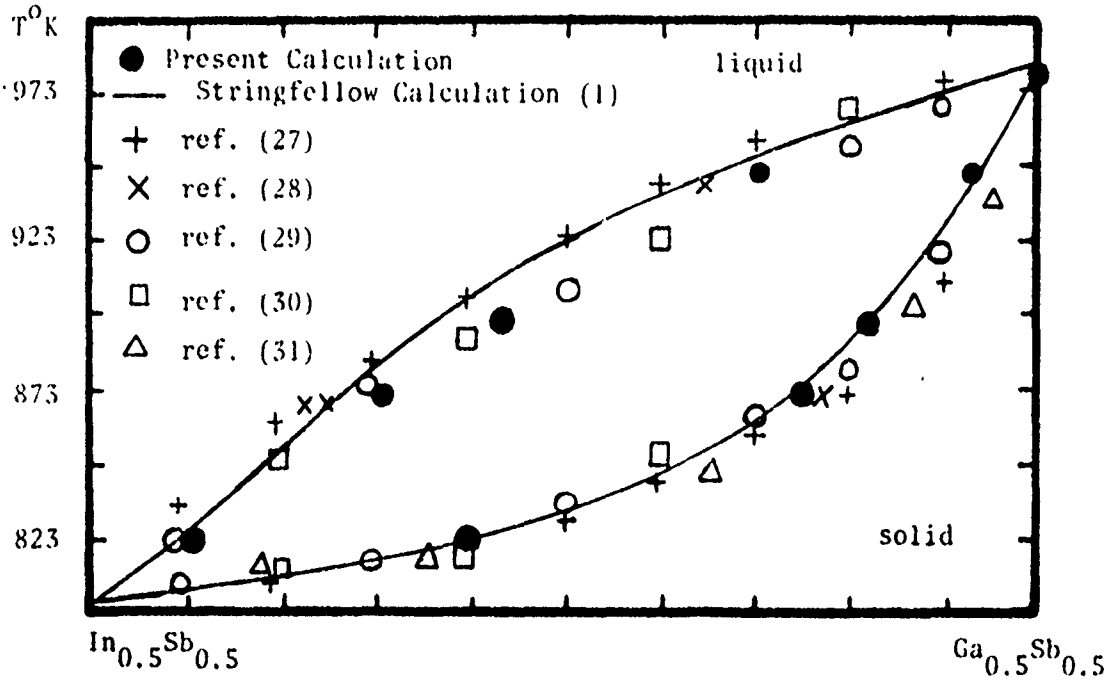

Figure 20. Calculated and Observed Equilibria Along the $In_{0.5}Sb_{0.5}$ - $Ga_{0.5}Sb_{0.5}$ Quasi-binary Join

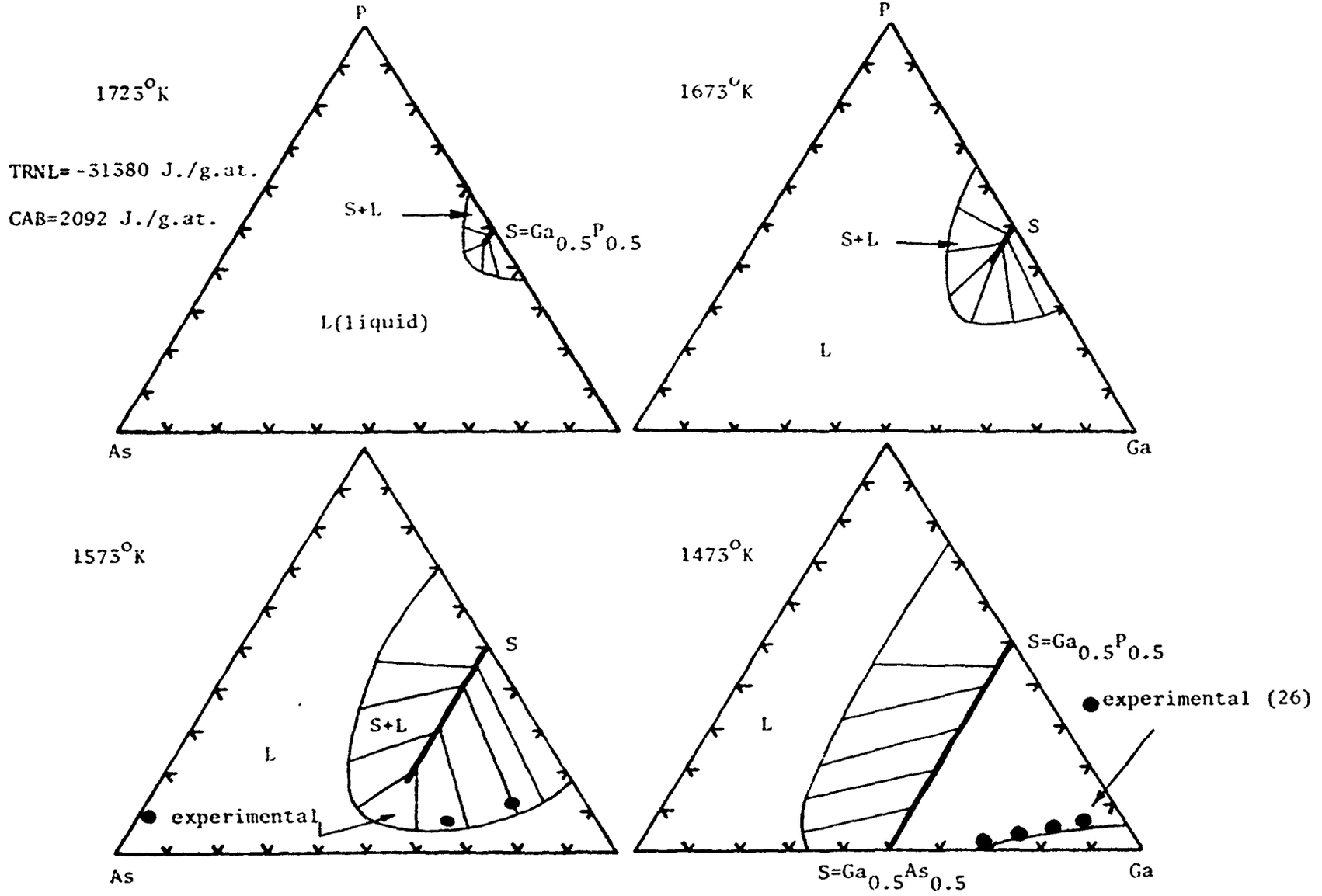

Figure 21. Calculated Partial Isothermal Sections in the Phosphorus-Gallium-Arsenic System. Experimental Values: ref. (26)

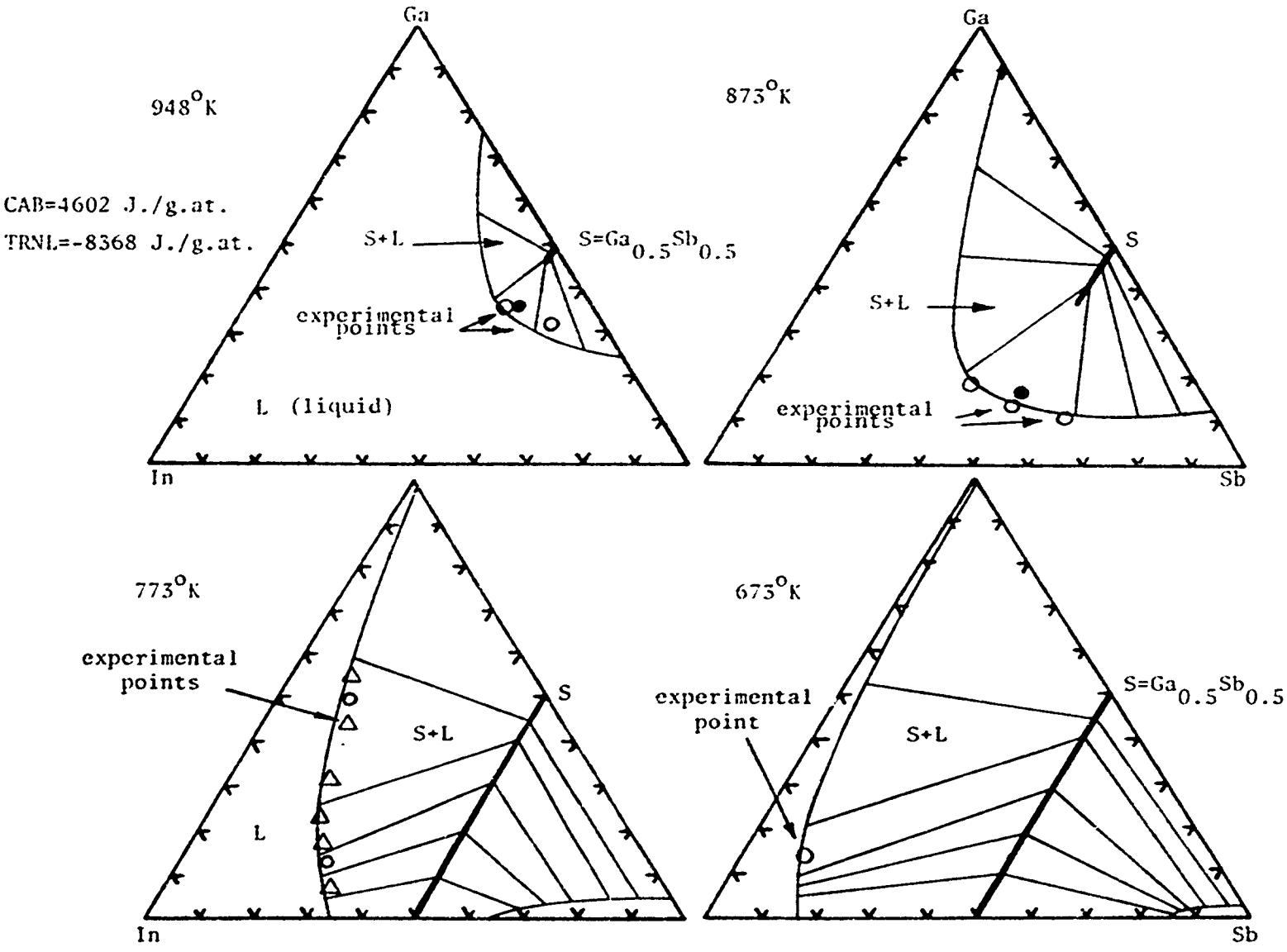

Figure 22. Calculated Partial Isothermal Sections in the Gallium-Antimony-Indium System. Experimental Values: ref. (28,30,32)

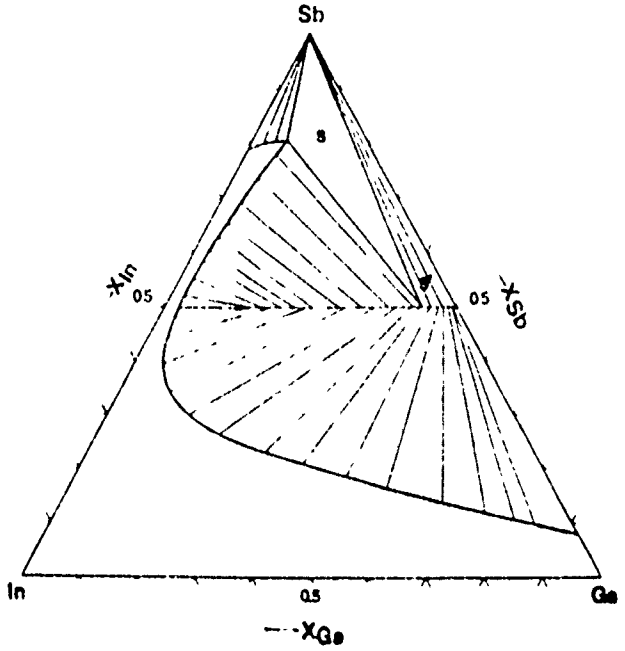

Figure 23. Calculated Partial Isothermal Section in the Sb-Ga-In System at 823°K [after ref. (7)]

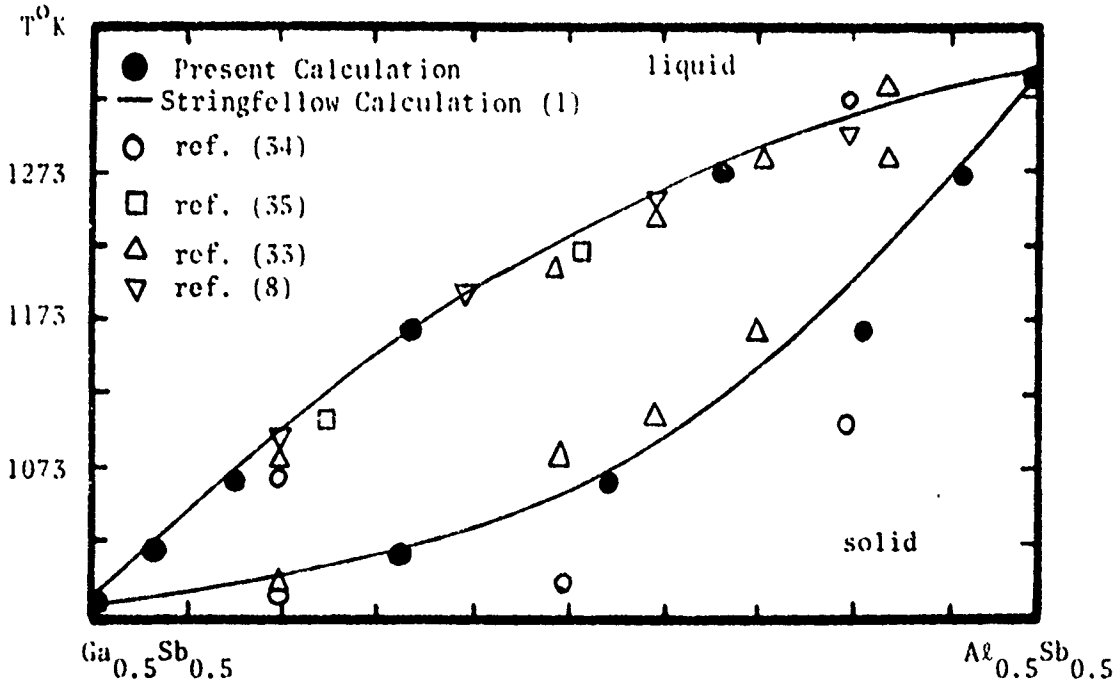

Figure 24. Calculated and Observed Equilibria Along the $Ga_{0.5}Sb_{0.5}$ - $Al_{0.5}Sb_{0.5}$ Quasi-binary Join

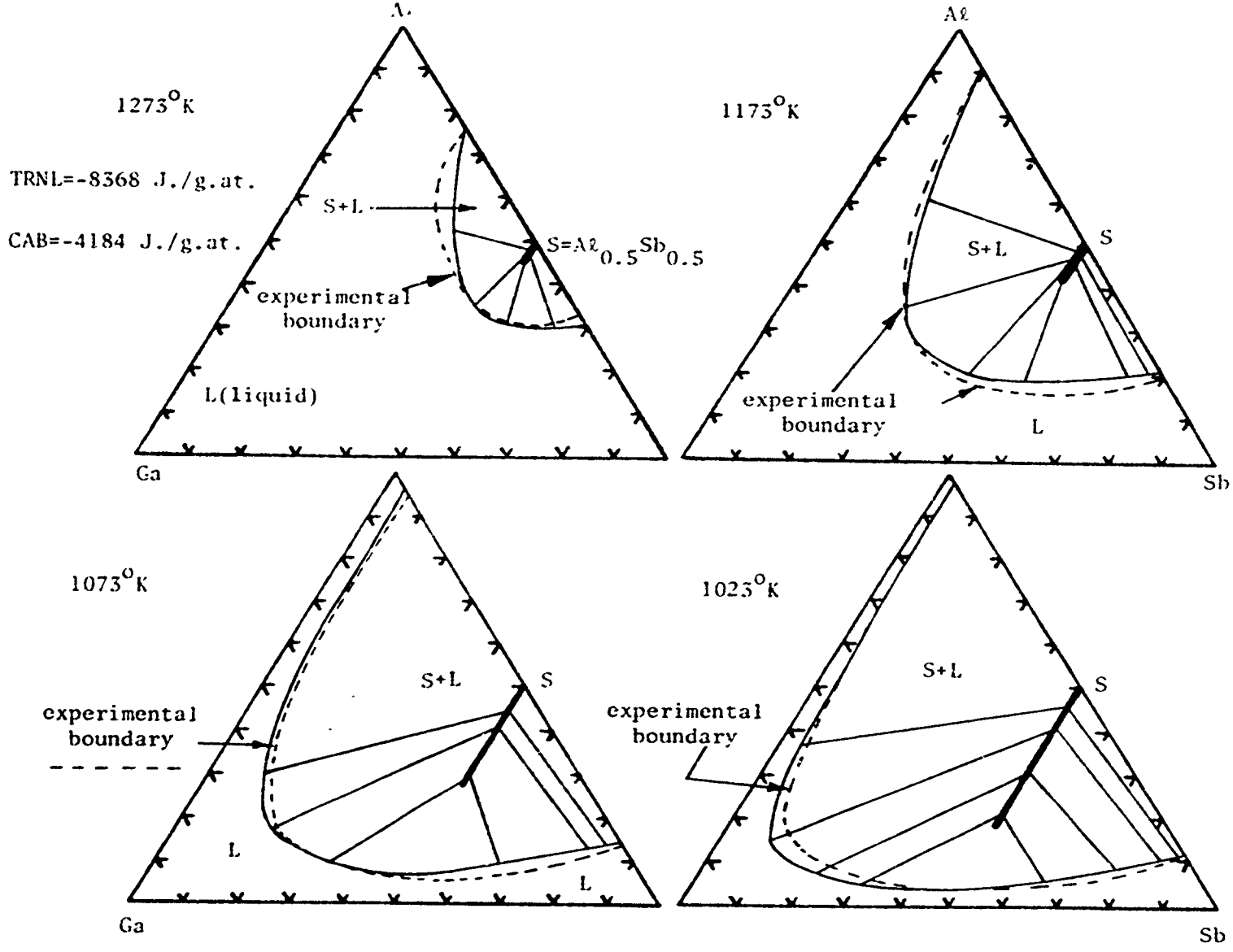

Figure 25. Calculated Partial Isolthermal Sections in the Aluminum-Antimony-Gallium System. Experimental Results: ----- ref. (36)

$Cd_{0.5}Te_{0.5}$-$Hg_{0.5}Te_{0.5}$ quasi-binary join. Liquid phase epitaxial (LPE) growth methods have been employed to circumvent this problem (37), but controlled growth requires a knowledge of the tie-lines between the alloy compound and the liquid. Such information can be generated experimentally with considerable effort. Alternatively, it is possible to use the CALPHAD method, which has been applied to a very wide range of systems, for calculating the ternary Cd-Te-Hg system from a knowledge of the component binary systems in order to provide the required information on tie-line composition. The description provided below provides an account of such calculations.

4. Description of the Vapor, Liquid and Zinc-blende Phases

Table 7 summarizes the current descriptions of the liquid(L), vapor(V) and zinc-blende(S), phases in the cadmium-tellurium-mercury system as a function of temperature (T, °K), pressure (P, atmospheres), atomic fraction tellurium(x), and atomic fraction of mercury(y). These equations, along with the associated lattice stability values relating the free energy of the vapor, liquid, fcc, and stable forms of cadmium, tellurium and mercury, have been assembled by employing existing (38,14-17) thermochemical and phase diagram data for the pure elements and binary systems. Figures 26-31 show the partial binary phase diagrams computed for the Te-Cd, Hg-Cd and Te-Hg systems at P=1 atmosphere and P=16 atmospheres. These phase diagrams follow directly from the ternary equations listed in Table 7 when they are reduced to binary systems for each of the edge binary systems in question. The small ternary terms assigned to the liquid phase (-33472xy(1-x-y)) and the zinc-blende phase (-4180y (1-2y)) Joules/g.at. were chosen in conformity with the experimental results along the $Cd_{0.5}Te_{0.5}$-$Hg_{0.5}Te_{0.5}$ quasi-binary join shown in Figures 32 and 33. Since the maximum value of these terms is attained at x=0.5 and y=0.25, it is apparent that the ternary correction term is at most about -1000 Joules/g.at. for the liquid phase and -500 Joules/g.at. for the zinc-blende phase at the x=0.5, y=0.25 composition. Table 8 compares calculated and observed thermochemical values for $Cd_{0.5}Te_{0.5}$ and $Hg_{0.5}Te_{0.5}$ at 298°K.

Figures 34-36 display calculated isothermal sections in the Cd-Te-Hg systems between 1 and 74 atmospheres at temperatures ranging from 773°K to 1213°K. These calculated isothermal sections show the tie-lines between the zinc-blende and liquid phases in addition to the three phase vapor/liquid/zinc-blende fields which are especially important in crystal growth operations. The calculations of tie-lines can be compared directly with the recent experimental results of Mroczkowski and Vydyanath, who determined tie-line compositions by means of "closed tube tipping experiments". In these experiments, crystals of the zinc-blende phase of fixed composition are equilibrated with the liquid phase in a graphite boat. After equilibration, the temperature was decreased by 5 to 7°C and the liquid was decanted. Subsequent electron microprobe analysis of the concentration profiles along the length of the crystal (from the zinc-blende single crystal phase into the polycrystalline phase, which forms when the contact liquid freezes) permits determination of the tie-line compositions (37). At 818°K, the following comparison can be made between the calculated and observed tie lines.

	Zinc-blende		Liquid	
Atomic Percent	Hg	Cd	Hg	Cd
Observed (37)	32.5	17.5	20.3	2.3
Calculated	32.5	17.5	19.5	2.0

This excellent comparison provides an independent check of the description of the liquid and zinc-blende free energies shown in Table 7. These equations can be used to compute the liquid/vapor/zinc-blende equilibria over a wide range of temperatures and pressures, which, in turn, can be used to define the conditions for stable conventional and LPE growth of Te-rich and Te-poor $(Cd,Hg)_{0.5}Te_{0.5}$ compositions.

5. Conclusions

The examples of calculated III-V and II-VI multi-component systems presented here illustrates the scope and utility of the method presented. The range of systems to which such computations can be applied will expand as additional binary systems are added to the data base.

TABLE 7

SUMMARY OF FREE ENERGY EQUATIONS DESCRIBING THE VAPOR LIQUID, AND ZINC-BLENDE PHASES IN THE CADMIUM-TELLURIUM-MERCURY SYSTEM
(All units in Joules per gram-atom (mole of atoms), °K)

L=liquid phase, V=vapor phase, S=zinc-blende phase, A=fcc
R=rhombohedral (stable Hg), T=trigonal (stable Te), E=hcp (stable Cd)
x=atom fraction Te, y=atom fraction Hg, P=pressure (atmospheres)
R=8.314 J/g.at.°K

Lattice Stability Values

$G^L_{Hg} - G^R_{Hg} = 2292-9.832T$; $\overline{T}=234°K$

$G^A_{Hg} - G^R_{Hg} = 2297-1.464T$

$G^V_{Hg} - G^L_{Hg} = 59174-93.303T+RT\ell nP$

$G^L_{Te} - G^T_{Te} = 17489-24.184T$; $\overline{T}= 723°K$

$G^A_{Te} - G^T_{Te} = 17489-15.816T$

$\frac{1}{2}G^V_{Te_2} - G^L_{Te} = 58409-45.982T+0.5RT\ell nP$

$G^L_{Cd} - G^E_{Cd} = 6192-10.418T$; $\overline{T}=594K$

$G^A_{Cd} - G^E_{Cd} = 1924-2.050T$

$G^V_{Cd} - G^L_{Cd} = 102,520-98.659T+RT\ell nP$

Ternary Phases

$$G^L = (1-x-y)G^L_{Cd} + xG^L_{Te} + yG^L_{Hg} + RT\,[(1-x-y)\ell n(1-x-y)+x\ell nx+y\ell ny]$$
$$-xy(x+y)^{-1}\,[(30962+5.02T)x+(3514+16.74T)y] + y(1-x-y)[-10878+4.184T]$$
$$+x(1-x-y)(1-y)^{-1}[(1-x-y)(112968-159T) -x(75312+20.92T)]- 33472\,xy(1-x-y)$$

$$G^V = (1-x-y)G^V_{Cd} + 0.5x\,G^V_{Te_2} + y\,G^V_{Hg}$$
$$+ RT((1-x-y)\ell n(1-x-y)+x\ell nx+y\ell ny)$$

$$G^S = (0.5-y)\,G^A_{Cd} + 0.5\,G^A_{Te} + y\,G^A_{Hg} + (1-2y)[-61191+13.075T]+2y[-26798+7.11T]$$
$$+ RT[y\ell ny + (0.5-y)\ell n(0.5-y)-0.5\ell n0.5] -4180y(1-2y)$$

$0 \leq y \leq 0.5$

TABLE 8

COMPARISON OF CALCULATED AND OBSERVED (16) FREE ENERGY OF FORMATION AT 298°K

Compound	$\Delta H[298]$ (J./g.at.)	$\Delta S[298]$ (J./g.at.°K)
$Cd_{0.5}Te_{0.5}$	-50900 ± 400 (obs.)	-4.18 ± 1.25 (obs.)
	-51500 (calc.)	-4.14 (calc.)
$Hg_{0.5}Te_{0.5}$	-15900 ± 2100 (obs.)	-6.28 ± 1.26 (obs.)
	-18050 (calc.)	-3.39 (calc.)

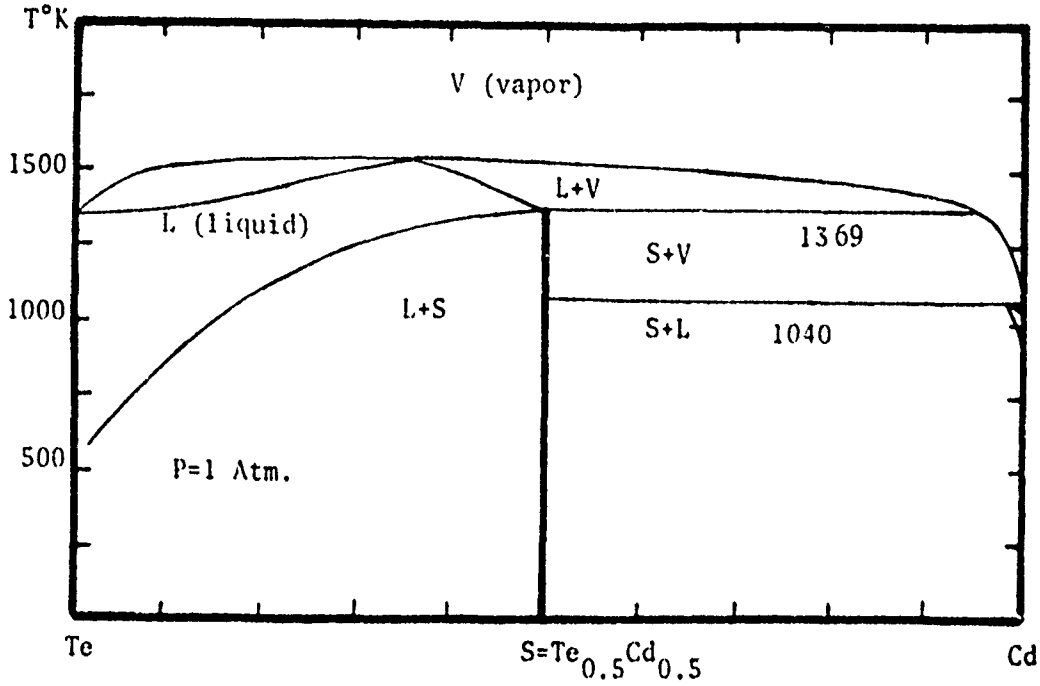

Figure 26. Calculated Partial Te-Cd Phase Diagram at 1 Atmosphere.

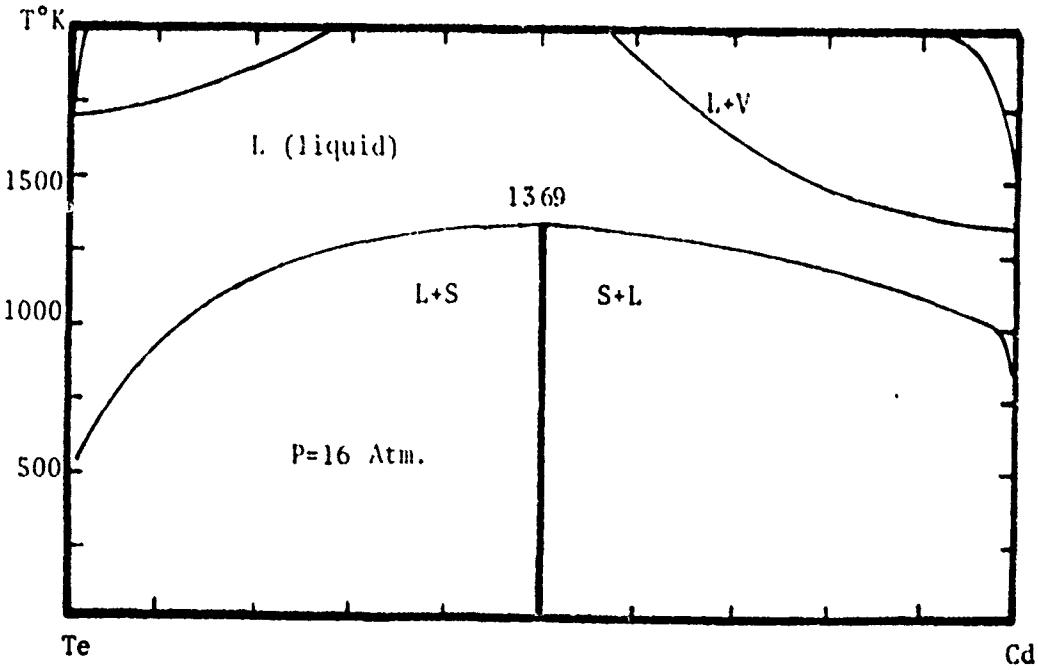

Figure 27. Calculated Partial Te-Cd Phase Diagram at 16 Atmospheres.

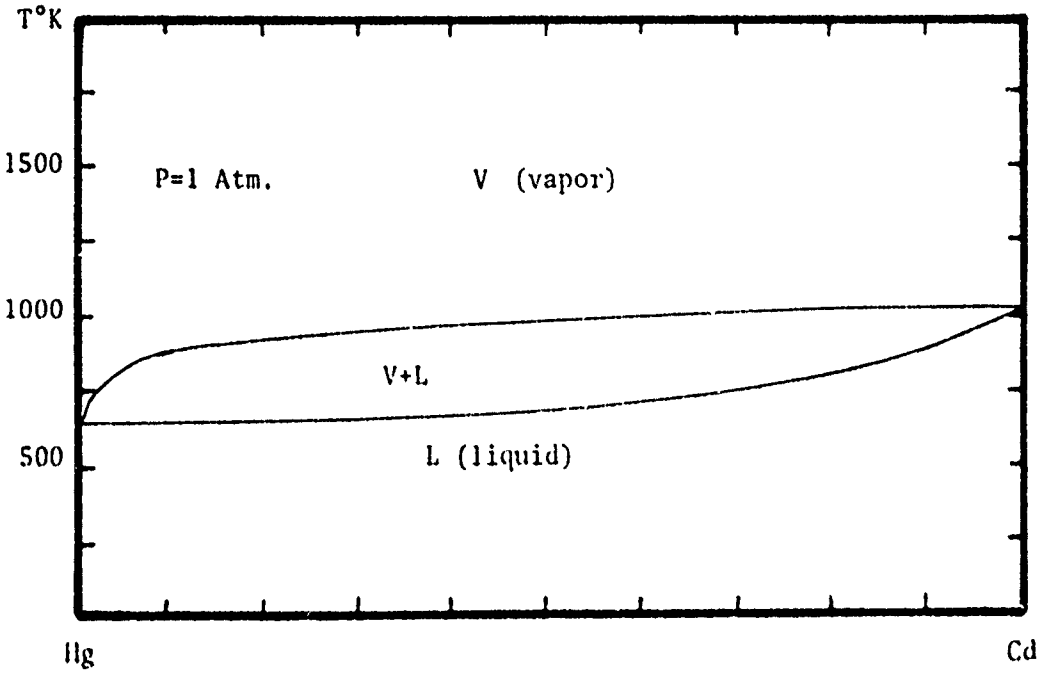

Figure 28. Calculated Partial Hg-Cd Phase Diagram at 1 Atmosphere.

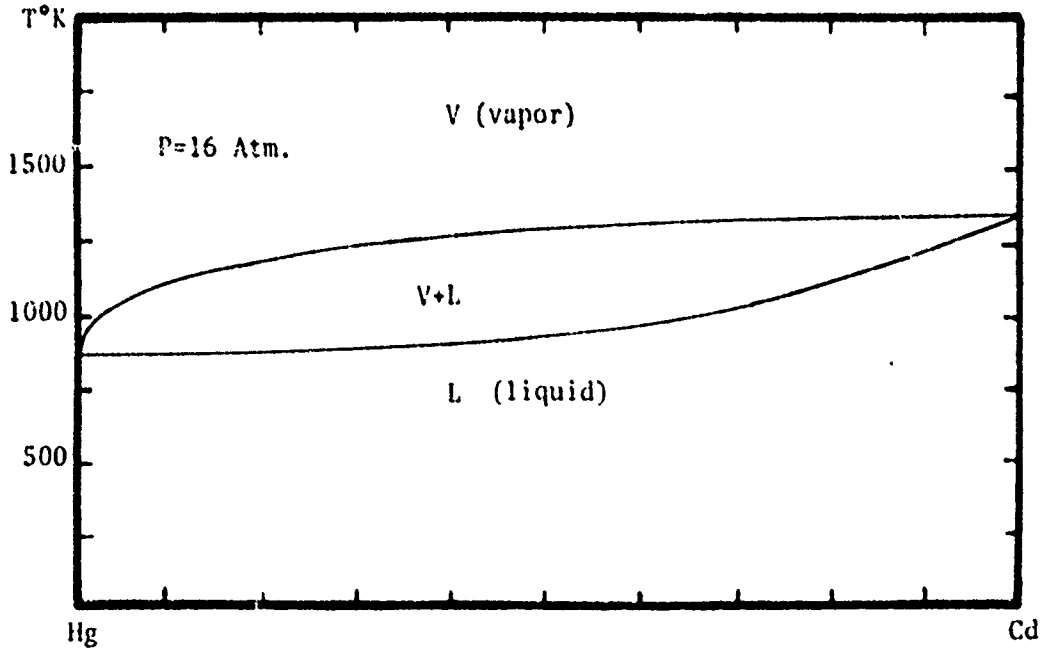

Figure 29. Calculated Partial Hg-Cd Phase Diagram at 16 Atmospheres.

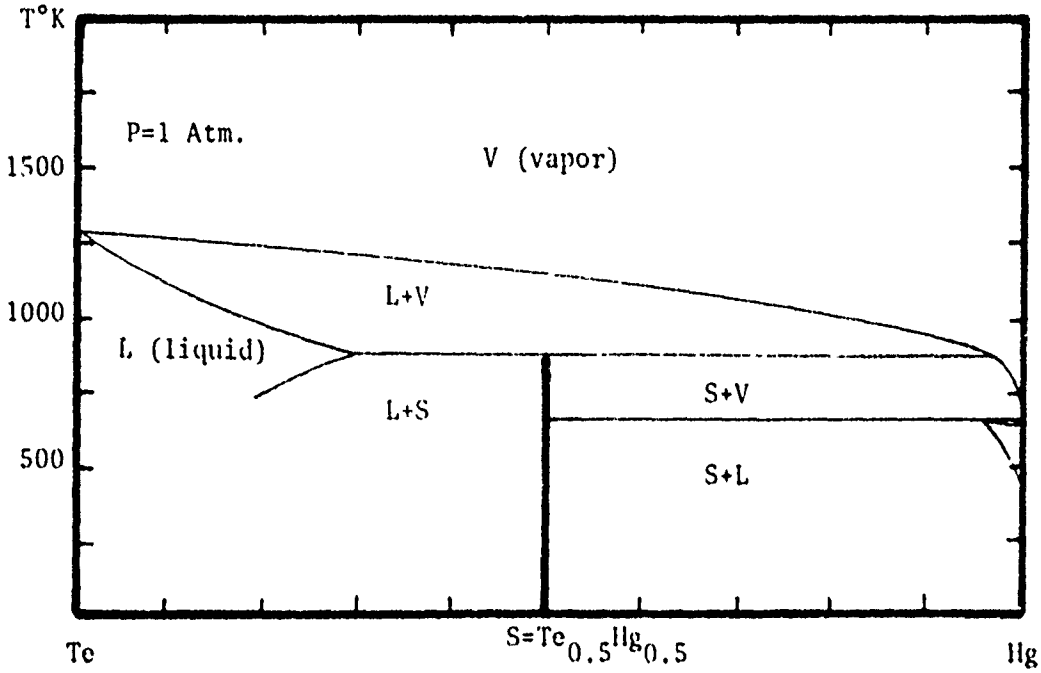

Figure 30. Calculated Partial Te-Hg Phase Diagram at 1 Atmosphere.

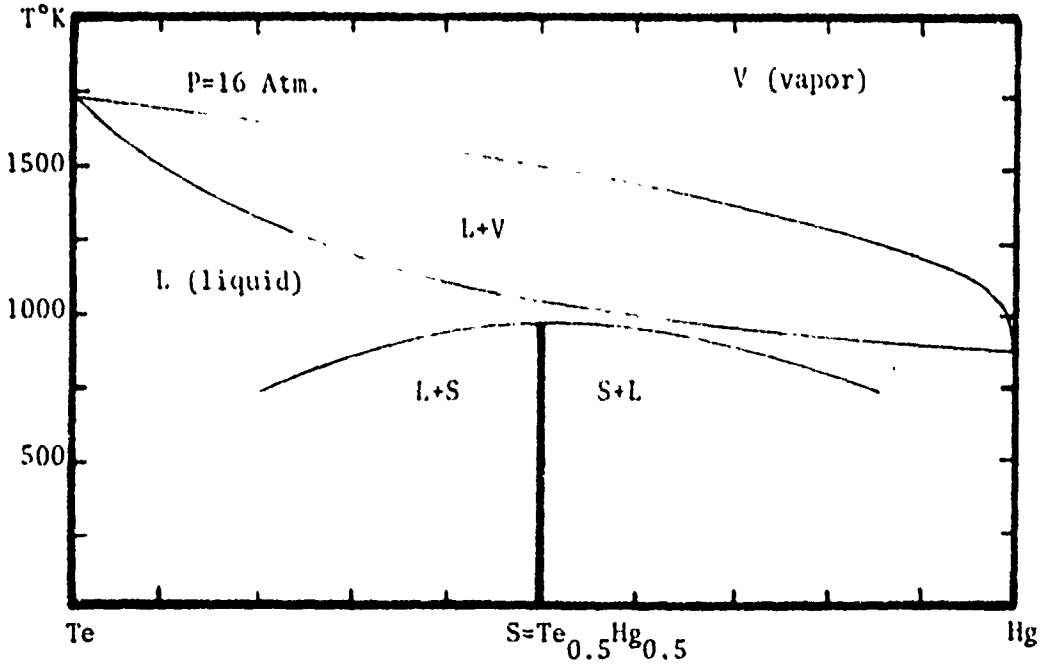

Figure 31. Calculated Partial Te-Hg Phase Diagram at 16 Atmospheres.

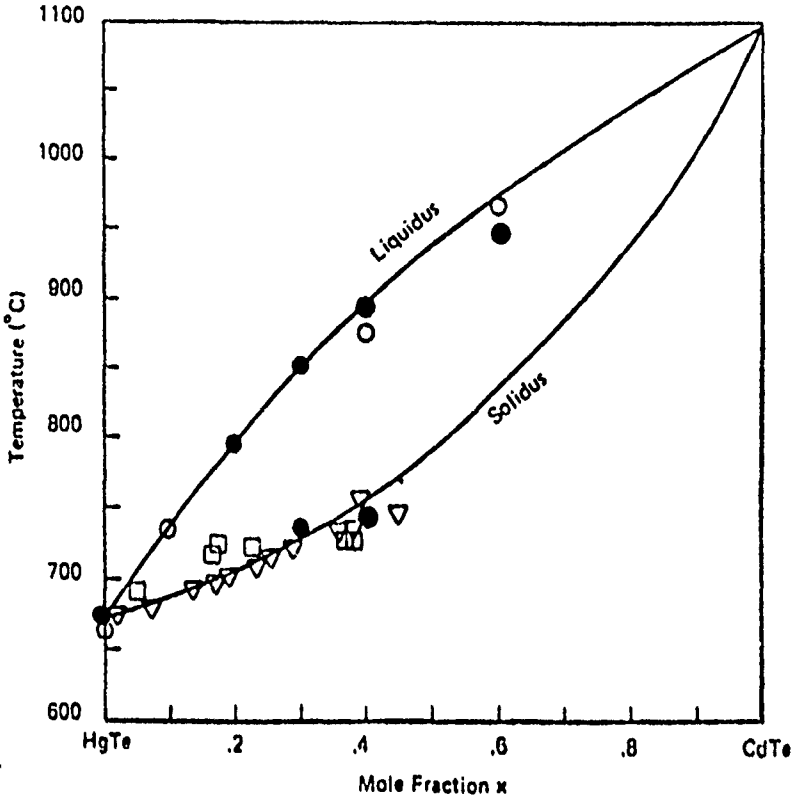

● – Steininger (39)
○ Liquidus Data – Blair and Newnham (40)
▽ Solidus Data – Harman and Strauss (41)
□ Solidus Data – Schmit and Speerschneider (42)

Figure 32. Liquidus and Solidus Curves for Pseudo-binary $Hg_{(1-x)}Cd_xTe$ Compositions (39)

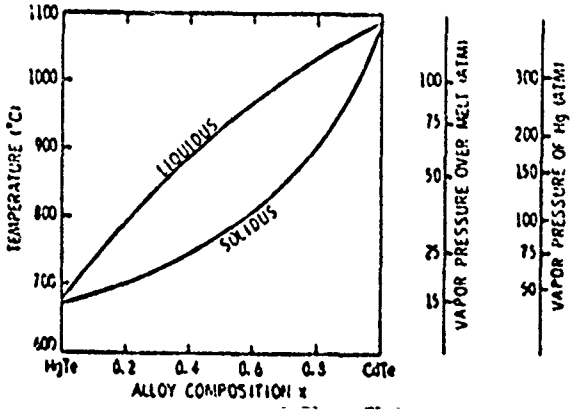

Figure 33. Composite P-T-x Diagram for the Pseudo-binary HgTe-CdTe System (39)

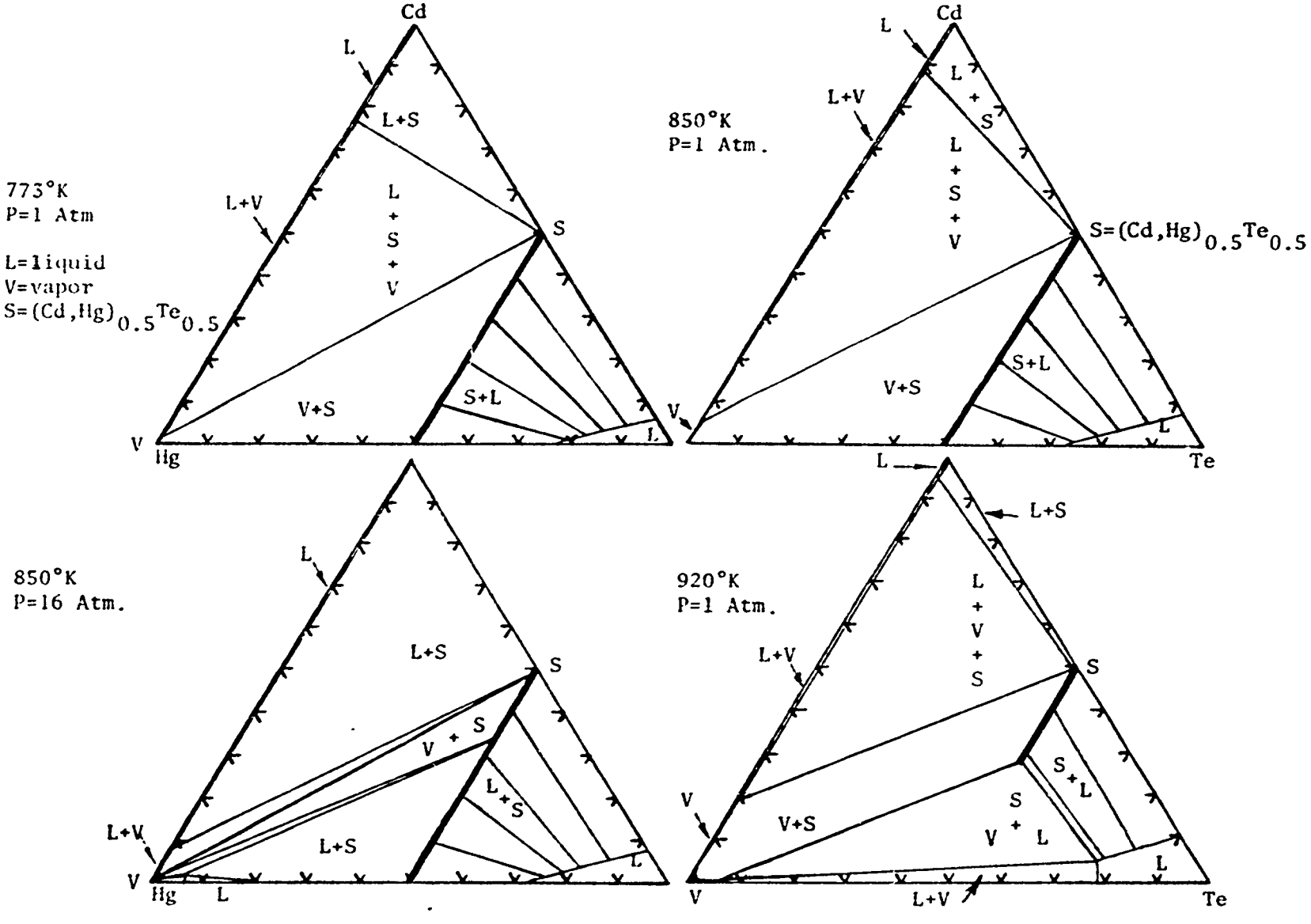

Figure 34. Calculated Isothermal Sections in the Cd-Te-Hg System

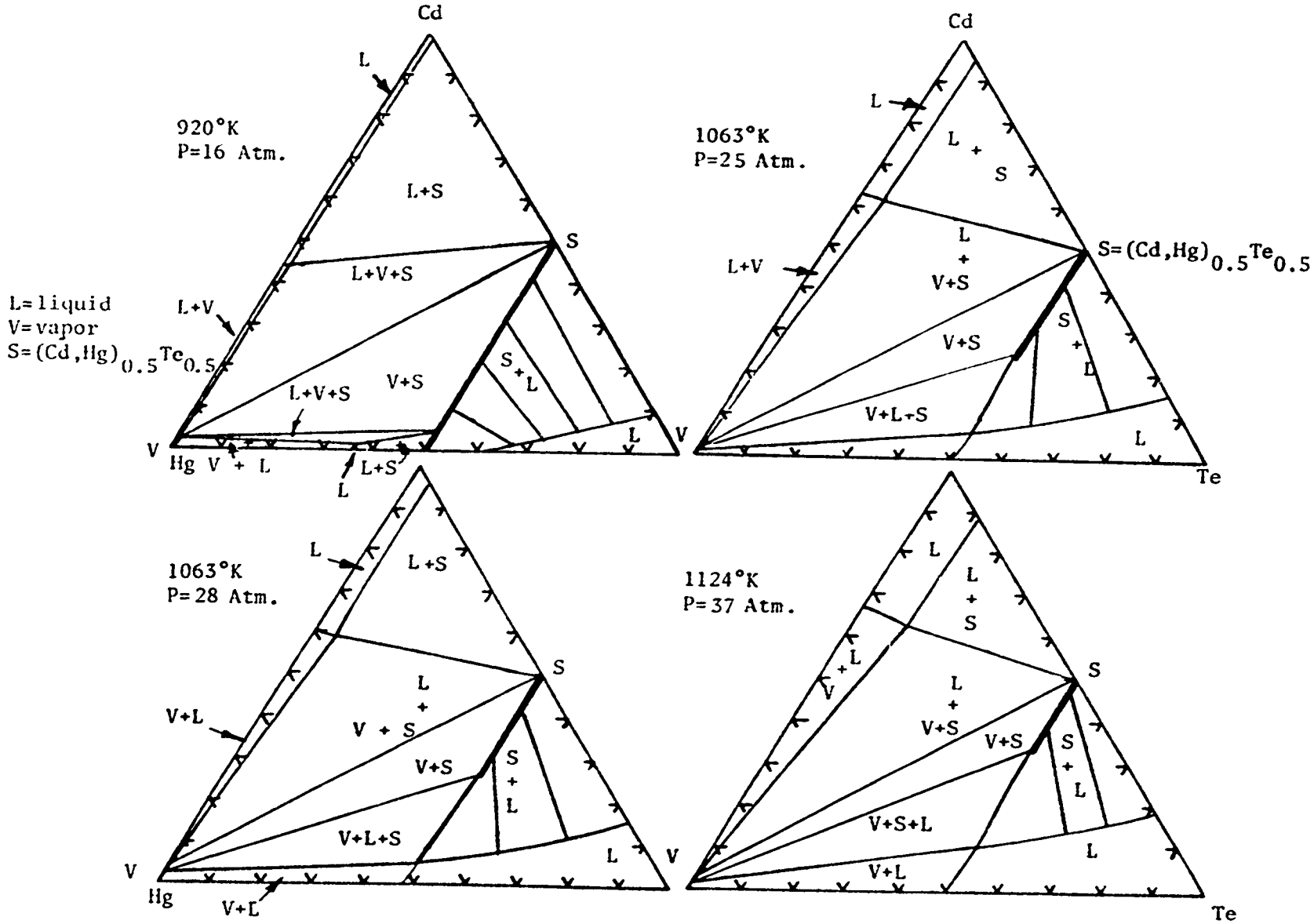

Figure 35. Calculated Isothermal Sections in the Cd-Te-Hg System

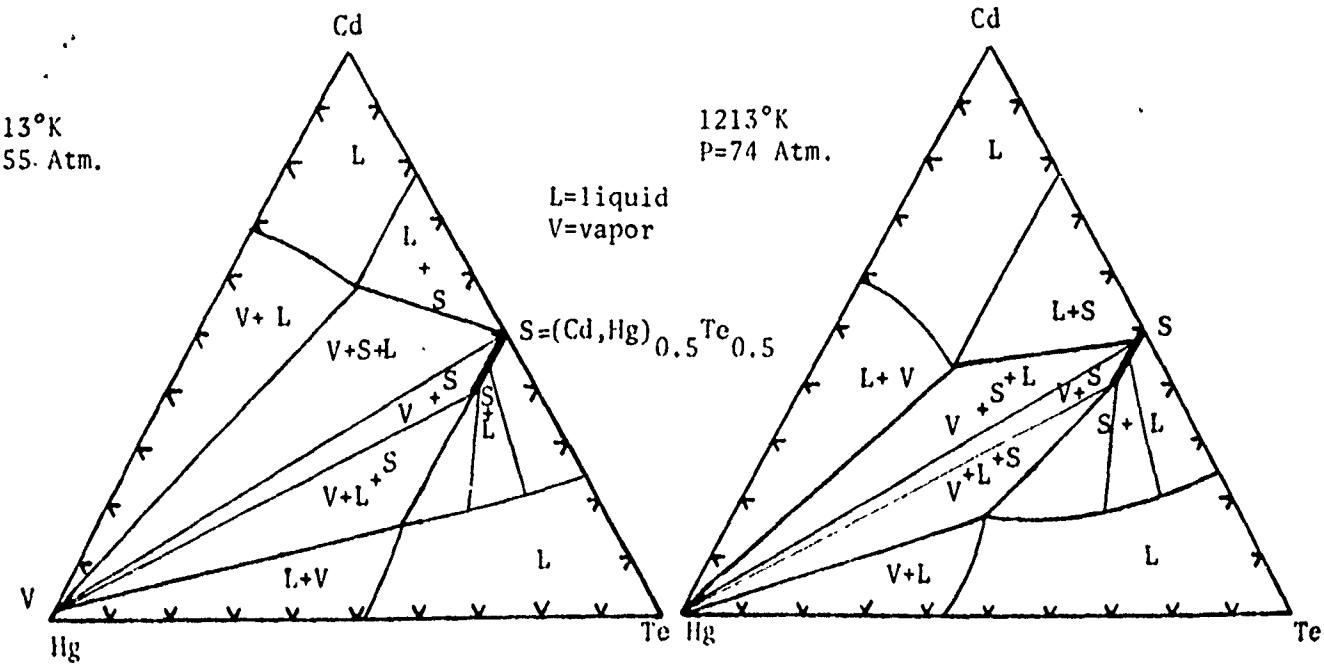

Figure 36. Calculated Isothermal Sections in the Cd-Te-Hg System at 1213°K

References

. G.B. Stringfellow, J. Phys. Chem. Solids 33 665 (1972).
. G.B. Stringfellow, Materials Res. Bulletin 6 371 (1971).
. G.B. Stringfellow and P.E. Greene, J. Electrochemical Soc. 117 1075 (1970).
. G.B. Stringfellow (Ibid.) 117 1301 (1970).
. G.B. Stringfellow, J. Phys. Chem. Solids 35 775 (1974).
. G.B. Stringfellow, J. Crystal Growth 27 21 (1974).
. I. Ansara, M. Gambino and J.P. Bros, J. Crystal Growth 32 101 (1976); CALPHAD 1 27, 40 (1977).
. K. Osamura, K. Nakajima and Y. Murakami, J. Electrochem. Soc. 126 1992 (1979).
. K. Osamura, J. Inoue and Y. Murakami, J. Electrochem. Soc. 119 102 (1972).
. K. Nakajima, K. Osamura and Y. Murakami, J. Electrochem. Soc. 122 1245 (1975).
. R.F. Brebrick, Met. Tr. 8A 403 (1977). Supplemented by CALPHAD 2 17 (1978).
. I. Ansara, J.P. Bros and C. Girard, CALPHAD 2 187 (1978).
. L. Kaufman, CALPHAD 1 7 (1977).
. L. Kaufman, CALPHAD 3 45 (1979).
. L. Kaufman, CALPHAD 3 275 (1979).
. O. Kubaschewski and C.B. Alcock, Metallurgical Thermochemistry, Fifth Edition, Pergamon Press, Oxford (1979).
. R. Hultgren, P.D. Desai, D.T. Hawkins, M. Gleiser and K.K. Kelley, Selected Values of the Thermodynamic Properties of Metals (and Binary Alloys), (2 volumes) ASM, Metals Park, Ohio (1973).
. M. Hansen and K. Anderko, Constitution of Binary Alloys, McGraw-Hill, N.Y. (1958).
. R.P. Elliott and F. Shunk, First and Second Supplements, Ibid. (1965).
. J.W. Wagner and A.G. Thompson, J. Electrochem. Soc., Spring Meeting (1970).
. W. Koster and W. Ulrich, Z. Metallkunde 49 365 (1958).
. J.C. Woolley and B.A. Smith, Proc. Phys. Soc. 72 214 (1950).

5. C. Shih and E.A. Peretti, Tr. ASM 48 709 (1956).
6. G.B. Stringfellow and P.E. Greene J. Electrochem. Soc. 118 805 (1971).
7. K. Osamura and Y. Murakami, Japan J. of App. Phys. 8 967 (1969).
8. M.B. Panish, J. Phys. Chem. Solids 30 1083 (1969).
9. V.B. Usimtsev, A.S. Timoshin and G.V. Kostin, Neorg. Mat. 7 2090 (1971).
10. G.M. Blom and T.S. Plaskett, J. Electrochem. Soc. 118 1831 (1971).
11. J.C. Woolley and D.G. Lees, J. Less-Common Metals 1 192 (1959).
12. J.C. Woolley B.A. Smith and D.G. Lees, Proc. Phys. Soc. London, 69B 1339 (1956).
13. J.C. Woolleyand B.A. Smith, Proc. Phys. Soc. London 72 214 (1958).
14. G.A. Antypas, J. Cryst. Growth 16 181 (1972).
15. A.S. Borschevskii, I.I. Burdiyan, E.Yu. Lubenskaya and E.V. Sokolova, Zh. Nauch. Khim 4 2824 (1959).
16. I.I. Burdiyan and A.S. Borschevskii, Sov. Phys. Tech. Phys. 3 2451 (1958).
17. J.F. Miller, H.L. Goering and R.C. Himes, J. Electrochem. Soc. 107 527 (1960).
18. K.Y. Cheng and G.L. Pearson, J. Electrochem. Soc. 124 753 (1977).
19. J.A. Mroczkowski and H.R. Vydyanath, "Liquid Phase Epitaxial Growth of $(Hg_{(1-x)}Cd_x)$ Te from Tellurium Rich Solutions Using a Closed Tube Tipping Technique", J. Electrochem. Soc. 128 655 (1981).
20. R.F. Brebrick and A.J. Strauss, J. Phys. Chem. Solids, 26 989 (1965).
21. J. Steininger, J. Elect. Materials, 5 299 (1976).
22. J. Blair and R.Newnham, Metallurgy of Elemental and Compound Semiconductors, Interscience Publishers Inc., New York (1961)vol. 12.
23. T.C. Harman and A.J. Strauss, J. Appl. Phys. (Suppl.) 32 2265 (1961).
24. J.L. Schmit and C.J. Speerschneider, Infrared Physics 8 247 (1968).
25. K. Osamura and Y. Murakami, J. Phys. Chem. Solids, 36 931 (1975).

CALCULATION OF ORDERING TEMPERATURES FOR THE QUASI-BINARY SECTION Fe_3Al - Fe_3Si

1. Introduction

Where limited experimental data is available, the method adopted by Inden (1-7) is attractive because it requires only two ordering parameters for each of the three component binary systems, provided the temperatures of interest are above any magnetic transition temperatures. These ordering parameters are the first and second nearest neighbor (chemical) interaction parameters denoted $W^{(1)}$ and $W^{(2)}$. These can be related to heats of formation as well as critical ordering temperatures, as will be shown in the following section. The Fe-Si binary system (Fig. 1) has already been characterized in some detail (3,4) and the previously determined values of $W^{(1)}_{Fe\text{-}Si}$ and $W^{(2)}_{Fe\text{-}Si}$ have been used unaltered in the present work Table I). Their validity has been confirmed by the successful prediction of ordering equilibria in ternary Fe-Si-Co alloys (8). The Fe-Al system is inherently more complicated (9,10) (Fig. 2) and several additional effects have been recently added by KÜster et al (11). Nonetheless the major features have been reproduced by the simplified Inden model(12). Only a minor change has been made in the value of $W^{(1)}_{Fe\text{-}Al}$ used previously by Inden (6) in the light of the available experimental data for Fe-Si-Al alloys (Table II). The derivation of suitable values of suitable $W^{(1)}_{Si\text{-}Al}$ and $W^{(2)}_{Si\text{-}Al}$ values poses a problem in so far that all experimentally accessible properties for these alloys refer to either FCC Aluminum or diamond cubic Silicon. One has therefore to extract the relevant values of $W^{(1)}_{Si\text{-}Al}$ and $W^{(2)}_{Si\text{-}Al}$ from whatever data is available for BCC ternary alloys.

2. Experimental Information on Fe-Al-Si Alloys

Lihl, Burger, Sturm and Ebel (14) have given a general indication of the location of the ordering region in Fe-Al-Si alloys (Fig. 3). However there is considerable divergence between this estimate and the investigation of Katsnel'son and Polishchuk (13). More weight has been given to the latter work as it utilized relative intensities of superlattice lines (Fig. 4) whereas the work by Ebel et al merely interpreted changes in d-spacing as ordering effects. An NMR study of $Fe_3Si_{(1-x)}Al_x$ alloys (15) suggests that Aluminum and Silicon substitute interchangeably on one specific sublattice, which confirms that the interaction energy between Silicon and Aluminum is relatively low.

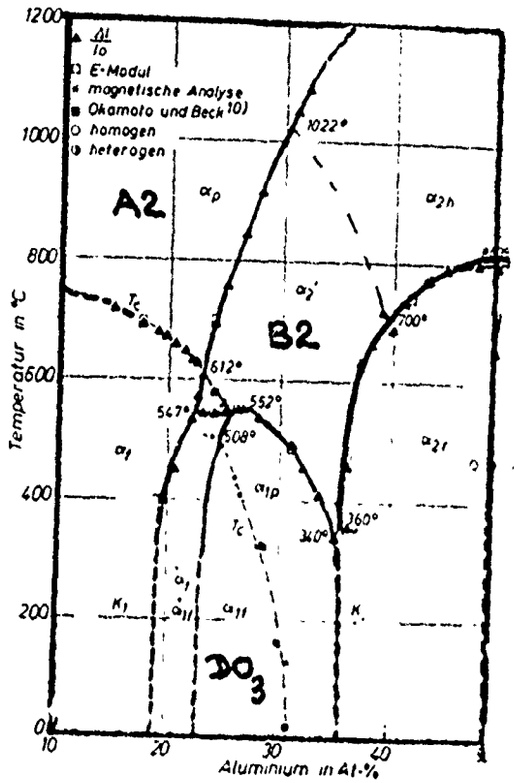

Fig. 1 Iron-Aluminum Diagram

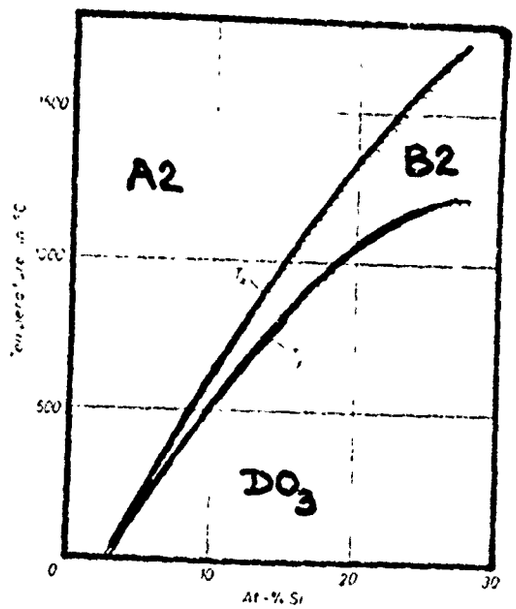

Fig. 1. Configuration diagram of bcc, paramagnetic iron-silicon solid solutions

Fig. 2 Iron-Silicon Diagram

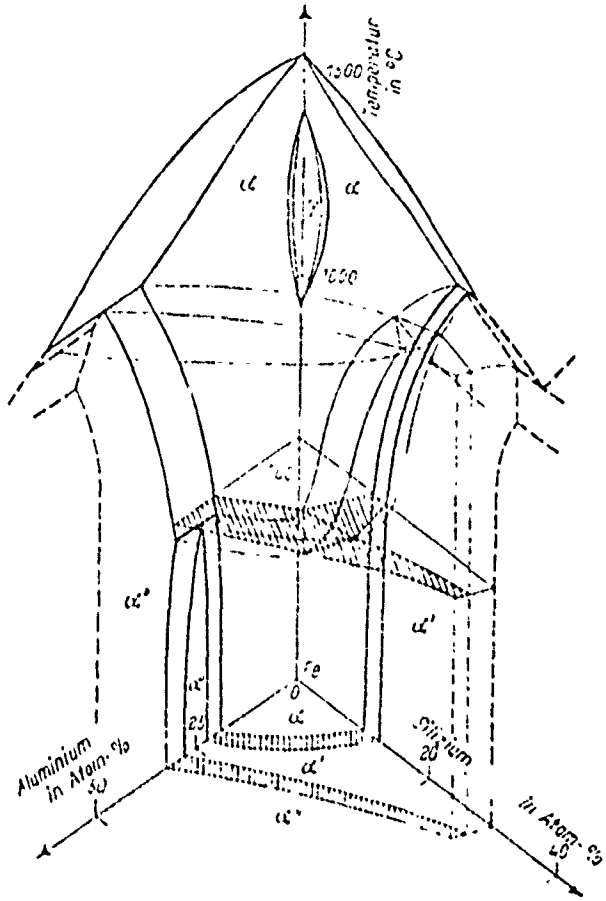

Fig. 3 Suggested Ternary Phase Boundaries for Fe-Al-Si alloys from F. Lihl et al (14)

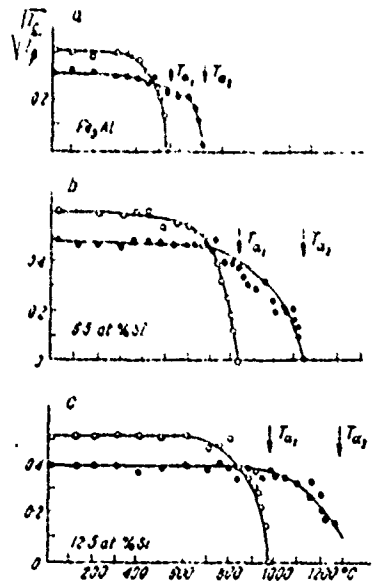

Fig. 4 Critical Temperatures suggested by the temperature dependence of superstructure lines from Katsnel'son (13)

3. Ordering Model

(a) Definition of order parameters

The main feature of the BWG model is the description of atomic distributions inside specifically defined sublattices. The choice follows from the kind of interaction between atoms. Any BCC lattice may be divided into four FCC sublattices, I, II, III, and IV, with the atomic configurations described by occupation probabilities 'p_i^L' of sublattice site 'L' by the component 'i'. (Fig. 5)

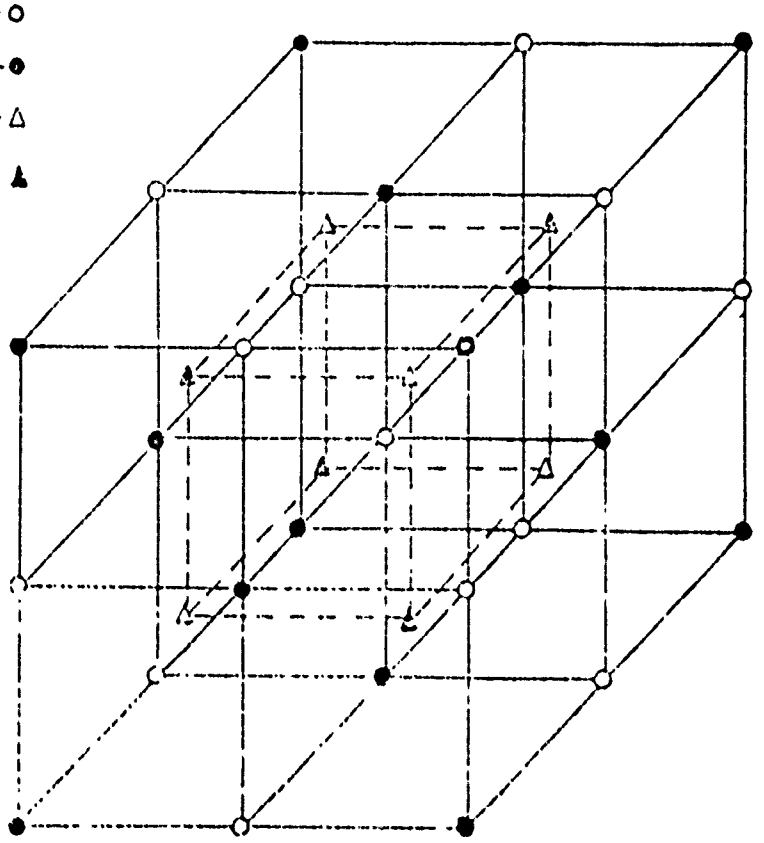

Fig. 5 Relative position of sublattices in the DO_3 structure.

The atomic configuration in a binary alloy A_CB_{1-C} can then be described with the aid of the following three parameters, which are a combination of the independent occupation probabilities p_i^L.

$$x = \tfrac{1}{4}\,(p_A^{I} + p_A^{II} - p_A^{III} - p_A^{IV}) \qquad (1a)$$

$$y = \tfrac{1}{2}\,(p_A^{III} - p_A^{IV}) \qquad (1b)$$

$$z = \tfrac{1}{2}\,(p_A^{I} - p_A^{II}) \qquad (1c)$$

The greatest value of these parameters corresponds to the highest degree of order, and the concentrations of A and B, (C_A and C_B) set limits on the values of x, y and z. For the binary case these are given by:

$$(a) \qquad 0 \leq x \leq C_B \qquad \text{for } 0 \leq C_B \leq 0.5 \qquad (2a)$$

$$(b) \qquad 0 \leq y \leq \min\,(C_A - x,\ C_B + x) \qquad (2b)$$

$$(c) \qquad 0 \leq z \leq \min\,(C_A + x,\ C_B - x) \qquad (2c)$$

Case 1

The random BCC lattice (A2) has an equal distribution of the atoms on the four sublattices and corresponds to $x = y = z = 0$.

Case 2

The state $x \neq 0$, $y = z = 0$ indicates 'A' preferentially occupying sublattices I and II ($x > 0$), or III and IV ($x < 0$). It follows that the number of AB neighbors in nearest neighbor (n.n) positions is increased, i.e. this corresponds to the B2 structure.

Case 3

It follows that $y \neq 0$, describes a surplus of A atoms in next nearest neighbor (n.n.n) positions, which corresponds to the DO_3 structure. As far as the present problem is concerned we need not consider z. (See Refs. 1,2)

(b) Free Energy Expressions and Interaction Parameters

The most stable atomic configuration then follows from the minimum value of the configurational free energy/mole ΔG^{BCC} which is given by:

$$\Delta G^{BCC}_{BINARY} = U^o - NC_AC_B\,(4W^{(1)} + 3W^{(2)}) - \frac{N}{4}\left[(8\,W^{(1)} - 6W^{(2)})\,x^2 + 3W^{(2)}\,(y^2 + z^2)\right] + \frac{NkT}{4}\sum_L\left[p_A^L \ln p_A^L + p_B^L \ln p_B^L\right] \qquad (3)$$

U^o is the internal energy of pure components; the second term is the energy of mixing; the third term gives the energy contribution due to ordering, and the fourth term is the entropy contribution of the configuration which is also expressed in terms of x, y, z. N is Avagadro's number, and k the Boltzmann constant. $W^{(1)}$ and $W^{(2)}$ are defined below and for eqn (3) to be valid, these must be expressed in k units where 1 k unit = 3.3×10^{-24} cal or 13.8×10^{-24} J. The values of $W^{(1)}$ and $W^{(2)}$ are related to the nearest and next nearest neighbor bond energies, $v_{ij}^{(k)}$ as follows:

$$W(1) = -2V_{AB}^{(1)} + V_{AA}^{(1)} + V_{BB}^{(1)} \qquad (4a)$$

$$W(2) = -2V_{AB}^{(2)} + V_{AA}^{(2)} + V_{BB}^{(2)} \qquad (4b)$$

According to this definition, positive values for $W^{(1)}$ and $W^{(2)}$ correspond to greater affinity between unlike atoms. All interchange energies are presumed to be independent of temperature and of environment of other atom sites where the interchange process is considered.

If the values of $W^{(1)}$ and $W^{(2)}$ are known, ΔG^{BCC} can be calculated with respect to the ordering parameters x, y, z using the necessary equilibrium conditions including particularly:

$$\frac{\partial G}{\partial x} = \frac{\partial G}{\partial y} = \frac{\partial G}{\partial z} = 0 \; ; \quad (T, C) \qquad (5)$$

and other subsidiary conditions.

(c) Expressions for critical ordering temperatures in binary alloys

The critical temperatures $T_x(A2/B2)$, $T_y(B2/DO_3)$, define the regions in which minimum free energy is obtained by the A2, B2 and DO_3 configurations respectively. For the binary case these are given by:

$$kT_x = kT^{A2/B2}_{(BWG)} = (8W^{(1)}_{BWG} - 6W^{(2)}_{BWG}) \cdot C_A C_B \qquad (6a)$$

$$kT_y = kT^{B2/DO_3}_{(BWG)} = 6W^{(2)}_{BWG} \cdot (C_A - x)(C_B + x) \qquad (6b)$$

where x is the appropriate value of the ordering coefficient at the temperature T_y.

Since $W^{(K)}$ are energy parameters, they are most easily determined from energy measurements like enthalpies of mixing of random alloys, or enthalpies of formation ΔH (C,T) of alloys with given atomic configurations. These entities can immediately be expressed by means of $W^{(K)}$ for a binary alloy $A_{1-C}B_C$ with reference to the pure components in the same crystal structure as the alloy formed. For BCC alloys:

$$\Delta H^{A2} = -N\,C(1-C)\left[4W^{(1)} + 3W^{(2)}\right] \qquad \ldots\ (7)$$

$$\Delta H^{B2} = -N\left[C(4W^{(1)} + 3W^{(2)}) - 6C^2\,W^{(2)}\right] \quad \text{for } C < 0.5$$

$$\Delta H^{DO_3} = -N\,C\,(4W^{(1)} + 3W^{(2)}) \quad \text{for } 0 < C < 0.25$$

$$\text{OR} \quad = -N\left[1.5W^{(2)} + C(4W^{(1)} - 3W^{(2)})\right] \quad \text{for } 0.25 < C < 0.5$$

$$\Delta H^{B32} = -N\left[C\,(4W^{(1)} + 3W^{(2)}) - 4C^2\,W^{(1)}\right] \quad \text{for } C < 0.5$$

$W^{(K)}_{BWG}$ values obtained from an analysis of critical temperatures (e.g. via equations 6a, 6b), can be related to the $W^{(K)}$ values in thermochemical equations (e.g. equ. 7) by a scale factor x (listed in Table 1). See References (1&2). (The differences between $W^{(K)}$ and $W^{(K)}_{BWG}$ are essentially due to the omission of short range order in the BWG model.)

4. Expressions for the Free Energy and critical ordering temperature in ternary alloys as used in the present work

In the ternary case there is a slight difference in the definition of the order parameters (5). If the total number of atoms is N, distributed over $4N_o$ lattice sites, the occupation probabilities p_i^L (i = A,B,C,; L = I, II, III, IV) are combined to give the order parameters as follows:

$$(a)\quad x_j = \tfrac{1}{4}\,(p_j^{I} + p_j^{II} - p_j^{III} - p_j^{IV}) \qquad (8a)$$

$$(b)\quad y_j = \tfrac{1}{2}\,(p_j^{III} - p_j^{IV}) \qquad (8b)$$

$$(c)\quad z_j = \tfrac{1}{2}\,(p_j^{I} - p_j^{III}) \qquad (8c)$$

with j = A, B

A similar condition to Equation (5) occurs except now there are two x parameters, two y parameters and two z parameters, corresponding to the degree of order of two solutes and not just one. For the purpose of determining T_x and T_y temperatures it is only necessary to consider x_A and x_B. The limiting values of x_A, x_B in the ternary case are:

(a) The maximum value of x_A is the smaller of a or (1-a). (9a)

(b) The maximum value of x_B is the smaller of b or $(c - x_A)$ (9b)

In the specific case of $Fe_3Al_{(1-x)}Si_x$ alloys, where a = Fe, b = Al and c = Si, this leads to a situation where (a) is always 0.75 and therefore $x_{A(max)} = 0.25$. Likewise since c = (1-a-b), $x_{B(max)} = -b$. The configurational free energy/mole ΔG of the three-component solid solution is then given by:

$$\begin{aligned}\Delta G^{(BCC)} = U_o - N\Big\{ & 4\,(C_AC_BW^{(1)}_{AB} + C_AC_CW^{(1)}_{AC} + C_BC_CW^{(1)}_{BC}) \\ & + 3(C_AC_BW^{(2)}_{AB} + C_AC_CW^{(2)}_{AC} + C_BC_CW^{(2)}_{BC})\Big\} \\ & - \frac{N}{2}\Big\{ E^R_{AC}\,x_A^2 + E^R_{BC}\,x_B^2 + (E^R_{AC} + E^R_{BC} - E^R_{AB})\,x_A\,x_B \\ & + 3W^{(2)}_{AC}\,(y_A^2 + z_A^2) + 3W^{(2)}_{BC}\,(y_B^2 + z_B^2) + 3(W^{(2)}_{AC} + W^{(2)}_{BC} \\ & - W^{(2)}_{AB})\,(y_Ay_B + z_Az_B)\Big\} - \frac{NkT}{4}\sum_i\sum_L p_i^{(L)} \ln p_i^{(L)}\end{aligned} \qquad \ldots (10)$$

where $E^R_{ij} = \left(8\,W^{(1)}_{ij} - 6W^{(2)}_{ij}\right)$

$$k\,T_x^{BWG}(A2/B2) = 0.5\left\{\sum_{ij} C_iC_jE_{ij} + \sqrt{\left(\sum_{ij} C_iC_jE_{ij}\right)^2 - 4C_AC_BC_C\,(E_{AC}E_{BC}) \cdots}\right.$$

$$\left. \cdots - \frac{1}{4}\left[E_{AC} + E_{BC} - E_{AB}\right]^2\right)\Big\} \qquad \ldots (11)$$

where ij = AB, AC, BC and $E_{ij} = \left(8W^{(1)}_{ij} - 6W^{(2)}_{ij}\right)_{BWG}$

$$k\,T_y^{BWG}(B2/L2_1) = 3\left\{\Omega + \sqrt{\Omega^2 - 4W^{(2)}_{AC}\,W^{(2)}_{BC} - \left[W^{(2)}_{AC} + W^{(2)}_{BC} \cdots\right.}\right.$$

$$\left.\left. \cdots - W^{(2)}_{AB}\right]^2\right\}_{BWG}(C_A - x_A)\,(C_B - x_B)\,(C_C + x_A + x_B)\Big\} \quad \ldots (12)$$

where $\Omega = (W^{(2)}_{AC})_{BWG}\,(C_B + C_C + x_A)\,(C_A - x_A)$

$$+ (W^{(2)}_{BC})_{BWG}\,(C_A + C_C + x_B)\,(C_B - x_B)$$

$$- \left[W^{(2)}_{AC} + W^{(2)}_{BC} - W^{(2)}_{AB}\right]_{BWG}(C_B - x_B)\,(C_A - x_A);$$

and x_A and x_B are the values of the order parameter in nearest neighbour positions at $T = T_y$.

5. Calculation of T_x and T_y for the Fe-Al-Si System

The following procedure was adopted to obtain optimum values of $W^{(1)}$ and $W^{(2)}$ (BCC Al-Si). Examination of various pairs of solutes shows that for BCC alloys $W^{(2)}/W^{(1)} \approx 0.5$, as is indeed the case for the other pairs concerned in the present case (Table I). It was therefore assumed that $W^{(2)}/W^{(1)}$ BCC (Al-Si) = 0.5. Inspection of the superlattice intensities Fig. (5) show that a considerable degree of order exists in the B2 lattice prior to DO_3 formation; the maximum theoretical values of x_A and x_B can therefore be used in preliminary calculations.

Trial values of $W^{(1)}_{Al\text{-}Si}$(BCC) were then inserted into equations until a reasonable fit was obtained for both T_x and T_y for a selected alloy composition.

As shown in (Fig. 6) there is a limit beyond which further changes in $W^{(1)}$ (and $W^{(2)}$) are counterproductive, which reflects the assumption that the real values of x_A and x_B are lower than the maximum values assumed in this preliminary calculation. Varying x_A and x_B in an iterative fashion can then be used to establish more realistic values of x_A and x_B as shown in (Table III). This result can be cross-checked for other trial compositions and a pattern established for the variation of x_A and x_B with composition. This appears to be a very simple variation, with x_A constant at 0.18 (compared to the initially assumed maximum value of 0.25), and x_B equal to a constant fraction of C_{Al} (the constant being the ratio $(x_A/x_A(max))$ or 0.72). These values of $W^{(1)}$, $W^{(2)}$, x_A and x_B when inserted into equations (11 & 12) yield the results shown in (Table IV), and a more direct comparison with experimental results is given in (Table V), and (Fig. 7).

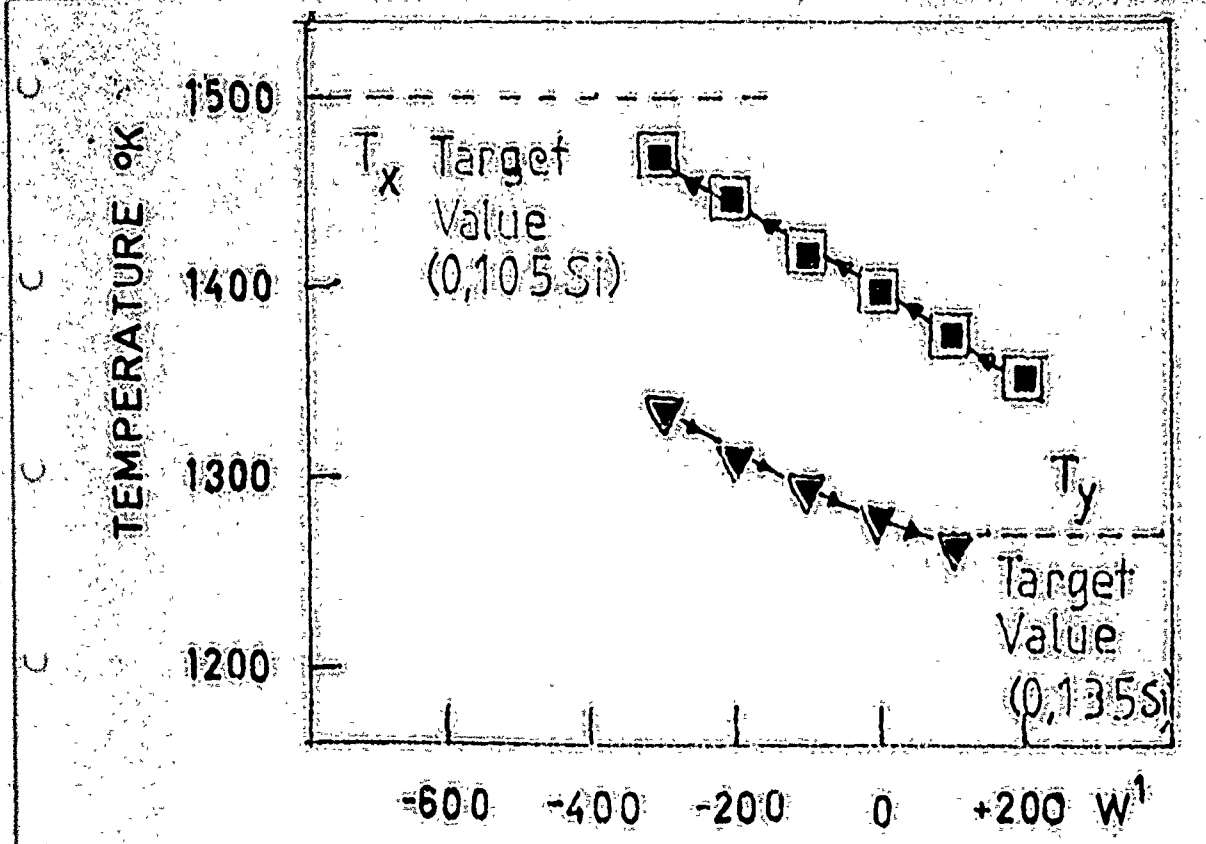

Trial Values of $W^{(1)}$ Al-Si

Fig. 6 Effect of varying $W^{(1)}$ Al-Si on calculated T_x and T_y temperatures using the assumption of full A2/B2 ordering at T_y.

6. Discussion

The degree of agreement obtained is very satisfactory, and further calculations in this system based on these interaction parameters should yield equally reliable results. There is some indication that the equilibrium values of x_A and x_B for the binary alloys Fe_3Al and Fe_3Si are in fact slightly higher than would be indicated by the simplifying assumptions just outlined (see Table II). Whether it is necessary to calculate equilibrium values of x_A and x_B vigorously for every composition instead of using the simplifying formula depends on the accuracy with which the ordering temperatures need to be known and also to some extent on the cooling rates required to attain equilibrium under practical conditions. Table VI gives some idea of the effect of small variations in ordering parameters. Additionally, the values of T_x and T_y shown in (Fig. 7) refer to the so-called constitutive phase boundaries and, analogous to the T_o lines of more common phase diagram calculations, assume no two phase regions exist. To establish the full phase diagram a more complex minimization program must be utilized (1, 2, 8) which is rather lengthy but requires no further new input data. It should also be noted that all calculations have been made on the basis that the temperatures of interest are above the magnetic transition temperatures in the system; if it is intended to investigate ordering below the Curie Temperature, additional terms have to be introduced into equations (10-12). In either circumstance the quoted values of $W^{(1)}$ and $W^{(2)}$ can be used to derive heats of formation for solid Al-Si BCC alloys which can be used to refine the calculation of the liquidus and solidus line in these systems, (17,18).

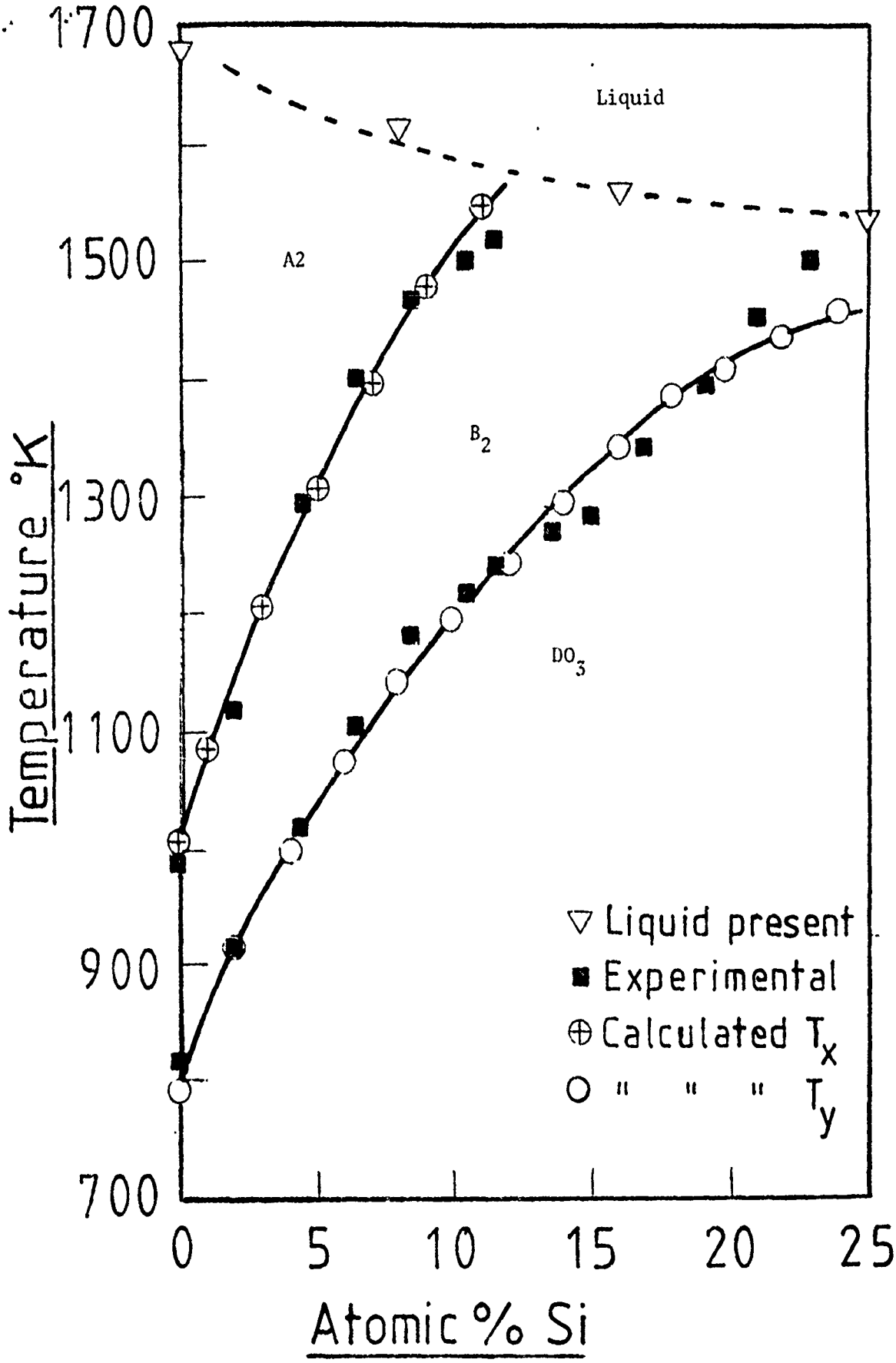

Fig. 7 Comparison of calculated and experimental ordering temperatures in the section Fe_3Al-Fe_3Si

7. References

1. G. Inden, Z. Metallk, 66 577 (1975)
2. G. Inden, Z. Metallk. 63 253 (1972)
3. G. Schlatte, G. Inden, W. Pitsch, Z. Metallk 65 94 (1974)
4. G. Inden, Z. Metallk. 68 529 (1977)
5. G. Inden, Thesis Techniche Hochschule Aachen (1970)
6. G. Inden, J. de Physique (C7) 38 373 (1977)
7. G. Inden, Physica 103B 82 (1981)
8. W. Meyer & G. Inden Phys. Stat Solidi (a) 56 481 (1979) (see also ibid 177)
9. P.R. Swann, W.R. Duff, R.M. Fisher Trans. Met Soc AIME 245 851 (1975).
10. S.M. Allen, J.W. Cahn, Acta Met 24 425 (1975)
11. W. Köster, T. Gödecke, Z. Metallk. 71 (12) 765 (1980)
12. G. Inden, Private Communication (1981)
13. A.A. Katsnel'son. V.Ye Polishchuk, Phys. Met. Metallog. 36 86 (1973) or (Fiz. Met. Metallog. 36 (2) 321)
14. F. Lihl, R. Burger, F. Sturn, H. Ebel, Arch. Eisenhutten W. 39 877 (1968)
15. V. Niculescu, K. Raj, T. Burch, J.I. Budnick, J. Phys, F. 7 (3) L73 (1977)
16. L. Chandrasekaran, Ph.D. Thesis, Univ. of Surrey (1980)
17. L. Kaufman, H. Nesor, CALPHAD 2 (4) 332 (1978)
18. P. Börner, E.T. Henig, H. Krieg, H.L. Lukas, G. Petzow, CALPHAD 4 (4) 241 (1980)

TABLE I

OPTIMIZED VALUES OF W_1 AND W_2 (k units)

X	SYSTEM	W	INDEN (6)	KATSNEL'SON (13)	USED IN THIS WORK	RATIO W_2/W_1
.68	FeAl	W_1	1005	1090 1063	1080	
	FeAl	W_2	539	583 547		
		(W_2/W_1)	0.54	0.52		0.50
	Al-Si	W_1			-480	
	Al-Si	W_2			-250	
		(W_2/W_1)				0.52
.71	Fe-Si	W_1	2010	-	2010	
	Fe-Si	W_2	1000	1067	1000	
		(W_2/W_1)	0.50	1000		0.50

TABLE II

DERIVATION OF A2/B2 ORDERING PARAMETERS FOR Fe_3Al

SHOWING THE EFFECT OF CHANGING $W^{(1)}$ (Fe-Al)

$W^{(1)} = 1080$ $W^{(2)} = 540$ $T_x = 1012K$

x_A	T_y	$(\delta\Delta G/\delta x_A)$
.17	789	-326
.18	794	-227
.19	798	-95
.20	801	+80
.21	804	+321
.22	807	+665

$W^{(1)} = 1005$ $W^{(2)} = 540$ calc $T_x = 900K$

x_A	T_y	$(\delta\Delta G/\delta x_A)$
.15	777	-93
.16	783	-15
.17	789	+81
.18	794	+204
.19	798	+360
.20	801	+560

TABLE III

TYPICAL TRIAL CALCULATION OF ORDER PARAMETERS AND T_y FOR A TERNARY ALLOY CONTAINING 75Fe, 13.5Al and 11.5Si

x_A	x_B	T_y	$\Delta G/\alpha x$	$\delta \Delta G/\delta x$
+.169	-.080	1243	+42	-41
+.171	-.081	1244	+25	-23
+.171	-.081	1244	+39	+13
+.172	-.081	1245	- 4	-41
+.172	-.082	1245	+ 8	- 4
+.173	-.082	1245	+21	+32
+.173	-.082	1246	-23	-23

Input Energy Parameters BWG Values in K Units

1005*, 540, -480, -250, 2010, 1000

Calculated T_x = 1516

* Note $W^{(1)}$ FeAl here is not the value finally adopted (1080)

TABLE IV

CALCULATED VALUES OF T_x AND T_y (°K)

Si%	T_x	Si%	T_y	(x_B)
.25	1890			
		.24	1458	-.007
.23	1855			
		.22	1433	-.022
.21	1816			
		.20	1403	-.036
.19	1773			
		.18	1370	-.050
.17	1724			
		.16	1334	-.065
.15	1671			
		.14	1293	-.079
.13	1613			
		.12	1247	-.094
.11	1548			
		.10	1196	-.108
.09	1477			
		.08	1139	-.123
.07	1397			
		.06	1074	-.137
.05	1307			
		.04	998	-.151
.03	1204			
		.02	908	-.166
.01	1083			
		0	794	-.180

W^1_{FeAl} 1080 W^1_{AlSi} - 480 W^1_{FeSi} 2010 $x_A = .18$ (at T_y)

W^2_{FeAl} 540 W^2_{FeAl} - 250 W^2_{FeAl} 1000 $x_B = C_B(-0.72)$

TABLE V

COMPARISON OF CALCULATED AND EXPERIMENTAL VALUES

Si(at%)	T_y(OK)		T_x(OK)	
	Exptl	Calcd	Exptl	Calcd
0.23%	1500	1446	-	1855
0.21	1450	1418	-	1816
0.195	1390	1392	-	1773
0.17	1340	1353	-	1724
0.15	1280	1314	-	1671
0.135	1270	1282	-	1613
0.115	1240	1235	1520	1565
0.105	1220	1259	1500	1531
0.085	1180	1154	1470	1458
0.065	1100	1091	1400	1376
0.045	102L	1018	1290	1283
0.02	910	908	1120	1147
0	820	794	980	1012

$x_A = .18 \quad x_B = -.72x\ C_B$

(Calculated value for T_x Fe_3Si is 1890°K)

TABLE VI

(a) The Effect of Arbitrarily Reducing the Order Parameters on the Calculated T_y Temperature for Fe75, Al 13.5, Si 11.5

x_A	x_B	calc T_y (°K)
.25	-.135	1264
.125	-.065	1182
.08	-.04	1115
.04	-.02	1035

(b) The Effect of varying the order parameters within the limits found for other compositions

x_A	x_B	calc T_y (°K)
.175	-.082	1245
.18	-.097	1235
.16	-.11	1181
.19	-.13	1202
.18	-.12	1201

CALCULATION OF THE FCC + BCC PHASE FIELDS IN DISORDERED Fe-Aℓ-Ni, Fe-Aℓ-Mn AND Fe-Ni-Mn ALLOYS BETWEEN 900°C and 1200°C

The ManLabs Data Bank was employed to compute the fcc/bcc two phase fields in the iron-aluminum-nickel, iron-aluminum-manganese and iron-nickel-manganese systems between 900°C and 1200°C for disordered alloys. The results are shown in Figures 1-3. Background information and details of the calculation are presented in Tables 1-8. The calculation of ternary equilibrium is done by employing CALPHAD descriptions of the binary systems to synthesize the ternary fcc and bcc disordered phases as illustrated in Tables 1-8. The procedure and numerical values have been published as referenced below.

1. L. Kaufman, CALPHAD 1 7 (1977)
2. L. Kaufman, CALPHAD 2 117 (1978)
3. D. Dew-Hughes and L. Kaufman, CALPHAD 3 175 (1979)
4. L. Kaufman and H. Nesor, CALPHAD 2 325 (1978)

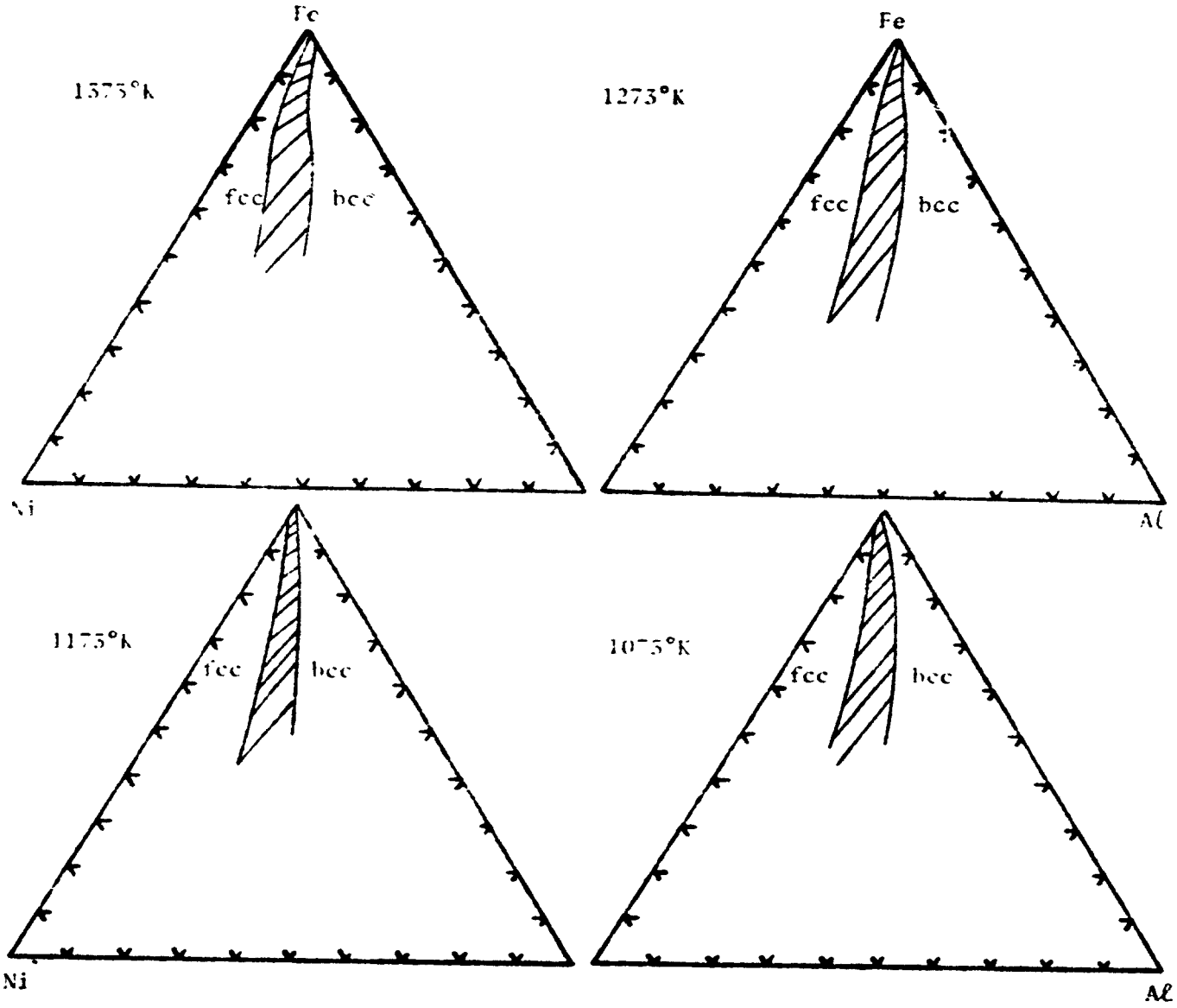

Figure 1. Calculated fcc/bcc Equilibrium Between Disordered Phases in the Iron-Aluminum-Nickel System Between 1373°K and 1073°K.

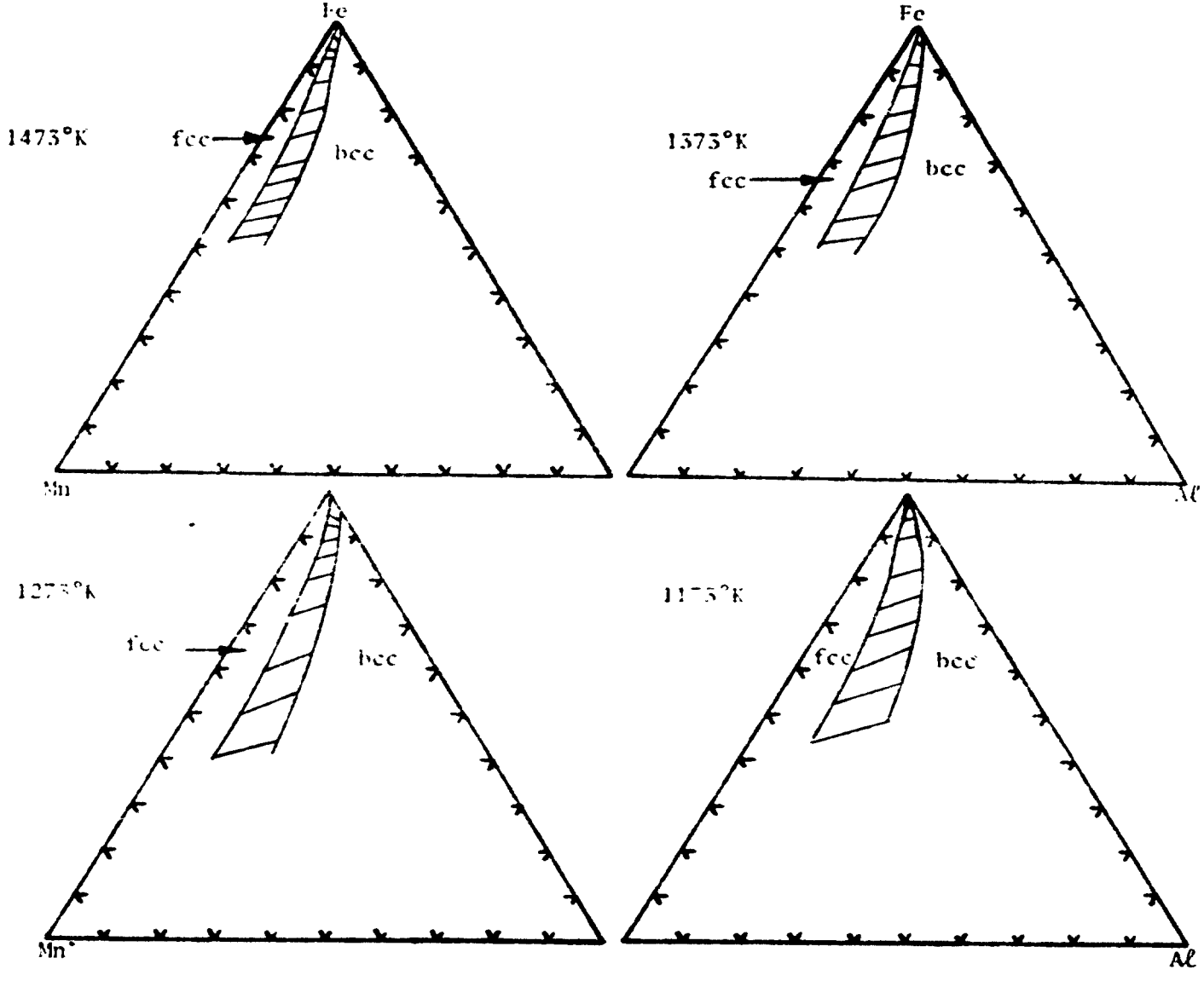

Figure 2. Calculated fcc/bcc Equilibrium Between Disordered Phases in the Iron-Aluminum-Manganese System Between 1473°K and 1173°K.

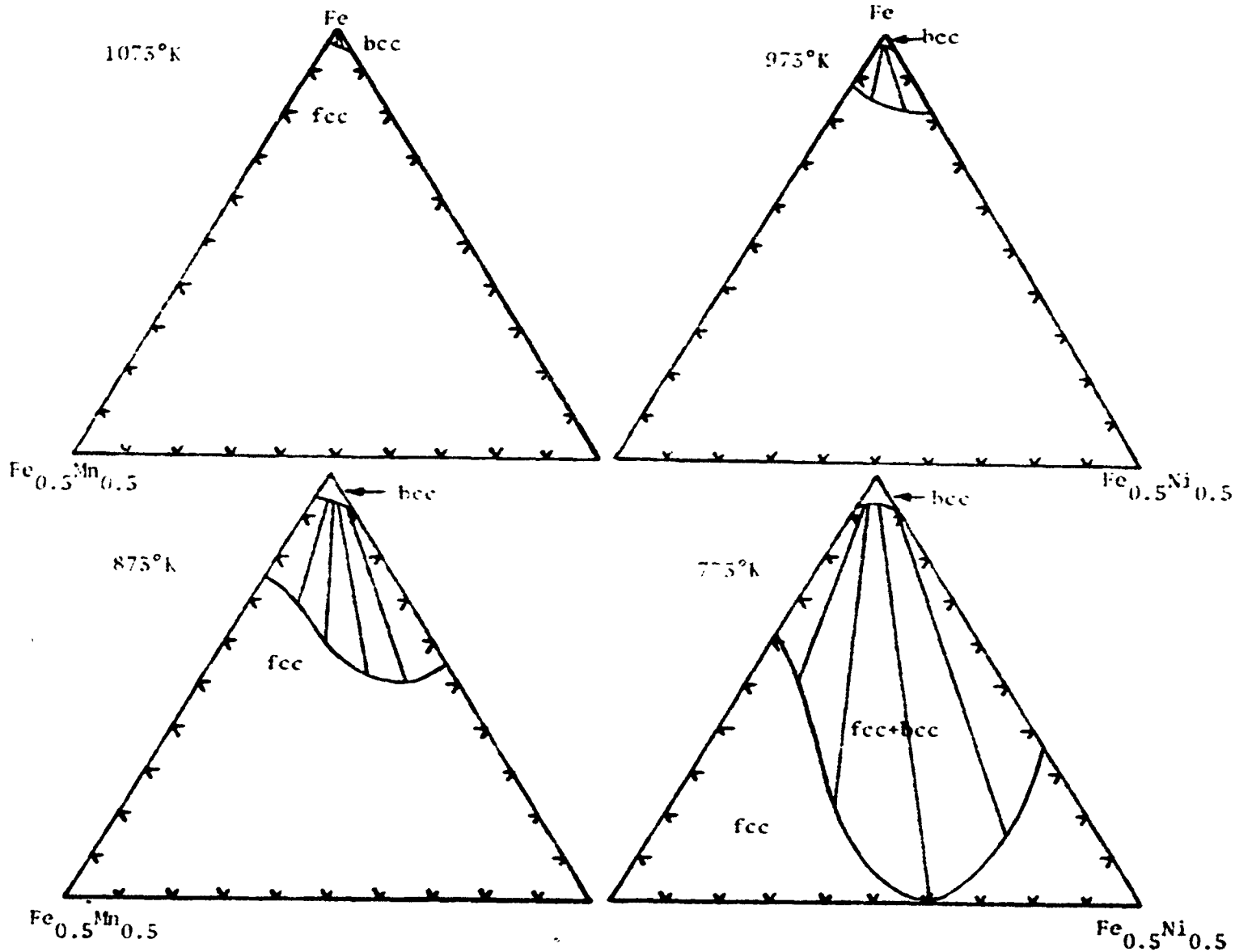

Figure 3. Calculated fcc/bcc Equilibrium Between Disordered Phases in the Iron-Nickel-Manganese System at 1073°K and 773°K.

TABLE 1

LATTICE STABILITY VALUES FOR THE ELEMENTS

(Units of J/mol and J/molK will be used throughout)

(L=Liquid, P=Primitive Cubic-βMn, K=Complex Cubic-αMn)

Element		Temperature Range K
Fe	${}^{\circ}G^{L} - {}^{\circ}G^{fcc} = 14744.416-8.1965T$	$1665 \leq T$
	${}^{\circ}G^{L} - {}^{\circ}G^{bcc} = 13807.2-7.6316T$	$1665 \leq T$
	${}^{\circ}G^{bcc} - {}^{\circ}G^{fcc} = -5235+9.4T-0.5295(E-2)T^{2}+0.9221(E-6)T^{3}$	$1100 \leq T \leq 1800$
	${}^{\circ}G^{fcc} - {}^{\circ}G^{bcc} = 6108.64-3.4618T-0.7472(E-2)T^{2}+0.51254(E-5)T^{3}$	$300 \leq T \leq 1100$
	${}^{\circ}G^{fcc} - {}^{\circ}G^{bcc} = 5451.752+7.4475(E-3)T^{2}-12(E-5)T^{3}+20.5434(E-8)T^{4}$	$0 \leq T \leq 300$
	${}^{\circ}G^{fcc} - {}^{\circ}G^{hcp} = 1828.4 - 4.686T$	$300 \leq T$
	${}^{\circ}G^{fcc} - {}^{\circ}G^{P} = -1151 - 0.837T$	$300 \leq T$
	${}^{\circ}G^{P} - {}^{\circ}G^{K} = -418 + 0.167T$	$300 \leq T$
Ti	${}^{\circ}G^{L} - {}^{\circ}G^{bcc} = 16233.92 - 8.368T$	$300 \leq T \leq 2400$
	${}^{\circ}G^{hcp} - {}^{\circ}G^{bcc} = -4351 + 3.7656T$	$300 \leq T \leq 2400$
	${}^{\circ}G^{hcp} - {}^{\circ}G^{fcc} = -3347.2$	$300 \leq T \leq 2400$
	${}^{\circ}G^{fcc} - {}^{\circ}G^{P} = -4184$	$300 \leq T$
	${}^{\circ}G^{P} - {}^{\circ}G^{K} = 2929$	$300 \leq T$
Mn	${}^{\circ}G^{L} - {}^{\circ}G^{bcc} = 14644 - 9.623T$	$1220 \leq T$
	${}^{\circ}G^{L} - {}^{\circ}G^{hcp} = 9205 - 7.113T$	$1220 \leq T$
	${}^{\circ}G^{L} - {}^{\circ}G^{fcc} = 16401 - 10.878T$	$1220 \leq T$
	${}^{\circ}G^{bcc} - {}^{\circ}G^{P} = 3975 - 2.887T$	$1220 \leq T$
	${}^{\circ}G^{P} - {}^{\circ}G^{K} = 2259 - 2.259T$	$1220 \leq T$
	${}^{\circ}G^{fcc} - {}^{\circ}G^{bcc} = 1477-0.51400T-2.7420(E-2)T^{2}+1.6534(E-6)T^{3}$	$400 \leq T \leq 1220$
	${}^{\circ}G^{fcc} - {}^{\circ}G^{P} = 611 + 13.101T-2.1240(E-2)T^{2}+0.8396(E-5)T^{3}$	$400 \leq T \leq 1220$
Al	${}^{\circ}G^{L} - {}^{\circ}G^{fcc} = 10711.04 - 11.506T$	
	${}^{\circ}G^{hcp} - {}^{\circ}G^{bcc} = -4602.4 + 3.01248T$	
	${}^{\circ}G^{hcp} - {}^{\circ}G^{fcc} = 5481.04 - 1.79912T$	
	${}^{\circ}G^{bcc} - {}^{\circ}G^{P} = -837$	
	${}^{\circ}G^{P} - {}^{\circ}G^{K} = -4187$	
Ni	${}^{\circ}G^{L} - {}^{\circ}G^{fcc} = 17614.64 - 10.209\ T$	
	${}^{\circ}G^{bcc} - {}^{\circ}G^{fcc} = 5564.72 - 1.046\ T$	$1000 < T$
	${}^{\circ}G^{bcc} - {}^{\circ}G^{fcc} = 3932.96+4.1087\ E\text{-}3\ T^{2}-0.4853\ E\text{-}5\ T^{3}+1.41\ E\text{-}9\ T^{4}$	$0 - 1800$
	${}^{\circ}G^{hcp} - {}^{\circ}G^{fcc} = 1046 + 1.2552\ T$	

$10^{m} = Em$

TABLE 2

THE IRON-MANGANESE SYSTEM

ANALYTICAL DESCRIPTION OF THE IRON-MANGANESE SYSTEM

Phase ϕ	$E_H^\phi = H_N^\phi - x_{Fe} {}^oH_{Fe}^\phi - x_{Mn} {}^oH_{Mn}^\phi$	$E_S^\phi = S^\phi - x_{Fe} {}^oS_{Fe}^\phi - x_{Mn} {}^oS_{Mn}^\phi + R[x_{Fe} \ln x_{Fe} + x_{Mn} \ln x_{Mn}]$	Composition Range	Comments
Liquid	$x_{Fe}x_{Mn}[-19874x_{Fe} - 21589x_{Mn}]$	$-x_{Fe}x_{Mn}16.987$	$0 \leq x_{Mn} \leq 1$	$1500 \leq T \leq 2000$ °Refers to Liquid
bcc	$x_{Fe}x_{Mn}[+4100x_{Fe} + 5188x_{Mn}]$	$x_{Fe}x_{Mn}[-4.686x_{Fe} - 1.506x_{Mn}]$	$0 \leq x_{Mn} \leq 1$	$300 \leq T \leq 2000$ °Refers to bcc
fcc	$x_{Fe}x_{Mn}(-18870)$	$-x_{Fe}x_{Mn}16.987$	$0 \leq x_{Mn} \leq 1$	$300 \leq T \leq 2000$ °Refers to fcc
P(βMn)	$x_{Fe}x_{Mn}[-13757x_{Fe} - 9113x_{Mn} - 1.4602\times10^{-3}T^2]$	$x_{Fe}x_{Mn}[-11.326x_{Fe} - 5.217x_{Mn} - 2.9204\times10^{-3}T]$	$0 \leq x_{Mn} \leq 1$	$800 \leq T \leq 1500$ °Refers to βMn
K(αMn)	$x_{Fe}x_{Mn}[-9665x_{Fe} - 5021x_{Mn}]$	$x_{Fe}x_{Mn}[-7.782x_{Fe} - 2.510x_{Mn}]$	$0 \leq x_{Mn} \leq 1$	$400 \leq T \leq 1200$ °Refers to αMn

EXPERIMENTAL THERMOCHEMICAL DATA FOR IRON-MANGANESE ALLOYS (8)

x_{Mn}	$E_H$fcc	$E_S$fcc	E_GL
	·····(1450K)·····		(1863K)
0.1	-1314	-1.238	397
0.2	-2456	-2.297	703
0.3	-3431	-3.167	924
0.4	-4204	-3.837	1054
0.5	-4728±1674	-4.255±0.837	1100±1674
0.6	-4925	-4.377	1054
0.7	-4690	-4.113	924
0.8	-3895	-3 391	703
0.9	-2389	-2.054	397

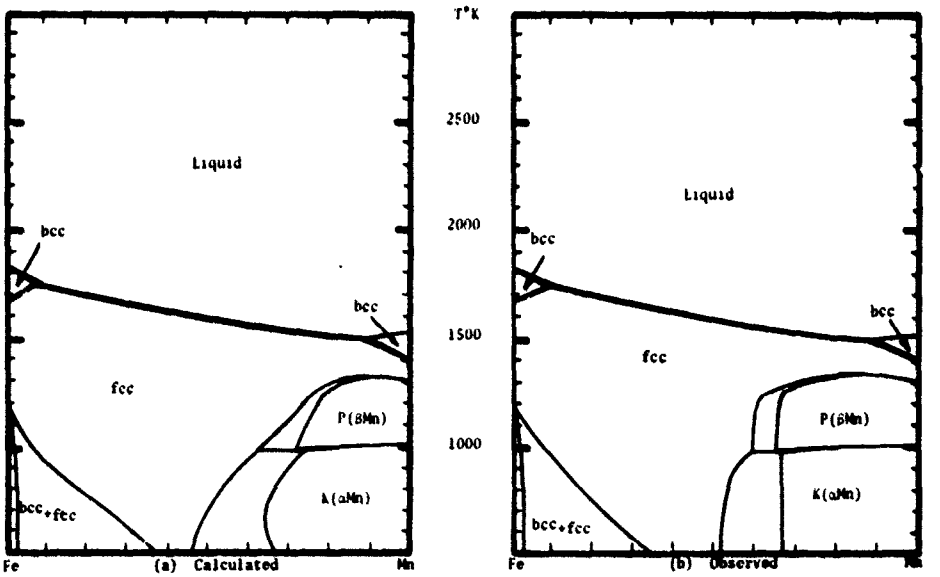

TABLE 3

THE IRON-ALUMINUM SYSTEM

Phase ϕ	$E_H^\phi = H_M^\phi - x_{Fe}{}^oH_{Fe}^\phi - x_{Al}{}^oH_{Al}^\phi$	$E_S^\phi = S^\phi - x_{Fe}{}^oS_{Fe}^\phi - x_{Al}{}^oS_{Al}^\phi + R[x_{Fe}\ln x_{Fe} + x_{Al}\ln x_{Al}]$	Composition Range	Comments
Liquid	$-x_{Fe}x_{Al}[x_{Fe}62760 + x_{Al}96232]$	$x_{Fe}x_{Al}[x_{Fe}4.602 - x_{Al}35.054]$	$0<x_{Al}<1$	800<T<1900 *Refers to Liquid
bcc	$-x_{Fe}x_{Al}[x_{Fe}58576 + x_{Al}175728]$	$x_{Fe}x_{Al}[x_{Fe}14.226 - x_{Al}71.128]$	$0<x_{Al}<1$	300<T<1900 *Refers to bcc
fcc	$-x_{Fe}x_{Al}[x_{Fe}51296 + x_{Al}112968]$	$x_{Fe}x_{Al}[x_{Fe}14.266 - x_{Al}71.128]$	$0<x_{Al}<1$	300<T<1900 *Refers to fcc

Compound	$\Delta H = H - x_{Fe}^o{}^oH_{Fe}^\phi - x_{Al}^o{}^oH_{Al}^\phi$	$\Delta S = S - x_{Fe}^o{}^oS_{Fe}^\phi - x_{Al}^o{}^oS_{Al}^\phi$	Composition	Comments
$Fe_{0.400}Al_{0.600}$	-25204	0.904	$x_{Al}^o = 0.600$	ϕ=bcc
$Fe_{0.333}Al_{0.667}$	-34060	-6.418	$x_{Al}^o = 0.667$	ϕ=bcc
$Fe_{0.286}Al_{0.714}$	-32562	-5.917	$x_{Al}^o = 0.714$	ϕ=bcc
$Fe_{0.250}Al_{0.750}$	-35146	-8.355	$x_{Al}^o = 0.750$	ϕ=bcc

SUMMARY OF EXPERIMENTAL THERMOCHEMICAL DATA FOR IRON-ALUMINUM ALLOYS

$(1-x)Fe(liquid) + xAl(liquid) \rightarrow Fe_{(1-x)}Al_x(liquid)(1873K)$

x	ΔG	ΔH	x	ΔG	x	ΔG
0.1	-9060±2500	-6110±2000	0.4	-21460±2500	0.7	-20050±2500
0.2	-14910	-11500	0.5	-22535	0.8	-16130
0.3	-18950	-16020	0.6	-22120	0.9	-9930

$(1-x)\ Fe^{bcc} + x\ Al^{fcc} \rightarrow Fe_{(1-x)}Al_x$

x	ΔG	ΔH[298K]	x	ΔG[1173K]	ΔH[298K]	x	ΔG[1173K]	ΔH[298K]
0.1	-9770±2500	-5770±2000	0.4	-24700±2500	-20000±2000	0.704	-24900±2500	-
0.2	-16800	-11000	0.5	-25850	-25100	0.750	-26350	-27900±2000
0.3	-21700	-15750	0.665	-25650	-26150			

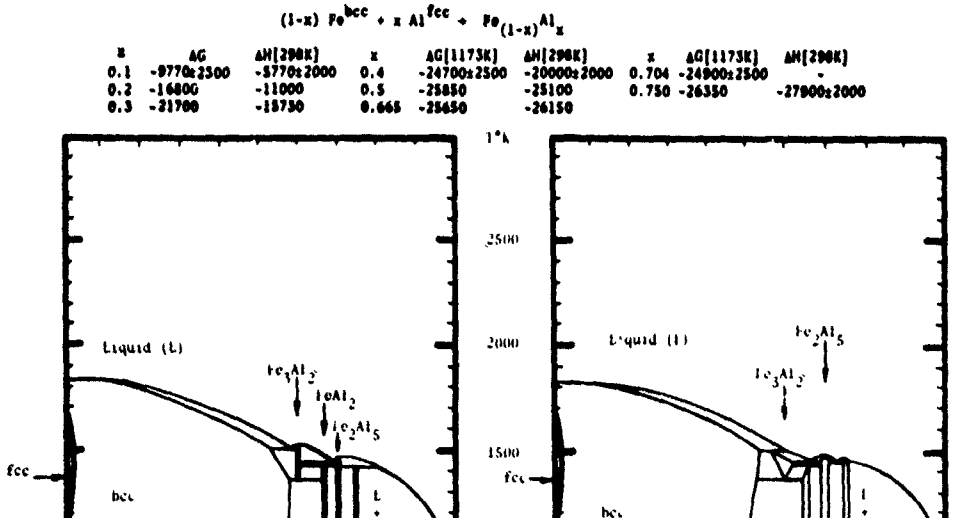

TABLE 4

ANALYTICAL DESCRIPTION OF THE IRON-NICKEL SYSTEM

Phase	$^{E}H^{\phi} = H_M - x_{Fe}\,{}^{\circ}H^{\phi}_{Fe} - x_{Ni}\,{}^{\circ}H^{\phi}_{Ni}$	$^{E}S^{\phi} = S^{\phi} - x_{Fe}\,{}^{\circ}S^{\phi}_{Fe} - x_{Ni}\,{}^{\circ}S^{\phi}_{Ni} - R[x_{Fe}\ln x_{Fe} + x_{Ni}\ln x_{Ni}]$	Composition Range	Comments
Liquid	$x_{Fe}x_{Ni}\,[-8368\,x_{Fe} - 32217\,x_{Ni}]$	$x_{Fe}x_{Ni}(-2.72x_{Fe} - 9.205x_{Ni})$	$0 < x_{Ni} < 1$	$0 < T < 1800K$
fcc	$x_{Fe}x_{Ni}[x_{Fe}(2092 + 3.8314\times10^{-3}T^2 - 3.2652\times10^{-6}T^3) + x_{Ni}(-34881 - 2.4404\times10^{-2}T + 2.0802\times10^{-5}T^3)]$	$x_{Fe}x_{Ni}[x_{Fe}(7.6628\times10^{-3}T - 4.8990\times10^{-6}T^2) + x_{Ni}(-4.8808\times10^{-2}T + 3.1203\times10^{-5}T^2)]$	$0 < x_{Ni} < 1$	$0 < T < 1800K$
bcc	$x_{Fe}x_{Ni}[x_{Fe}(1339 - 1.3275\times10^{-3}T^2 + 3.1740\times10^{-6}T^3) + x_{Ni}(-16276 - 3.5412\times10^{-2}T^2 + 2.6382\times10^{-5}T^3)]$	$x_{Fe}x_{Ni}[x_{Fe}(-2.655\times10^{-3}T + 4.761\times10^{-6}T^2) + x_{Ni}(-7.0824\times10^{-2}T + 3.9573\times10^{-5}T^2)]$	$0 < x_{Ni} < 1$	$0 < T < 1800$
Compound	$\Delta H = H - x^{*}_{Fe}\,{}^{\circ}H^{fcc}_{Fe} - x^{*}_{Ni}\,{}^{\circ}H^{fcc}_{Ni}$	$\Delta S = S - x^{*}_{Fe}\,{}^{\circ}S^{fcc} - x^{*}_{Ni}\,{}^{\circ}S^{fcc}_{Ni}$	Composition	Comments
$Fe_{0.25}Ni_{0.75}$ $AuCu_3$ Structure	-15592	-10.83	$x^{*}_{Ni} = 0.75$	

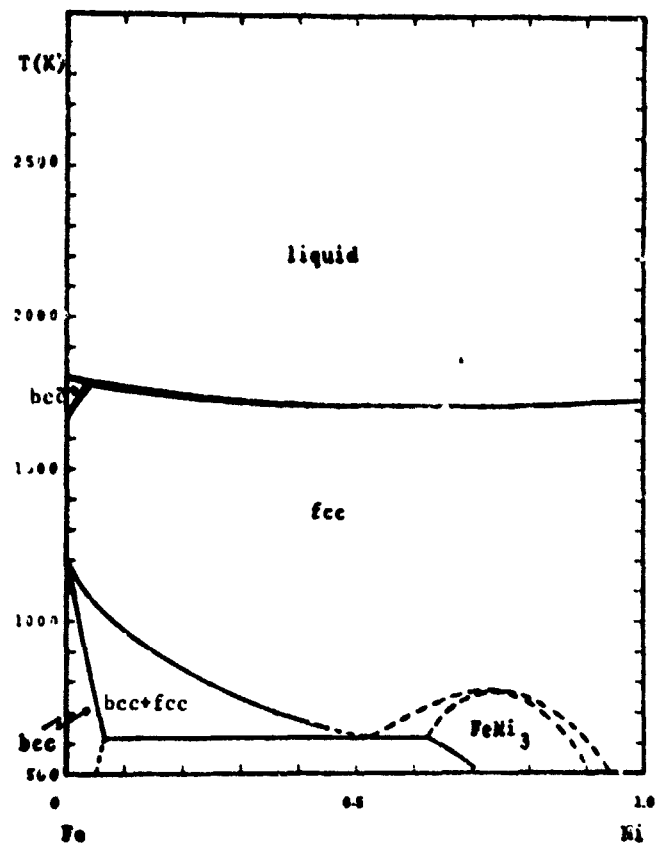

FIG. 38 (observed) (40)

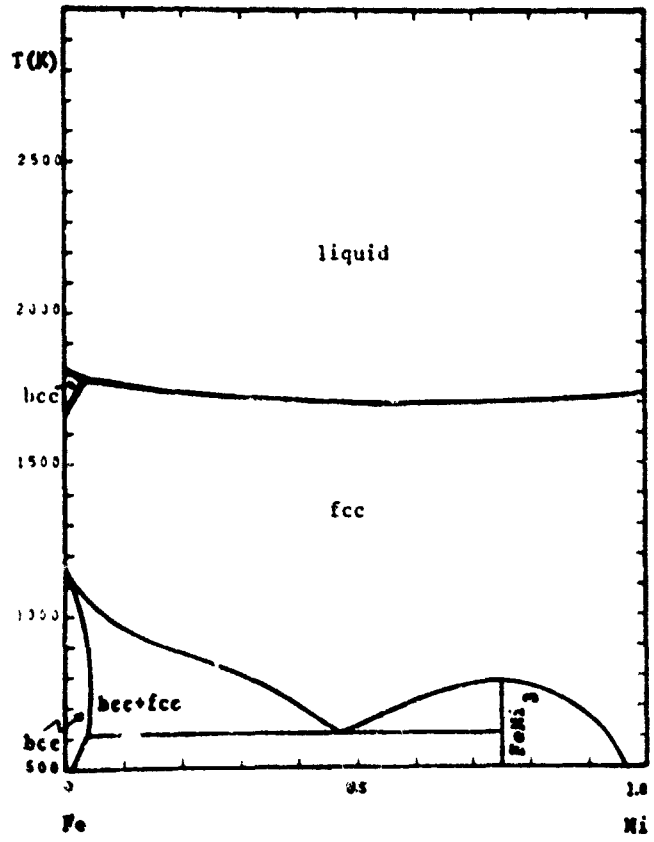

FIG. 39 (calculated) (36)

TABLE 5

ANALYTICAL DESCRIPTION OF THE ALUMINUM-NICKEL SYSTEM

Phase ϕ	${}^{E}H^{\phi}=H_M^{\phi}-x_{Al}{}^{\circ}H^{\phi}_{Al}-x_{Ni}{}^{\circ}H^{\phi}_{Ni}$	${}^{E}S^{\phi} = S^{\phi} - x_{Al}{}^{\circ}S^{\phi}_{Al} - x_{Ni}{}^{\circ}S^{\phi}_{Ni} + R[x_{Al}\ln x_{Al} + x_{Ni}\ln x_{Ni}]$	Composition Range	Comments
Liquid	$x_{Al}x_{Ni}[x_{Ni}(-203376-1.3924\times10^{-1}T^2+5.4626\times10^{-5}T^3)+x_{Al}(-92081-1.3924\times10^{-1}T^2+5.4626\times10^{-5}T^3)]$	$x_{Al}x_{Ni}[x_{Ni}(138.15-27.848\times10^{-2}T+81.939\times10^{-6}T^2)+x_{Al}(130.206-27.848\times10^{-2}T+81.939\times10^{-6}T^2)]$	$0 \leq x_{Ni} \leq 1$	$300 \leq T \leq 2000K$ °Refers to liquid
fcc	$x_{Al}x_{Ni}[x_{Ni}(-189987-1.3924\times10^{-1}T^2+5.4626\times10^{-5}T^3)+x_{Al}(-19907-1.3924\times10^{-1}T^2+5.4626\times10^{-5}T^3)]$	$x_{Al}x_{Ni}[x_{Ni}(149.452-27.848\times10^{-2}T+81.939\times10^{-6}T^2)+x_{Al}(182.506-27.848\times10^{-2}T+81.939\times10^{-6}T^2)]$	$0 \leq x_{Ni} \leq 1$	$300 \leq T \leq 2000$ K °Refers to fcc
bcc	$x_{Al}x_{Ni}[x_{Ni}(-220984-1.3924\times10^{-1}T^2+5.4626\times10^{-5}T^3)+x_{Al}(-281662+0.92048\times10^{-1}T^2-3.6116\times10^{-5}T^3)]$	$x_{Al}x_{Ni}[x_{Ni}(141.084-27.848\times10^{-2}T+81.939\times10^{-6}T^2)+x_{Al}(-220.622+18.410\times10^{-2}T-54.174\times10^{-6}T^2)]$	$0 \leq x_{Ni} \leq 1$	$300 \leq T \leq 2000$ K °Refers to bcc
Compound	$\Delta H_M = H_M - x^{m}_{Al}{}^{\circ}H_{Al} - x^{m}_{Ni}{}^{\circ}H_{Ni}$	$\Delta S = S - x^{m}_{Al}{}^{\circ}S_{Al} - x^{m}_{Ni}{}^{\circ}S_{Ni}$	Composition	Comments
$Al_{0.75}Ni_{0.25}$	$-33465-2.611\times10^{-2}T^2+1.0242\times10^{-5}T^3$	$20.00-5.222\times10^{-2}T+1.5364\times10^{-5}T^2$	$x^{m}_{Ni}=0.25$	°Refers to fcc
$Al_{0.6}Ni_{0.4}$	$-49352-0.33418\times10^{-1}T^2+1.3110\times10^{-5}T^3$	$26.84-6.683\times10^{-2}T+1.9665\times10^{-5}T^2$	$x^{m}_{Ni}=0.40$	°Refers to fcc
$Al_{0.25}Ni_{0.75}$	$-38878-2.611\times10^{-2}T^2+1.0242\times10^{-5}T^3$	$27.57-5.222\times10^{-2}T+1.5364\times10^{-5}T^2$	$x^{m}_{Ni}=0.75$	°Refers to fcc

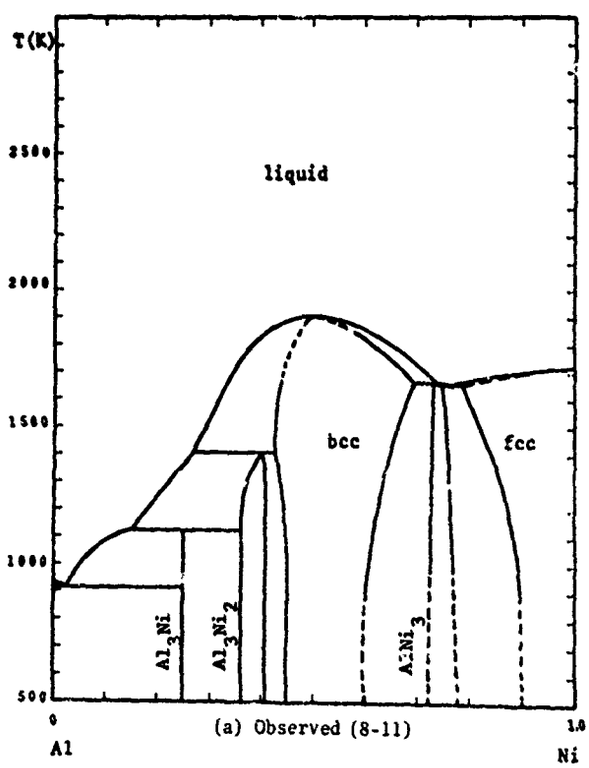

(a) Observed (8-11)

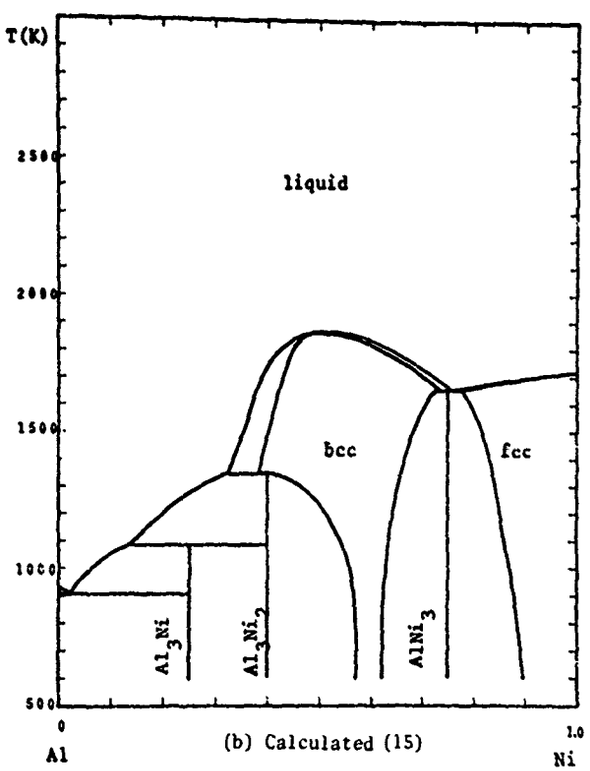

(b) Calculated (15)

TABLE 6

ANALYTICAL DESCRIPTION OF THE MANGANESE-NICKEL SYSTEM

Phase ϕ	$E_H^\phi = H_M^\phi - x_{Mn}{}^\circ H_{Mn}^\phi - x_{Ni}{}^\circ H_{Ni}^\phi$	$E_S^\phi = S^\phi - x_{Mn}{}^\circ S_{Mn}^\phi - x_{Ni}{}^\circ S_{Ni}^\phi + R[x_{Mn} \ell n x_{Mn} + x_{Ni} \ell n x_{Ni}]$	Composition Range	Comments
Liquid	$-x_{Mn}x_{Ni}[64434x_{Mn}+76986x_{Ni}]$	$-x_{Mn}x_{Ni}10.878$	$0 \leq x_{Ni} \leq 1$	$1200 \leq T \leq 1800$ ° Refers to Liquid
bcc	$-x_{Mn}x_{Ni}[45606x_{Mn}+58158x_{Ni}]$	$-x_{Mn}x_{Ni}3.640$	$0 \leq x_{Ni} \leq 1$	$1200 \leq T \leq 1500$ ° Refers to bcc
fcc	$-x_{Mn}x_{Ni}[51882x_{Mn}+64434x_{Ni}]$	$-x_{Mn}x_{Ni}10.878$	$0 \leq x_{Ni} \leq 1$	$300 \leq T \leq 1800$ ° Refers to fcc
P(βMn)	$-x_{Mn}x_{Ni}[63178x_{Mn}+39330x_{Ni}]$	$-x_{Mn}x_{Ni}17.991$	$0 \leq x_{Ni} \leq 1$	$700 \leq T \leq 1500$ ° Refers to βMn
K(αMn)	$-x_{Mn}x_{Ni}[63178x_{Mn}+39330x_{Ni}]$	$-x_{Mn}x_{Ni}17.991$	$0 \leq x_{Ni} \leq 1$	$400 < T < 1200$ ° Refers to αMn

Compound	$\Delta H = H - x^*_{Mn}{}^\circ H^\theta_{Mn} - x^*_{Ni}{}^\circ H^\theta_{Ni}$	$\Delta S = S - x^*_{Mn}{}^\circ S^\theta_{Mn} - x^*_{Ni}{}^\circ S^\theta_{Ni}$	Composition	Comments
$Mn_{0.750}Ni_{0.250}$	-27379	-17.730	$x^*_{Ni} = 0.250$	θ = K(αMn)
$Mn_{0.667}Ni_{0.333}$	-14028	+1.302	$x^*_{Ni} = 0.333$	θ = fcc
$Mn_{0.500}Ni_{0.500}$	-18891	+1.360	$x^*_{Ni} = 0.500$	θ = bcc
$Mn_{0.333}Ni_{0.667}$	-16777	-0.557	$x^*_{Ni} = 0.667$	θ = fcc
$Mn_{0.250}Ni_{0.750}$	-15208	-2.040	$x^*_{Ni} = 0.750$	θ = fcc

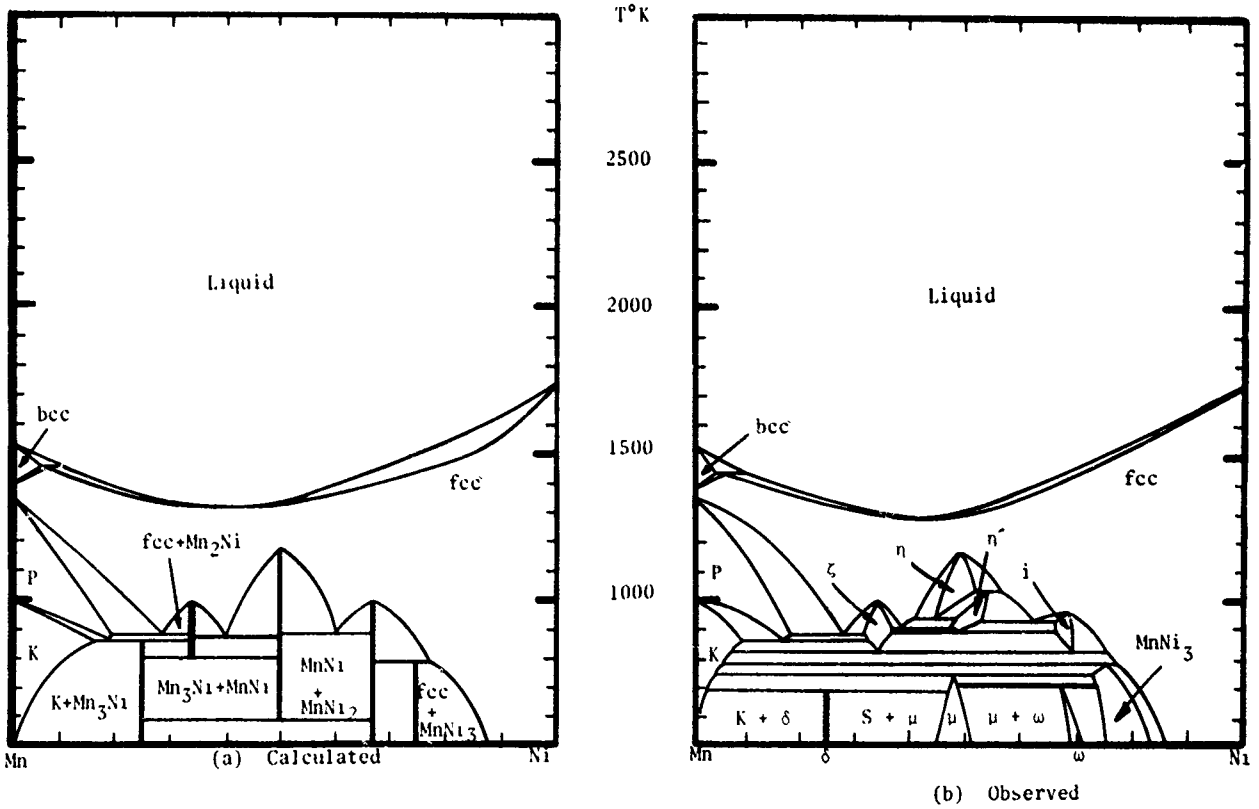

TABLE 7

ANALYTICAL DESCRIPTION OF THE ALUMINUM-MANGANESE SYSTEM

Phase ϕ	$E_H^\phi = H_M^\phi - x_{Al}\,{}^\circ H_{Al}^\phi - x_{Mn}\,{}^\circ H_{Mn}^\phi$	$E_S^\phi = S^\phi - x_{Al}\,{}^\circ S_{Al}^\phi - x_{Mn}\,{}^\circ S_{Mn}^\phi + R[x_{Al}\ell n x_{Al} + x_{Mn}\ell n x_{Mn}]$	Composition Range	Comments
Liquid	$-x_{Al}x_{Mn}57321$	$-x_{Al}x_{Mn}22.761$	$0<x_{Mn}<1$	$800<T<1800$ °Refers to Liquid
bcc	$-x_{Al}x_{Mn}73220$	$-x_{Al}x_{Mn}22.761$	$0<x_{Mn}<1$	$1000<T<1700$ °Refers to bcc
fcc	$-x_{Al}x_{Mn}[x_{Al}48116+x_{Mn}69036]$	$-x_{Al}x_{Mn}22.761$	$0<x_{Mn}<1$	$300<T<1500$ °Refers to fcc
P (β-Mn)	$-x_{Al}x_{Mn}[x_{Al}95814+x_{Mn}983$,]	$-x_{Al}x_{Mn}41.84$	$0<x_{Mn}<1$	$300<T<1500$ °Refers to P(β-Mn)
K(α-Mn)	$x_{Al}x_{Mn}[x_{Al}41840-x_{Mn}89956]$	$-x_{Al}x_{Mn}41.84$	$0<x_{Mn}<1$	$300<T<1500$ °Refers to K(α-Mn)

Compound	$\Delta H = H - x_{Al}^* {}^\circ H_{Al}^\theta - x_{Mn}^* {}^\circ H_{Mn}^\theta$	$\Delta S = S - x_{Al}^* {}^\circ S_{Al}^\theta - x_{Mn}^* {}^\circ S_{Mn}^\theta$	Composition	Comments
$Al_{0.857}Mn_{0.143}$	-16717	-8.166	$x_{Mn}^*=0.143$	θ=fcc
$Al_{0.800}Mn_{0.200}$	-21539	-10.015	$x_{Mn}^*=0.200$	θ=fcc
$Al_{0.615}Mn_{0.385}$	-23184	-5.390	$x_{Mn}^*=0.385$	θ=fcc
$Al_{0.450}Mn_{0.550}$	-20711	-1.491	$x_{Mn}^*=0.550$	θ=fcc

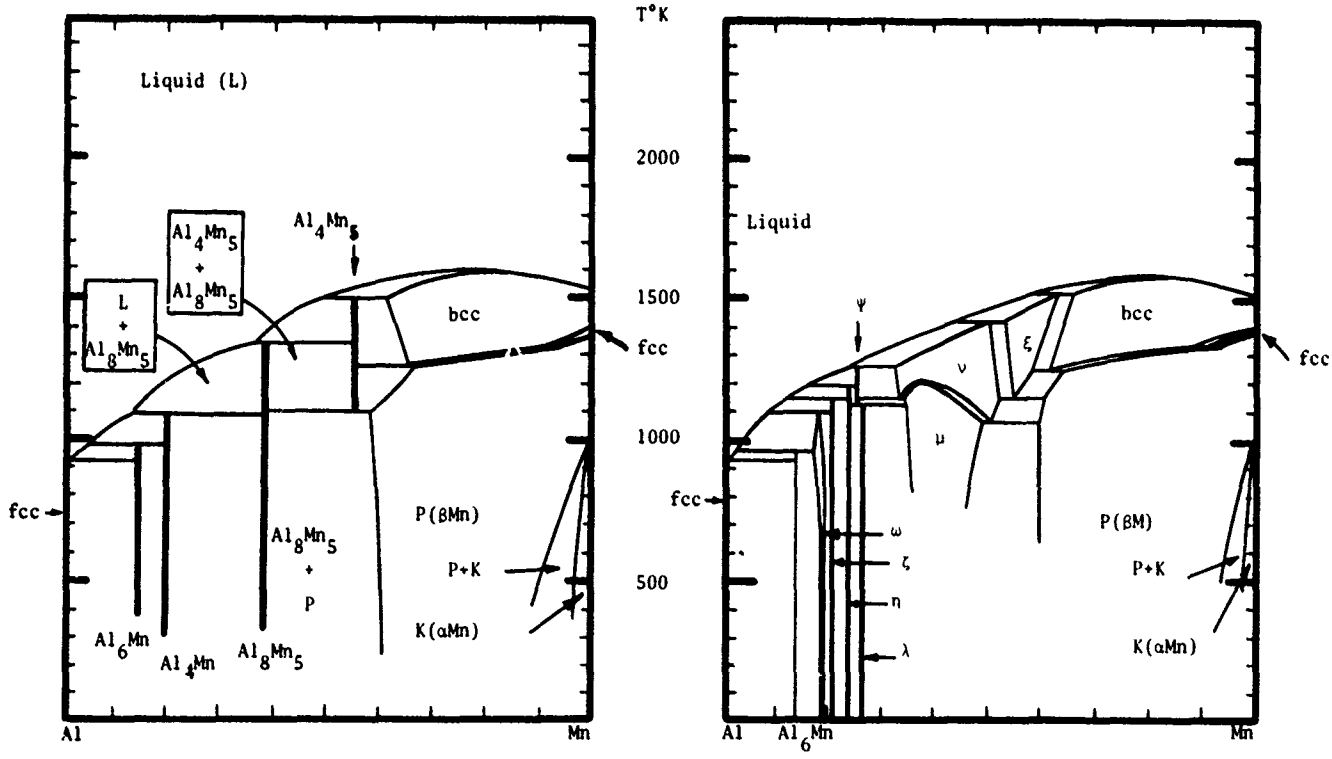

(a) Calculated

(b) Observed

TABLE 8

DESCRIPTION OF THE FREE ENERGY OF TERNARY PHASES

Definition of the free energy of the bcc phase of the Fe-Aℓ-Ni system $x=x_{Aℓ}$, $y=y_{Ni}$ can readily be stated as

$$G^{bcc} = (1-x-y)G^{bcc}_{Fe}+xG^{bcc}_{Aℓ}+yG^{bcc}_{Ni}+RT[(1-x-y)ℓn(1-x-y)+xℓnx+yℓny]$$
$$+\frac{(1-x-y)x}{(1-y)}[(1-x-y)BFEAL+xBALFE]+\frac{(1-x-y)y}{(1-x)}[(1-x-y)BFENI+yBNIFE]$$
$$+\frac{xy}{x+y}[xBALNI+yBNIAL] \qquad (1)$$

Similarly the free energy of the fcc phase can be written as

$$G^{fcc} = (1-x-y)G^{fcc}_{Fe}+xG^{fcc}_{Aℓ}+yF^{fcc}_{Ni}+RT[(1-x-y)ℓn(1-x-y)+xℓnx+yℓny]$$
$$+\frac{(1-x-y)x}{(1-y)}[(1-x-y)AFEAL+xAALFE]+\frac{(1-x-y)y}{(1-x)}[(1-x-y)AFENI+yANIFE]$$
$$+\frac{xy}{x+y}[xAALNI+yANIAL] \qquad (2)$$

On the basis of Eqs (1) and (2) the partial molar free energies of iron, nickel and aluminum in the fcc phase and the bcc phase can be written for the orientation Fe-Aℓ-Ni considered above. Thus with $x=x_{Aℓ}$ and $y=y_{Ni}$ the partial free energies in the fcc phase are given by Eqs (3)-(5)

$$\bar{G}^{fcc}_{Fe} = G^{fcc}_{Fe} + RTℓn(1-x-y) + x^2AFEAL + y^2AFENI$$
$$+xy(AFEAL+AFENI-AALNI) + x^2[\frac{x(2-y)}{(1-y)^2} - 1](AALFE-AFEAL)$$
$$+y^2[\frac{y(2-x)}{(1-x)^2} - 1](ANIFE-AFENI) - \frac{xy^2}{(x+y)}(ANIAL-AALNI) \qquad (3)$$

$$\bar{G}^{fcc}_{Aℓ} = G^{fcc}_{Aℓ} + RTℓnx + (1-x)^2AFEAL + y^2AFENI$$
$$-y(1-x)(AFEAL+AFENI-AALNI)+[\frac{x(2-y)}{(1-y)^2}+\frac{(2-3x-2y)}{x(1-y)} -1]x^2(AALFE-AFEAL)$$
$$+y^2[\frac{y}{1-x} -1](ANIFE-AFENI) + \frac{y^2}{(x+y)^2}[y(1-x)-x^2](ANIAL-AALNI) \qquad (4)$$

TABLE 8 (CONCLUDED)

and

$$\bar{G}_{Ni}^{fcc} = G_{Ni}^{fcc} + RT\ell ny + x^2AFEAL + (1-y)^2AFENI$$

$$-x(1-y)(AFEAL+AFENI-AALNI) + x^2[\frac{x}{1-y} - 1](AALFE-AFEAL)$$

$$+y^2[\frac{y(2-x)}{(1-x)^2} + \frac{(2-3y-2x)}{y(1-x)} - 1] (ANIFE-AFENI)$$

$$+ \frac{xy}{(x+y)^2}[2x+y-xy-y^2](ANIAL-AALNI) \qquad (5)$$

Similar equations can be written for the partial free energies for iron, aluminum and nickel in the bcc phase merely by replacing the symbols fcc and A by bcc and B in Equations (3)-(5).

Tables 2-7 contain the explicit equations for the A and B values in all of the six binary systems of interest to compute the fcc/bcc equilibria in Fe-Aℓ-Mn, Fe-Ni-Mn and Fe-Mn-Aℓ. In addition, Table 1 contains the free energy differences between the fcc and bcc forms of Fe, Aℓ, Ni and Mn so that the relative free energies of the fcc and bcc phases in each ternary can be specified. Simultaneous equilibration of the partial free energies of <u>each</u> component in the fcc and bcc phase permits calculation of the tie lines across the two phase fields. The latter are shown in Figures 1-3.

AFOSR/NE
Attn: Captain Steve Wax
Bldg. #410
Bolling AFB
Washington, D.C. 20332

AFML/LLS
Attn: Branch Chief
W-P AFB, Ohio 45433

U.S. Army Research Office
Metallurgy & Materials Sciences
P.O. Box 12211
Research Triangle Park, NC 27709

Office of Naval Research
Attn: Dr. A.M. Diness
800 N. Quincy Street
Arlington, VA 22203

Materials Research Lab (AMMRC)
Attn: Dr. R.N. Katz
Watertown, MA 02172

Prof. A.H. Heuer
Prof. T.E. Mitchell
Dept. of Materials Science
Northwestern University
Evanston, Illinois 60201

Dr. D.D. Cubicciotti
Stanford Research Institute
Materials Research Center
Menlo Park, California 94025

Dr. C. Sehagian
ESMC
Rome Air Development Center
Hanscom AFB, MA

Dr. M. Drexage
ESMC
Rome Air Development Center
Hanscom AFB, MA

Dr. A. Armington
ESMC
Rome Air Development Center
Hanscom AFB, MA

AFML/LLM
Attn: Branch Chief
W-P AFB, Ohio 45433

AFML/LLN
Attn: Branch Chief
W-P AFB, Ohio 45433

AFML/MBM
Attn: W.L. Baun
W-P AFB, Ohio 45433

N.S.F. (Materials Res.)
Attn: R.J. Reynik
1800 G Street, N.W.
Washington, DC 20550

U.S. Naval Research Laboratory
Attn: Dr. R.W. Rice, Chem. Div.
Washington, DC 20375

Professor T.Y. Tien
University of Michigan
Materials Engineering
Ann Arbor, Michigan 48105

Dr. E.F. Lange
Dr. A.G. Evans
Rockwell International
Science Center
Thousand Oaks, California 91360

Dr. Fred S. Pettit
Pratt & Whitney Aircraft
East Hartford, Conn. 06108